

**THE EPIGENETIC ROLE OF THE KLEEFSTRA SYNDROME
PROTEIN EHMT1 IN SYNAPTIC SCALING
AND IN COGNITION**

Marco Benevento

ISBN: 978-94-92380-34-0

Donders series number: 280

Image: *Maybe an architecture, but more likely a techno-plant* by architect Felice Gualtieri, Lab-OFF®, Trebisacce (CS), Italy

Layout & printing: Off Page, Amsterdam

Copyright © 2017 by Marco Benevento. All rights reserved.
No part of this book may be reproduced, stored in a retrieval system or transmitted in any form or by any means, without prior permission of the author.

THE EPIGENETIC ROLE OF THE KLEEFSTRA SYNDROME PROTEIN EHMT1 IN SYNAPTIC SCALING AND IN COGNITION

Doctoral Thesis

to obtain the degree of doctor
from Radboud University Nijmegen
on the authority of the Rector Magnificus prof. dr. J.H.J.M. van Krieken,
according to the decision of the Council of Deans
to be defended in public on Tuesday, May 23, 2017
at 10.30 hours

by

Marco Benevento

Born on November 13, 1977
in Rome, Italy

PROMOTOR COMMITTEE

Supervisor(s): Prof. dr. J.H.L.M. van Bokhoven

Co-supervisor(s): Dr. N. Nadif Kasri
Dr. H. Zhou

Doctoral Thesis Committee: Prof. dr. G.J.M. Martens
Prof. dr. L.T. Kozicz
Dr. A. Barco (Instituto de Neurociencias de Alicante, Spain)

THE EPIGENETIC ROLE OF THE KLEEFSTRA SYNDROME PROTEIN EHMT1 IN SYNAPTIC SCALING AND IN COGNITION

Proefschrift
ter verkrijging van de graad van doctor
aan de Radboud Universiteit Nijmegen
op gezag van de rector magnificus prof. dr. J.H.J.M. van Krieken,
volgens besluit van het college van decanen
in het openbaar te verdedigen op dinsdag 23 mei 2017
om 10.30 uur precies

door

Marco Benevento
geboren op 13 november 1977
te Rome, Italië

PROMOTIECOMMISSIE

Promotor: Prof. dr. J.H.L.M. van Bokhoven

Copromotoren: Dr. N. Nadif Kasri
Dr. H. Zhou

Manuscriptcommissie: Prof. dr. G.J.M. Martens
Prof. dr. L.T. Kozicz
Dr. A. Barco (Instituto de Neurociencias de Alicante, Spanje)

TABLE OF CONTENTS

Chapter 1	General Introduction	11
	Partially published in: <i>Neurobiology of learning and memory</i> 2015, 124:88-96. doi: 10.1016/j.nlm.2015.06.013	
Chapter 2	Histone Methylation by the Kleefstra Syndrome Protein EHMT1 Mediates Homeostatic Synaptic Scaling	27
	Published in: <i>Neuron</i> 91:341-55. doi: 10.1016/j.neuron.2016.06.003	
Chapter 3	EHMT1 is required for synaptic scaling in cortical neurons derived from human induced pluripotent stem cells	71
	(Manuscript in preparation for publication)	
Chapter 4	Heterozygous knockout of Euchromatin histone methyltransferase-1 increases pattern separation ability and hippocampal cell proliferation	85
	Published in: <i>Scientific Reports</i> , 10;7:40284. doi: 10.1038/srep40284	
Chapter 5	General Discussion	105
Appendix	Summary	117
	List of abbreviations	119
	References	123
	List of publications	129
	Acknowledgements (Dankwoord)	131

*...to all the Kleefstra families, who I had the gift to meet in Coventry (UK),
in August 2013. I dedicate them the findings described in this thesis.*

... a Giuseppe, Silvana, Alessandro e Sandra.

¹Department of Cognitive Neuroscience, Radboudumc, 6500 HB Nijmegen, The Netherlands; Donders Institute for Brain, Cognition, and Behaviour, Centre for Neuroscience, 6525 AJ Nijmegen, The Netherlands.

²Department of Cognitive Neuroscience, Radboudumc, 6500 HB Nijmegen, The Netherlands; Department of Human Genetics, Radboudumc, 6500 HB Nijmegen, The Netherlands; Donders Institute for Brain, Cognition, and Behaviour, Centre for Neuroscience, 6525 AJ Nijmegen, The Netherlands.

³Department of Cognitive Neuroscience, Radboudumc, 6500 HB Nijmegen, The Netherlands; Department of Human Genetics, Radboudumc, 6500 HB Nijmegen, The Netherlands; Donders Institute for Brain, Cognition, and Behaviour, Centre for Neuroscience, 6525 AJ Nijmegen, The Netherlands. Electronic address: n.nadif@donders.ru.nl

Neurobiology of learning and memory. 2015;124:88-96.

doi: 10.1016/j.nlm.2015.06.013

one

GENERAL INTRODUCTION

Part of this chapter has been published as a review

Marco Benevento¹, Marise van de Molengraft¹, Rhode van Westen¹,
Hans van Bokhoven², Nael Nadif Kasri³

The word “epigenetic” is derived from the ancient Greek prefix “ἐπι” (epi-), which means “on top of”, and the Greek word “γένος” (genos), which means “gene” or “race”. The term epigenetics generally refers to a set of heterogeneous cellular mechanisms that finely control gene expression at multiple levels. At the biochemical level, these mechanisms include DNA methylation of cytosine residues and post-translational modifications (PTMs) of histones. All modifications share the same characteristic; they have the capacity to reversibly modulate transcriptional activity while leaving the DNA sequence itself unaffected. This enables dynamic gene transcription patterns in the nucleus in response to environmental or developmental stimuli.

Chromatin is a structure that consists of DNA and histones, whose function is to package DNA into a smaller volume within the nucleus and to control gene expression. Depending on the condensation state, chromatin can be distinguished into euchromatin and heterochromatin. Euchromatin is the decondensed form, which is associated with genomic regions that are transcriptionally permissive, whereas heterochromatin is compacted and can exist in two forms; i) facultative, which is actively involved in gene expression and ii) constitutive, which is obligatorily silenced. The histone protein is the core structure of the nucleosome. Each nucleosome consists of 147-164 base pairs of DNA wrapped around an octamer of histone proteins, which includes two copies of histone H2A, H2B, H3 and H4 each (reviewed by Felsenfeld and Groudine, 2003). Of these proteins, histone 3 (H3) is the most extensively studied. Histone tails protrude from the nucleosome to areas that are typically accessible for the chemical modifications, such as acetylation, methylation, phosphorylation, and others (Figure 1.1) (Cedar and Bergman, 2009; Rose and Klose, 2014; Rothbart and Strahl, 2014).

These modifications are installed by *writer enzymes*, such as histone acetyltransferases (HATs) and histone methyltransferases (HMTs); removed by *eraser enzymes*, such as histone deacetylases (HDACs) and histone demethylases (HDMs); and interpreted by *reader enzymes*, proteins that bind specific chromatin marks or are found in transcription repressor and activator complexes that regulate DNA accessibility by the basic transcription machinery (Kleefstra et al., 2014; Ronan et al., 2013). Writer, eraser and reader enzymes specifically target one or a few modifications. For example, the writer enzyme Euchromatic histone methyltransferase-1 (EHMT1) catalyses histone 3 lysine 9 (H3K9) mono- and dimethylation, but not trimethylation

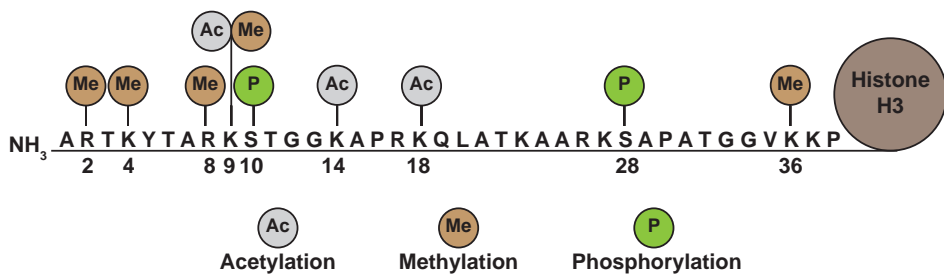


Figure 1.1. Model figure depicting histone post-translational modifications (PTMs) and residues modified in histone H3.

(Figure 1.2) (Tachibana et al., 2005). The combinatorial nature of histone PTMs impact on gene expression has been postulated to generate a histone code which cells use as “epigenetic memory” of previous transcriptional states, yet this model is still under debate (Comoglio and Paro, 2014; de Pretis and Pelizzola, 2014; Lesne et al., 2015; Rando, 2012).

Recently, numerous studies have implicated dynamic changes in DNA methylation and histone PTMs in the formation or consolidation of long-term memories in specific memory-related brain regions. In addition, pathways up and downstream of the chromatin modifying enzymes were found to be part of the signaling pathways governing synaptic plasticity and long-term behavioral memory (Fonseca, 2016; Sweatt, 2016; Day and Sweatt, 2011b; 2011a; Kramer, 2013; Levenson and Sweatt, 2005; Lipsky, 2013). Consequently, disturbances in epigenetic states can impede plasticity and underlie cognitive disorders (Benevento et al., 2016; Barco, 2014; Kleefstra et al., 2014; Schaefer et al., 2011). Most of the studies on epigenetics in cognition have focused on DNA methylation and histone H3 (de)-acetylation and have been summarized in recent reviews (Gräff and Mansuy, 2008; Gräff et al., 2012b; Miller et al., 2010; Penney and Tsai, 2014; Zovkic et al., 2013). While DNA methylation is generally considered to inhibit gene transcription and histone acetylation is considered to be activating, histone methylation can achieve both gene activation and repression.

Histone methylation initially received less attention, because it was long assumed to be rigid and therefore of little interest to dynamic processes involved in cognition, such as learning and memory. Because the half-life of histone methylation is as long as the histone protein itself [reviewed by (Bannister et al., 2002), demethylation was thought to happen only passively through cell division. However the discovery of an ‘eraser’ enzyme that removes histone methylation, histone demethylase LSD1 (Shi et al., 2004), suggested that histone methylation could also be dynamically regulated. In general, the outcome of histone methylation depends on (a) the type of amino acid being modified, arginine (R) or lysine (K); (b) the extent of methylation (mono-, di- or trimethylation), and (c) the location of the modified residue on the histone tail (Figure 1.1). In particular, histone H3 methylation has been shown to modulate enduring changes in gene expression to regulate memory formation and neural plasticity (Sharma et al., 2016; Fischer et al., 2007; Gräff and Mansuy, 2008; Gupta et al., 2010; Gupta-Agarwal et al., 2012; 2014; Lubin et al., 2011; Parkel et al., 2013).

THE REPRESSIVE COMPLEX EHMT1/EHMT2

Dimethylation of lysine 9 of Histone H3 (H3K9me2) is a PTM typically present in both euchromatin and heterochromatin at the promoters of silenced genes. H3K9me2 in euchromatic regions is catalysed by the heterodimerization of EHMT1 (KMT1D or GLP) with EHMT2 (KMT1C or G9a) (Figure 1.2) (Tachibana et al., 2002). Indeed chemical inhibitors or genetic manipulations of either EHMT1 or EHMT2 has shown (*in vivo* and *in vitro*) to reduce H3K9me2 levels via specific EHMT1/EHMT2 inhibition of methyltransferase activity (Del Rio and Varchi, 2016; Qing and Wang, 2016; Chang et al., 2009; Kubicek et al., 2007; Vedadi et al., 2011). Biologically, the EHMT1/EHMT2 repressive complex is important for governing transcriptional

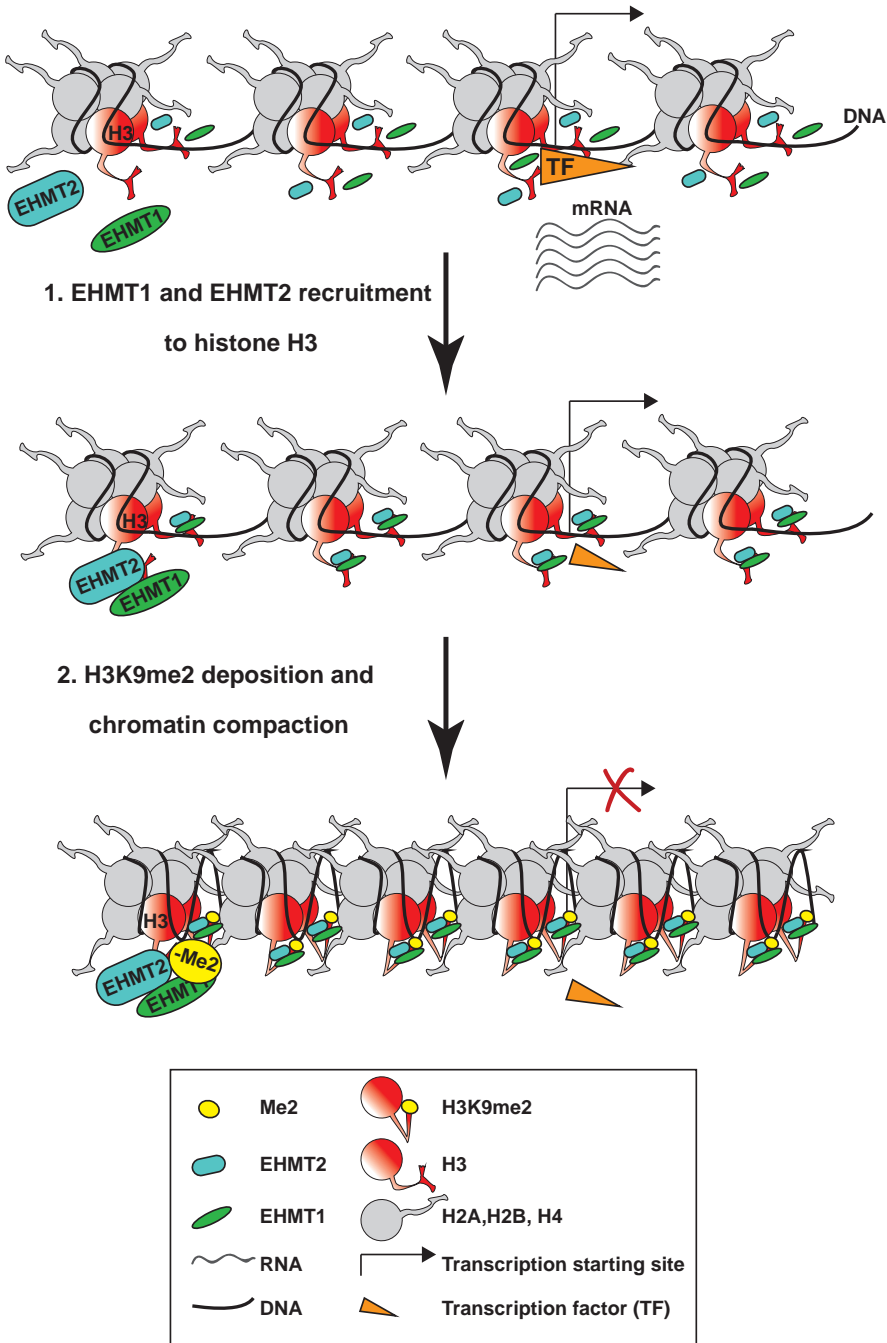


Figure 1.2. Model depicting EHMT1/EHMT2 mediated mechanism of nucleosomal compaction when EHMT1 (green stretched oval) and EHMT2 (light blue rounded rectangle) associate to a certain given stimulus. Nucleosomal compaction as showed in the figure represses gene transcription (red cross) by impeding transcription factors (orange triangle) binding to the promoter. Figure legend in the black-lined box.

output during development and cell differentiation (Tachibana et al., 2002, 2005; Fiszbein et al., 2016; Zhang et al., 2016; Cougot et al., 2016). This is best reflected by the fact that both, *Ehmt1*^{-/-} and *Ehmt2*^{-/-} mice, show severe developmental delays and early embryonic lethality (Tachibana et al., 2008). At the level of gene regulation it has been suggested that the EHMT1/EHMT2 complex prevents the re-expression of time locked developmental genes by interacting with Polycomb and REST/NSRF repressor complexes (Mozzetta et al., 2014; Roopra et al., 2004). In terms of cellular maturation, the EHMT1/EHMT2 repressor complex is required for the commitment of human hematopoietic stem cells and brown adipose cells (Chen et al., 2012; Schones et al., 2014). Specifically in the nervous system, loss of EHMT2 function led to increased cell proliferation and disorganized layering in the retina (Katoh et al., 2012), and also resulted in a switch of neuronal subtypes, from dopamine receptor D2 expressing (Drd2) neurons to Drd1 neurons in the mouse nucleus *Accumbens* (nAc) (Maze et al., 2014). Finally, EHMT1 and EHMT2 govern the heterochromatic silencing of olfactory receptor genes, which is essential for the diversification of olfactory neurons (Lyons et al., 2014). Overall these studies identified EHMT1 and EHMT2 as a crucial repressive complex during development and neuronal cell differentiation.

H3K9 METHYLATION IN LEARNING AND MEMORY

In recent years, numerous studies have provided evidence that changes in histone lysine methylation, leading to gene expression activation or repression, are also required for the formation and consolidation of long-term memory (LTM) in particular brain regions. Specifically, the expression of H3K4me3 and H3K9me2 marks were found to be transiently and dynamically regulated in rat CA1 hippocampus, entorhinal cortex (EC) and lateral amygdala (LA) following contextual fear-conditioning, a form of learning in which an aversive stimulus (e.g. an electrical shock) is associated with a particular neutral context (Gupta et al., 2010; Gupta-Agarwal et al., 2012; 2014). H3K9me2 levels together with H3K4me3, an active mark for transcription (Akbarian and Huang, 2009; Schneider et al., 2004), are transiently increased in CA1 hippocampal neurons one hour after training rats in the contextual fear-conditioning paradigm, returning to baseline (H3K4me2) or even decreasing to levels below baseline (H3K9me2) twenty-four hours after training (Gupta et al., 2010). Of note, the novel context exposure alone was sufficient to trigger an increase in H3K9me2, but not H3K4me3, levels in CA1. Mice deficient in the H3K4-specific histone methyltransferase, *Mll*, displayed deficits in contextual fear conditioning, suggesting that H3K4 methylation is required for proper long-term consolidation of contextual fear memories (Gupta et al., 2010). Interestingly, methylation dynamics of H3K9me2 and H3K4me3 were found to be different in the EC and LA (Gupta-Agarwal et al., 2012; 2014). While the levels of both H3K9me2 and H3K4me3 increased in the EC one hour after contextual fear conditioning training, H3K9me2 protein levels were unaltered and H3K4me3 levels were reduced in the EC twenty-four hours after training compared to naïve animals (Gupta-Agarwal et al., 2012). In the LA, H3K9me2 levels were increased one hour following auditory fear conditioning and this increase persisted until

twenty-five hours following behavioral training. In contrast, H3K4me3 remained unchanged in the LA following training (Gupta-Agarwal et al., 2014). The differences observed in histone methylation dynamics in contextual and auditory fear conditioning hint towards a specific role for the respective marks during memory formation and/or consolidation. Indeed, infusing a EHMT2 inhibitor, BIX-01924, in the CA1 impaired contextual fear memory twenty-four hours after training, whereas contextual fear memory was increased when BIX-01924 was delivered to the EC (Gupta et al., 2010; Gupta-Agarwal et al., 2012). Moreover, EHMT2 inhibition in the EC had an effect on the contextual association as BIX-01924-infused rats displayed elevated freezing behavior twenty-four hours and seven days after training, compared to vehicle treated animals (Gupta-Agarwal et al., 2012). Inhibition of EHMT2 using the selective EHMT2 inhibitor UNCO224 (Liu et al., 2009) in the LA also impaired fear memory, whereas inhibiting a H3K9me2 demethylase LSD1, with *trans*-2-phenylcyclopropylamine (t-PCP) (Benelkebir et al., 2011; Binda et al., 2010), enhanced fear memory. Collectively these data indicate that bidirectional regulation of H3K9me2 in the LA is a regulator of fear memory. The differences observed between the various brain regions suggest that methylation marks, in particular H3K9me2, could act as a molecular hub that underlies cellular connectivity between EC, CA1 and LA. Interestingly, the changes in methylation seen after behavioral training were very often accompanied with a change in the expression of the respective enzymes mediating the methylation (e.g. EHMT2 or EHMT1), indicating that transcriptional regulation of EHMT1/EHMT2 often precedes the changes in methylation.

The importance of EHMT2 and EHMT1 in fear memory formation and consolidation has similarly been demonstrated using conditional knockout mice in which either EHMT1 or EHMT2 was removed in *CamK2a* expressing neurons, in the postnatal forebrain. Specifically, memory formation was impaired in *Ehmt1^{fl/fl} CamK2a-Cre* mice twenty-four hours after training in the contextual fear conditioning paradigm (Schaefer et al., 2009). Moreover, conditional knockdown of *Ehmt1/Ehmt2* showed decreased explorative behavior, reduced sucrose preference and less anxiety-related behavior in the elevated plus maze. Interestingly, these phenotypes partially overlapped with phenotypes observed in mice with haploinsufficiency in *Ehmt1* (*Ehmt1^{+/-}*), a mouse model for Kleefstra syndrome (KS) (Balemans et al., 2010; 2013). KS is caused, amongst others, by the heterozygous loss of EHMT1/GLP (Willemsen et al., 2012). The syndrome is characterized by intellectual disability, general developmental delay, childhood hypotonia, cranio-facial abnormalities and autistic-like behavioral problems (Kleefstra et al., 2009; 2006; Nillesen et al., 2011; Willemsen et al., 2012). In contrast to the *Ehmt1^{fl/fl} CamK2a-Cre* mice, *Ehmt1^{+/-}* mice showed increased fear memory during acquisition and retention twenty-four hours after contextual fear conditioning training, but impaired fear memory extinction when the mice were re-exposed for five consecutive days after tone-stimuli association (Balemans et al., 2013). Furthermore *Ehmt1^{+/-}* mice displayed typical autistic features such as reduced exploration, increased anxiety, altered social interaction (Balemans et al., 2010) and craniofacial abnormalities (Balemans et al., 2014).

Finally, a critical role for EHMT1/EHMT2 function in LTM was also found in *Drosophila*, in which the *Drosophila* orthologue EHMT was mutated (*EHMT^{DD}*). Behavioral analyses identified

EHMT as a regulator of peripheral dendrite development, larval locomotor behavior, non-associative learning, and courtship memory. The requirement for EHMT in memory was mapped to predominantly mushroom body neurons, the learning and memory centre in *Drosophila*. Interestingly, memory was restored by EHMT re-expression during adulthood, indicating that cognitive defects are reversible in EHMT mutants (Kramer et al., 2011).

From a cellular perspective *Ehmt1*^{+/-} mice and *Drosophila* (*EHMT^{DD}*) showed altered neuronal architecture (Balemans et al., 2013; Kramer et al., 2011). Morphological analysis by reconstructing hippocampal CA1 pyramidal neurons revealed a reduction in complexity and in the total length and branches of CA1 apical dendrites. A similar dendritic phenotype was observed in *Drosophila* type 4 multiple dendrites neurons (Kramer et al., 2011). *Ehmt1*^{+/-} mice also showed a reduction in spine density in CA1 pyramidal neurons, in particular stubby and mushroom types were decreased in *Ehmt1*^{+/-} mice compared to wildtype (Balemans et al., 2013). However, postnatal deletion of either *Ehmt1* or *Ehmt2* did not affect neuronal architecture of CA1 nor Drd1 neurons (Schaefer et al., 2009), indicating that the repressive EHMT1/EHMT2 complex might play a specific role during early development.

Long-term potentiation (LTP) is considered to be the cellular mechanism for long-term memory formation (Kessels and Malinow, 2009; Makino and Malinow, 2009; Malenka and Malinow, 2011; Malinow and Malenka, 2002). The requirement of EHMT1/EHMT2 for memory formation is also reflected at the synaptic level. Blockage of EHMT2 by bath application of BIX-01294 impeded long lasting-LTP (L-LTP) induction at the Schaffer collateral SC-CA1 synapses, but not in the temporoammonic pathway (TA-CA1) (Gupta-Agarwal et al., 2012), nor was LTP altered at the CA1-CA3 synapse in the *Ehmt1*^{+/-} mice. However, inhibition of EHMT2/EHMT1 complex during protein synthesis-independent LTP (early LTP) reinforces both early-LTP and synaptic tagging and capture in the hippocampal CA1, through increases in Brain Derived Neurotrophic Factor (BDNF) levels (Sharma et al., 2016). At the basal level however, paired-pulse facilitation (PPF) was increased in *Ehmt1*^{+/-} mice, indicative for a pre-synaptic deficit associated with reduced release probability (Balemans et al., 2013). Furthermore, whole-cell patch clamping revealed that miniature excitatory postsynaptic currents frequencies, but not amplitudes, were significantly reduced in *Ehmt1*^{+/-} CA1 pyramidal neurons, correlating with the reduction observed in PPF and decrease in mature spine density (Balemans et al., 2013).

The differences observed at the level of structure, physiology and behavior between the animal models - heterozygous versus conditional and pharmacological models - reveal a complex scenario, but all point towards a spatio-temporal specific requirement for the EHMT1/EHMT2 repressor complex in regulating neural connectivity and the formation or consolidation of long-term memories in the hippocampus (Table 1.1). Although perturbations of H3K9me2 clearly alter many aspects of neuronal function, given the many homeostatic feedback pathways that influence neural circuit and brain development, it is unclear which perturbations are directly causal and which are induced secondarily as a consequence of altered brain function.

Although the role of the repressive complex EHMT2/EHMT1 in fear memory has been established, still very little is known regarding the downstream target genes being repressed

Table 1.1. Summary comparative table of the major behavioral and functional findings from three different studies using different means to manipulate EHMT2/EHMT1 function .

	<i>Ehmt1</i> ^{+/-} mouse (Bailemans et al., 2010, 2012)	<i>Ehmt1</i> ^{2-/-fl;CamK2a-Cre} (Schaeffer et al., 2009)	EHMT1/2 inhibition (Gupta et al., 2012)	
			CA1 infusion	EC infusion
Exploration	decreased	decreased	non-tested	non-tested
Social interaction	decreased	non-tested	non-tested	non-tested
Anxiety	enhanced	decreased	non-tested	non-tested
Fear memory (cued-CFC)	enhanced	decreased	decreased	enhanced
Fear extinction (cued-CFC)	no extinction	non-tested	non-tested	enhanced
Dendritic branching	decreased	no difference	non-tested	non-tested
Dendritic spine density	decreased	no difference	non-tested	non-tested
Basal e-phys properties	no difference	no difference	non-tested	non-tested
LTP-induction	no difference	non-tested	decreased	no difference
Presynaptic plasticity	enhanced	non-tested	enhanced	non-tested

by this complex. Equally little is known regarding the upstream activation pathways. A possible mechanism that controls the activity-dependent regulation of EHMT2, has recently been proposed (Gupta-Agarwal et al., 2014), in which the NMDA receptor subunit GluN2B via ERK activation was shown to differentially recruit EHMT2 and LSD1 to the target gene promoters in the LA via ERK activation. Interestingly, fear memory deficits associated with NMDAR or ERK blockage could be rescued by the inhibition of LSD1, suggesting that H3K9me2 enhancement within the LA is downstream of NMDAR and ERK activation (Gupta-Agarwal et al., 2014). In this context it also of interest to note that the developmental NMDAR subunit switch from GluN2B to GluN2A, which is critical for learning and memory (Sheng et al., 1994; Williams et al., 1993; Yashiro and Philpot, 2008), at least in part involves the regulation of H3K9me2 levels (Rodenas-Ruano et al., 2012). NMDA receptor mediated Ca²⁺ influx is known to result in signal transduction that induces *de novo* gene expression underlying LTP (Zhao et al., 2005). The GluN2B-to-GluN2A switch is required for learning and memory, as GluN2B restricts AMPA receptor incorporation into the synapse (Hall et al., 2007), lowers the LTP threshold, increases the LTP magnitude (Yashiro and Philpot, 2008), and promotes spine growth and dendrite patterning (Espinosa et al., 2009; Lee et al., 2010; Ultanir et al., 2007). During the developmental GluN2B-to-GluN2A switch, chromatin immunoprecipitation (ChIP) experiments showed that REST/NRSF, EHMT2 and H3K9me3 were enriched at the *Grin2b* promoter in postnatal day 15 (P15) mice, time points which coincided with a reduction in LTP induction (Gray et al., 2011; Rodenas-Ruano et al., 2012). Since the H3K9me3 mark is transient, the long-lasting repression of GluN2B is more likely mediated by additional mechanisms, such as the persistent change in H3K27me3 at P15. Interestingly, a recent study linked EHMT1/EHMT2 to the PRC2 repressor complex indicative of a H3K9me2, H3K9me3 crosstalk with H3K27me3 in order to repress genes during neuronal development (Mozzetta et al., 2014). However, at P60 the levels of H3K9me3 at

the *Grin2b* promoter decreased, while the H3K27me3 stayed elevated. This could point towards a mechanism in which long-term gene repression is initiated by crosstalk between H3K9me2-3 and H3K27me3 and is further maintained by different effectors.

It is clear that chromatin remodeling mediated gene regulation is a finely tuned and complex process, which requires the integration of different converging pathways onto histone modifying enzymes and DNA methyltransferases. The further understanding of the “code” and crosstalk between the histone PTMs and DNA-methylation will be extremely helpful to comprehend mechanisms of activity-driven gene expression.

INTERFERENCE OF HISTONE METHYLATION AND ADDICTION

Chronic consumption of “recreational” drugs, such as cocaine can lead to devastating psychiatric effects, which are caused by long-lasting changes in the brain’s dopaminergic reward system. One well-characterized reward brain-system affected by cocaine intake is the Ventral-Tegmental Area (VTA) and nAc axis. The VTA projects dopaminergic afferents to the nAc. Cocaine acts as a dopamine reuptake inhibitor (Rothman, 1990) increasing neuronal activity in the nAc. In recent years, numerous studies have untangled how cocaine-induced chromatin remodelling, at specific loci, affects gene expression, physiology and behavior. Repeated cocaine administration increased *FosB/DFosB* mRNA levels and H3K9/14-acetylation at the *FosB* promoter in mice (Heller et al., 2014; Maze et al., 2010). In contrast, cocaine treatment decreased global H3K9me2 levels, and specifically reduced mRNA levels of both, *Ehmt1* and *Ehmt2* compared to other histone lysine methyltransferases twenty-four hours after the last cocaine presentation in the mouse nAc (Maze et al., 2010). At the behavioral level, knockdown of EHMT2 by locally (Ac) injecting an AAV-Cre in *Ehmt2*^{fl/fl} mice significantly increased the effects of cocaine in the conditioning place preference (CPP) paradigm. In contrast, CPP memory for cocaine exposure was decreased when EHMT2 was over-expressed in the nAc (Maze et al. 2010). These findings directly linked H3K9me2 to the expression of synaptic plasticity observed upon addictive behavior. Neuronal architecture was also affected by cocaine exposure. Local EHMT2 overexpression or EHMT2 knockdown in the nAc respectively, blocked or enhanced the increase in spine density on neurons from the nAc in mice that were chronically exposed to cocaine (Maze et al., 2010), whereas EHMT2 manipulation alone did not affect spine density, gene expression or behavior. In terms of gene regulation cocaine causes an increase in glutamatergic drive onto nAc (Ungless et al., 2001) and enhances the expression of target genes implicated in cocaine-induced plasticity (Graham et al., 2007; Russo et al., 2009). Using microarrays the authors found two interesting aspects; a) repeated cocaine exposure led to enhanced gene expression compared to animals that were acutely treated with cocaine and b) overexpression of EHMT2 (HSV-EHMT2) in the nAc was sufficient to block the cocaine-dependent increase in gene expression (Maze et al., 2010). Amongst others, *FosB* and *Bdnf* expression were increased by chronic cocaine consumption (Nestler, 2014b; 2014a). EHMT2 and H3K9me2 enrichment

in *FosB*/ Δ *FosB* and *Bdnf* IV promoters was reduced when animals were chronically treated with cocaine (Maze et al., 2010). Interestingly, chronic HDAC1 inhibition by implanting mini-osmotic pumps delivering HDAC inhibitor MS-275 (Kennedy et al., 2013) attenuated cocaine-related increase in locomotor sensitivity. Simultaneously, it induced an increase in *Ehmt2* mRNA and global H3K9me2 expression in the nAc, thus counteracting the cocaine-induced decrease in H3K9me2. This indicated that EHMT2 serves as a mediator for the inhibition of addictive behavior observed after HDAC inhibition. At a functional level, repeated cocaine consumption has been shown to cause an increase in frequency of GABA_A receptor-mediated miniature inhibitory postsynaptic currents (mIPSCs) in striatonigral medium spiny neurons in mice (Dixon et al., 2010). Reinstating EHMT2 expression through MS-275 HDAC1 inhibition suppressed the cocaine-dependent expression of GABA-receptor genes *Gabra1*, *Gabra3* and *Gabrb2*, while it blocked the cocaine-dependent increase in mIPSCs frequency (Kennedy et al., 2013). This study further highlighted the possibility that EHMT2-mediated chromatin remodeling through H3K9me2 could serve as a therapeutic target and venue to counteract drug-dependent psychiatric effects through gene repression. Indeed, site specific targeting of a specific locus within the *FosB*/ Δ *FosB* promoter by using zinc finger-proteins (ZFPs) fused with EHMT2 C-terminal or using transcription activator like effectors (TALEs) have recently shown to be sufficient to counteract cocaine-induced plasticity (Heller et al., 2014).

Interestingly, the dynamic response of H3K9me2 is not only restricted to cocaine addiction since similar epigenetic responses have been observed upon ethanol exposure. Qiang and colleagues (Qiang et al., 2011) showed that chronic intermittent ethanol withdrawal in primary cortical neurons lead to a global and local decrease in H3K9 di- and trimethylation at the *Grin2b* gene promotor. Ethanol exposure reduced the global expression levels of the HMTs *Ehmt2*, *Suv39h1* and *Setdb1*, but not the activity of HATs or HDACs. Moreover, EHMT2-mediated H3K9me2 was shown to critically regulate ethanol-induced neurodegeneration and associated loss of cognition in rodents (Subbanna and Basavarajappa, 2014; Subbanna et al., 2013). Consequently, inhibiting EHMT2 before ethanol exposure at P7 prevented ethanol-induced deficits in LTP, memory and social cognition (Subbanna et al., 2014). Similarly, nicotine exposure induced chromatin remodeling by decreasing H3K9me2 protein levels and *Ehmt1*/*Ehmt2* mRNA levels in mouse cortical extracts both *in vitro* and *in vivo* (Chase and Sharma, 2013). Chromatin immunoprecipitation (ChIP) analysis further showed that nicotine caused a decrease in H3K9me2 enrichment at *Bdnf* I, IV and IXa promoters thereby inducing an increase in *Bdnf* mRNA transcription. These results indicate that EHMT2-mediated chromatin remodeling is involved in different types of substance-dependence. Hence, the underlying mechanisms might serve as a potential drug target and deserves further attention.

EHMT1/EHMT2 IN COGNITIVE DISORDERS

Defects in epigenetic mechanisms may contribute to the development of several cognitive disorders. Many of these disorders involve, among others, memory impairment, learning deficits and neurodevelopmental delays (van Bokhoven, 2011; Barco, 2014; Kelly et al., 2010;

Kleefstra et al., 2014; Peña et al., 2014; Portela and Esteller, 2010). Intellectual disability (ID) is a common neurodevelopmental disorder arising before the age of 18 that affects approximately 1–3% of the population. ID is defined by an intelligence quotient (IQ) lower than 70, associated with deficits in conceptual, social and adaptive skills. KS is an example of an emerging number of ID disorders caused by genes encoding epigenetic regulators of neuronal gene activity (Kleefstra et al., 2014). KS, previously known as the 9q subtelomeric deletion syndrome (9qSTDs) is caused by haploinsufficiency of the *EHMT1* gene. Heterozygous (or de novo) intragenic mutations and 9q34 microdeletions encompassing the entire gene can both be responsible for this syndrome which is characterized by ID, hypotonia, and typical dysmorphisms, and may be associated with congenital heart and/or renal defects and epilepsy (Kleefstra et al., 2006; Willemsen et al., 2012). Behavioral phenotypes include sleep disturbances and apathy. The effects of the mutation in the *EHMT1* gene on a molecular, cellular and behavioral level have been extensively investigated in *Drosophila* and mouse models (Balemans et al., 2010; 2013; 2014; Kramer et al., 2011; Parkel et al., 2013; Schaefer et al., 2009). Decreased levels of H3K9me2, the most studied marker for *EHMT1* activity so far, have been found in particular in the hippocampus and other brain regions of heterozygous *Ehmt1* knockout mice (*Ehmt1*^{-/-}), and were shown to lead to deviant neuronal morphology as well as aberrant dendritic spine formation, indicating alterations in plasticity in the brain. Additionally, a number of other epigenetic regulators have been found to play a role in the development of KS phenotypic spectrum (KSS). Kleefstra and colleagues (Kleefstra et al., 2012) described four genes which were found to be defective in KSS patients: *MBD5*, *MLL3*, *SMARCB1* and *NR1H3*. Of these, *MBD5*, *MLL3* and *NR1H3* genetically interacted with *EHMT1*, and *SMARCB1* influenced *EHMT1* through its interaction with *MLL3*. *EHMT1* is thus part of a larger epigenetic module underlying human cognitive disorders.

EHMT1/EHMT2 IN NEURODEGENERATION

Disorders such as Alzheimer's, Parkinson's, and Huntington's disease have been linked to age-related cognitive decline. This predominantly affects declarative, episodic and working memory, which is associated with decreased neuronal plasticity. The epigenetic (dys) regulation underlying aging is related to a loss of open chromatin, mediated by reduced histone acetylation and by an increase in DNA methylation (Akbarian et al., 2013) and repressive histone methylations (Fischer, 2014; Gräff et al., 2012a; Traynor and Renton, 2015; Wood et al., 2010). For example, histone methylation involves defects in axon myelination and white matter lesions which are found both in aging and in neurodegenerative diseases and, recently described, in KS patients (He et al., 2016; Yankner et al., 2008). Although, the involvement of histone methylation in aging has been proposed it remains unanswered to what extent histone methylation contributes to the progression of age related cognitive decline and associated changes in dendritic branching, spine density or LTP threshold, nor is it understood whether preventing the activity of histone methyltransferases will restore the loss of memory functions associated with aging. Specifically, in mouse models H3K9

methylation was found to increase with age, which was amplified further in an Alzheimer mouse model (3xTg-AD) (Walker et al., 2013). Recently a widespread loss of heterochromatin in tau-induced neurodegenerative *Drosophila* and mouse models, and in human AD have also been observed (Frost et al., 2014). In particular, a reduction of H3K9me2 was observed in these neurodegenerative models, linking decreased H3K9me2 to neurodegeneration. As a result, large-scale analyses from human AD brains revealed a widespread transcriptional increase in genes that are silenced in controls.

Further evidence for histone methylation in cognitive decline is found in Huntington's disease, a neurodegenerative disorder associated with gene expression changes early in the disease course (Borovecki et al., 2005; Sugars and Rubinsztein, 2003). It has been shown that H3K9me2 is increased in both patients and mouse models (Gardian et al., 2005; Ryu et al., 2006), and that acetylation is decreased. Interestingly, the application of HDAC inhibitors caused an arrest in neurodegeneration and lowered the level of H3K9me2. The resulting opening of chromatin leads to increased expression of glutathione S-transferase, striatin calmodulin-binding protein 3, ubiquitin-specific protease 29, proteasome subunit α type 3 and the proteasome 26 S subunit (ATPase 3), but it decreased expression of apoptotic genes, such as caspase 9, caspase 8/FADD-like apoptosis regulator, and proteasome 26 S subunit (non-ATPase 10) (Gardian et al., 2005). This suggests that HDAC inhibitors work through histone acetylation and H3K9me2 to selectively modulate gene expression critical for neuronal survival and neuroprotection.

Interestingly, there is some evidence that a neurodegenerative process might also be involved in the pathophysiology of KS. A 'regressive' phenotype has been observed in KS patients, which was associated with the *GLP/EHMT1* gene. In particular, these patients showed signs of progressive apathy and showed multifocal subcortical signal abnormalities in MRI studies (Verhoeven et al., 2011). Thus, life-long decreased H3K9me2 levels, as in the case in KS, could potentially lead to neurodegeneration at later stages in life. Longitudinal studies following KS patients will reveal whether this pathophysiology will be more widespread amongst KS patients. Studies using KS animal models have however, to date, not reported any neurodegenerative phenotype.

THESIS AIM AND OUTLINE

The study of the contribution of epigenetic factors in controlling the expression of genetic programs related to cognition and development in response to environmental changes is a novel and fascinating neurobiological frontier. The aim of this thesis is to advance the knowledge of the epigenetic mechanisms that regulate dynamic changes of neuronal synaptic properties and in neurodevelopmental mechanisms related to cognition. The findings highlighted in this manuscript relate to the contribution of the epigenetic factor Euchromatic Histone Methyltransferase 1 (EHMT1) in regulating synaptic properties, cognition and neuronal development.

In **chapter 2**, I describe the requirement of EHMT1 for a specific form of non-hebbian synaptic plasticity, i.e. homeostatic plasticity. In this section, I describe how EHMT1 through histone methylation controls synaptic scaling in response to chronic changes in neuronal network activity.

In **chapter 3**, I validate the results obtained in Chapter 2 in a human cellular model for KS. To this end I optimized a method to reliably produce excitatory neurons from hiPSCs derived from control volunteers and Kleefstra syndrome patients haploinsufficient for *EHMT1*.

In **chapter 4**, I highlight the contribution of EHMT1 to cognition and adult hippocampal neurogenesis. In this chapter, I show that a mouse model for KS, haploinsufficient for *Ehmt1* displays an improved pattern separation and increased proliferation of neuronal stem cells in the adult dentate gyrus.

Finally, in **chapter 5** I summarize and discuss the main findings of this thesis.

¹Department of Cognitive Neuroscience, Radboudumc, 6500 HB Nijmegen, the Netherlands; Donders Institute for Brain, Cognition, and Behaviour, Centre for Neuroscience, 6525 AJ Nijmegen, the Netherlands.

²Department of Molecular Biology, Faculty of Science, Radboud University, 6500 HB Nijmegen, the Netherlands.

³Department of Human Genetics, Radboudumc, 6500 HB Nijmegen, the Netherlands; Donders Institute for Brain, Cognition, and Behaviour, Centre for Neuroscience, 6525 AJ Nijmegen, the Netherlands.

⁴Department of Human Genetics, Radboudumc, 6500 HB Nijmegen, the Netherlands; Department of Molecular Developmental Biology, Faculty of Science, Radboud University, 6500 HB Nijmegen, the Netherlands.

⁵Department of Cognitive Neuroscience, Radboudumc, 6500 HB Nijmegen, the Netherlands; Department of Human Genetics, Radboudumc, 6500 HB Nijmegen, the Netherlands; Donders Institute for Brain, Cognition, and Behaviour, Centre for Neuroscience, 6525 AJ Nijmegen, the Netherlands.

⁶Department of Cognitive Neuroscience, Radboudumc, 6500 HB Nijmegen, the Netherlands; Department of Human Genetics, Radboudumc, 6500 HB Nijmegen, the Netherlands; Donders Institute for Brain, Cognition, and Behaviour, Centre for Neuroscience, 6525 AJ Nijmegen, the Netherlands. Electronic address: n.nadif@donders.ru.nl.

Neuron. 2016 Jul 20;91(2):341-55.

Doi: 10.1016/j.neuron.2016/06/003

two

HISTONE METHYLATION BY THE KLEEFSTRA SYNDROME PROTEIN EHMT1 MEDIATES HOMEOSTATIC SYNAPTIC SCALING

Marco Benevento¹, Giovanni Iacono², Martijn Selten¹, Wei Ba¹, Astrid Oudakker¹,
Monica Frega¹, Jason Keller¹, Roberta Mancini¹, Elly Lewerissa¹, Tjitske Kleefstra³,
Hendirk G. Stunnenberg², Huiqing Zhou⁴, Hans van Bokhoven⁵, Nael Nadif Kasri⁶

ABSTRACT

Homeostatic plasticity, a form of synaptic plasticity, maintains the fine balance between overall excitation and inhibition in developing and mature neuronal networks. Although the synaptic mechanisms of homeostatic plasticity are well characterized, the associated transcriptional program remains poorly understood. We show that the Kleeftstra syndrome-associated protein EHMT1 plays a critical and cell-autonomous role in synaptic scaling by responding to attenuated neuronal firing or sensory drive. Chronic activity deprivation increased the amount of neuronal dimethylated H3 at lysine 9 (H3K9me2), the catalytic product of EHMT1 and an epigenetic marker for gene repression. Genetic knockdown and pharmacological blockade of EHMT1 or EHMT2 prevented the increase of H3K9me2 and synaptic scaling up. Furthermore, BDNF repression was preceded by EHMT1/2-mediated H3K9me2 deposition at the *Bdnf* promoter during synaptic scaling up, both *in vitro* and *in vivo*. Our findings suggest that H3K9me2-mediated changes in chromatin structure govern a repressive program that controls synaptic scaling.

INTRODUCTION

Experience-dependent neuronal activity is crucial for promoting long-lasting modifications at functional synapses during development and in adulthood. To preserve neural network stability, a mechanism exists that maintains firing rates within a physiological range of activity. Neurons can continuously adapt their firing rates through synaptic and intrinsic cellular mechanisms, a process generally referred to as homeostatic plasticity (Turrigiano and Nelson, 2004; Turrigiano, 2012). Disrupted homeostatic plasticity appears in several neurodevelopmental disorders, including Fragile X syndrome, Rett syndrome and Tuberous Sclerosis, suggesting that improper circuit refinement during development contributes to cognitive impairment (Cortés-Mendoza et al., 2013; Soden and Chen, 2010; Zhong et al., 2012).

Synaptic scaling, a well-characterized form of homeostatic plasticity, stabilizes neuronal network activity by balancing excitation and inhibition. This occurs through bidirectional modulation of cell-wide synaptic strength, where prolonged unidirectional neuronal activity receives negative feedback (Turrigiano, 2012). An important mechanism underlying synaptic scaling at glutamatergic synapses involves regulated trafficking of AMPA receptors into and out of the post-synaptic membrane (Diering et al., 2014; Pozo and Goda, 2010; Turrigiano, 2012). Chronic network activity elicits AMPA receptor removal, whereas chronic suppression increases synaptic AMPA receptor abundance (Goold and Nicoll, 2010). Mounting evidence indicates that the intricate regulation of AMPA receptor trafficking during synaptic scaling requires *de novo* gene transcription and depends on intracellular Ca^{2+} -signaling (Ibata et al., 2008; Thiagarajan et al., 2005). Experiments have indeed shown that bidirectional scaling is prevented by the transcription inhibitor actinomycin-D (Goold and Nicoll, 2010; Han and Stevens, 2009; Ibata et al., 2008). Also, chronic neuronal activity or suppression respectively activates or inactivates calcium/calmodulin-dependent protein kinase type IV (CaMKIV) (Goold and Nicoll, 2010; Ibata et al., 2008). This indicates that gene transcription through CaMKIV signaling plays a pivotal role in bidirectional scaling. Specifically, transcriptional repression of *Arc* and *Bdnf* is required for synaptic scaling up during chronic network suppression (Béïque et al., 2011; Gao et al., 2010; Rutherford et al., 1998; Shepherd et al., 2006).

Since synaptic scaling requires gene transcription, a picture is emerging that implicates epigenetic regulation in homeostatic plasticity. Several studies have shown that DNA-methylation at the *Bdnf* promoter is dynamically regulated in an activity-dependent manner (Chang et al., 2010; Levenson et al., 2006; Lubin et al., 2008; Martinowich et al., 2003). Also methyl-CpG binding protein 2 (MeCP2) and Tet3 are required for synaptic scaling (Blackman et al., 2012; Qiu et al., 2012; Zhang et al., 2014; Zhong et al., 2012; Yu et al., 2015) and the REST/NRSF complex is required for intrinsic homeostatic plasticity induced by sustained electrical activity in hippocampal neurons (Pozzi et al., 2013). While evidence that epigenetic mechanisms are critical for synaptic scaling is mounting, it is currently unknown which chromatin modifications are involved and how they are regulated.

Disrupted epigenetic regulation is commonly found in neurological disorders such as intellectual disability (ID) (Kleefstra et al., 2014), autism spectrum disorder (ASD) (De Rubeis,

2014) and schizophrenia (McCarthy et al., 2014). Haploinsufficiency of the euchromatic histone-lysine N-methyltransferase 1 (*EHMT1*) gene causes Kleefstra syndrome (Kleefstra et al., 2009; 2006; 2012) and is associated with some cases of ASD (Talkowski et al., 2012) and schizophrenia (Kirov et al., 2012). EHMT1 (EHMT1) together with its paralog EHMT2 (EHMT2) form a chromatin remodeling complex that catalyzes the dimethylation of histone H3 at lysine 9 (H3K9me2), a PTM associated with transcriptional repression (Tachibana et al., 2005). Interestingly, H3K9me2 is an epigenetic mark that is dynamically regulated in the hippocampus and nucleus *Accumbens* during contextual fear memory formation, addiction and stress (Boulle et al., 2014; Chase and Sharma, 2013; Covington et al., 2011; Gupta et al., 2010; Gupta-Agarwal et al., 2012; 2014; Heller et al., 2014; Maze et al., 2010). Genetic and pharmacological manipulations of EHMT1/2 *in vivo* have also shown that EHMT signaling is important for long-term memory formation both in mouse and *Drosophila* (Balemans et al., 2013; Gupta-Agarwal et al., 2012; Kramer et al., 2011; Schaefer et al., 2009).

Here, we report that H3K9me2 is bidirectionally regulated by chronic changes in neuronal activity. We show that EHMT1 and EHMT2 are part of a complex that regulates a transcriptional program essential for synaptic scaling. Specifically, EHMT1 and EHMT2 are required for the increase in H3K9me2 when network activity is chronically inhibited and for synaptic scaling up *in vitro* and *in vivo*. Moreover, we found that EHMT1 and EHMT2 repressed *Bdnf* expression during synaptic scaling up by increasing H3K9me2 at *Bdnf* promoter IV. We posit that EHMT1 and EHMT2 act as cell-autonomous epigenetic regulators that govern a repressive program required for synaptic scaling up.

RESULTS

Neuronal activity elicits dynamic effects on synaptic scaling via H3K9me2

We first investigated whether chronic neuronal network manipulation alters the methylation levels of H3K4 (H3K4me1, H3K4me3), H3K9 (H3K9me2) or H3K27 (H3K27me3). We treated cultures of rat primary cortical neurons for 48 hours (h) beginning at 11 days *in vitro* (DIV) with either 1 μ M tetrodotoxin (TTX) or 10 μ M picrotoxin (PTX) to induce homeostatic scaling up or scaling down, respectively (Turrigiano et al., 1998). The fluorescence intensity of immunolabeled H3K9me2 (Vedadi et al., 2011) revealed that nuclear H3K9me2 increased significantly in TTX-treated compared to untreated neurons, whereas H3K9me2 decreased significantly in neurons treated with PTX (Figure 2.1A and 2.1B). In a mixed primary culture, H3K9me2 was most prominently detected in MAP2-positive neurons (Figure 2.1A). Accordingly, we did not observe any network activity-dependent changes in H3K9me2 within MAP2-negative glial cells (Figure 2.1B), suggesting that changes in H3K9me2 were restricted to neurons.

Although we did observe less pronounced changes in H3K4me3 and H3K27me3, they were not bidirectionally correlated with synaptic scaling up or down (Figure 2.2).

Synaptic scaling is a progressive process that develops gradually over a time period of 48h (Ibata et al., 2008; Sutton et al., 2006). To evaluate the temporal dynamics of H3K9 dimethylation induced by TTX, we measured H3K9me2 fluorescence at sequential time points

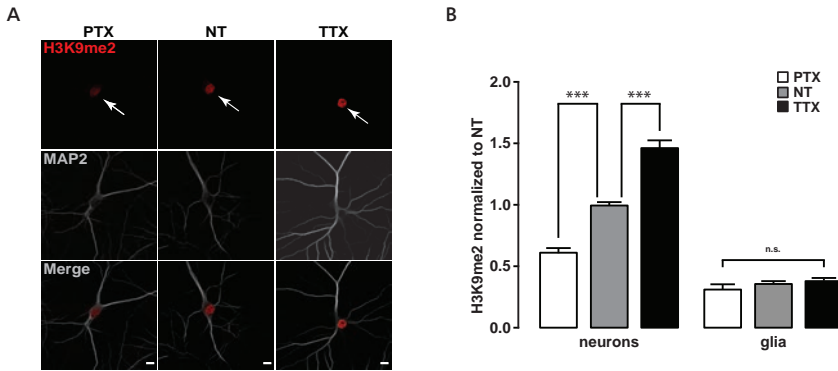


Figure 2.1. EHMT1 is required for network activity dependent H3K9me2 dynamics. **A)** Representative confocal images of H3K9me2 immunoreactivity in untreated (NT) and neurons treated with PTX or TTX for 48h. Scale bar 5 μ m. (continues next page). **B)** Quantitative analysis of H3K9me2 levels in neurons (MAP2 positive) and glial (MAP2 negative cells) treated with PTX or TTX for 48h and untreated (NT). Data are represented as mean \pm SEM. ***, $p < 0.001$; $n = 34-41$; n.s., non significant; glia $p > 0.05$; one-way ANOVA.

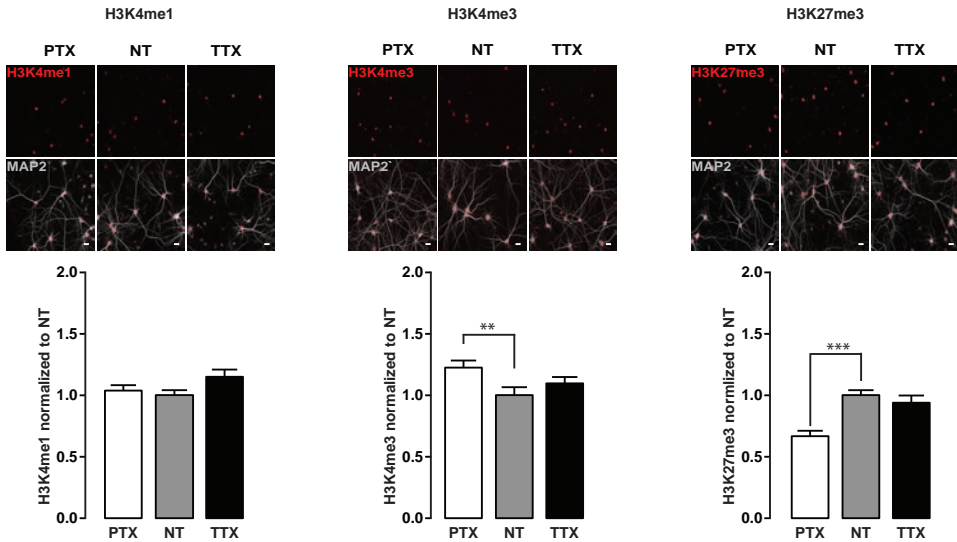


Figure 2.2. Changes in histone methylation marks during synaptic scaling. Representative images of H3K4me1, H3K4me3 and H3K27me3 immunoreactivity and relative intensity levels quantifications expressed as mean \pm SEM fold change from NT cultures. Scale bars, 20 μ m. **, $p < 0.01$; ***, $p < 0.001$. H3K4me1: NT, TTX, PTX, $n = 31-48$. one-way ANOVA. H3K4me3: NT, TTX, PTX, $n = 24-30$. one-way ANOVA. H3K27me3: NT, TTX, PTX, $n = 31-39$. one-way ANOVA.

after adding TTX. H3K9me2 fluorescence was significantly elevated by 12h, further enhanced at 24h, and plateaued from 36-48h after TTX treatment (Figure 2.3A). Synaptic scaling is also a reversible process (Goel and Lee, 2007; Goel et al., 2011); therefore, we investigated the effect of removing TTX on H3K9me2 in our neuronal cultures. Cultures were first treated with TTX for 48h, the medium was then refreshed with pre-conditioned untreated culture medium,

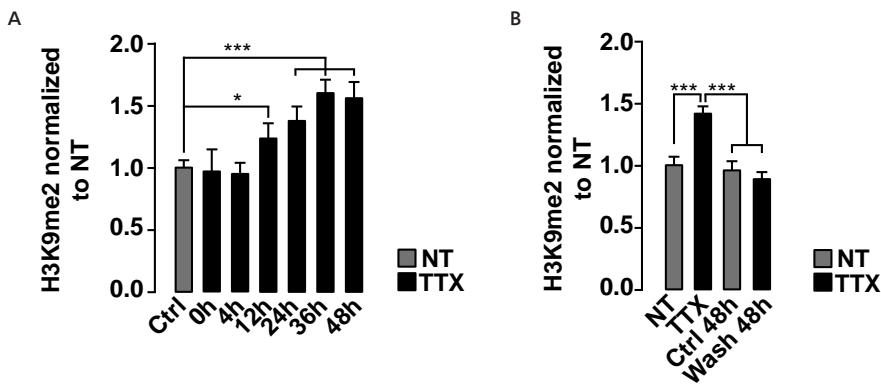


Figure 2.3. H3K9me2 increases after TTX treatment are gradual and reversible. **A)** Quantitative analysis of time course of H3K9me2 levels in TTX-treated neurons. Data are represented as mean±SEM. *, $p<0.05$; ***, $p<0.001$; n.s., non significant; n=20-25; one-way ANOVA. **B)** Analysis of reversibility of TTX-induced H3K9me2 changes. H3K9me2 intensity expressed as mean±SEM fold change from NT cultures. ***, $p<0.001$; n=23-27; one-way ANOVA.

and H3K9me2 fluorescence intensity was measured 48h later. Interestingly, after TTX was withdrawn, we found that H3K9me2 fluorescence in treated neurons returned to an intensity equal with untreated neurons (Figure 2.3B).

Various protocols that reduce Ca^{2+} influx are used to induce synaptic scaling in cultured neurons. These include blocking L-type calcium channels or AMPA receptor function respectively with nimodipine or CNQX for 48h (Lee et al., 2013; Wierenga et al., 2005; Thiagarajan et al., 2005, Ibata et al., 2008). Either nimodipine or CNQX alone increased H3K9me2 fluorescence but they occluded the TTX-induced increase in H3K9me2 (Figure 2.4A and 2.4B). In contrast, blocking NMDA-dependent calcium influx with APV for 48h did not increase H3K9me2 nor was there a cumulative effect when combined with TTX (Figure 2.4A and 2.4B) (Turrigiano et al., 1998). Furthermore, the TTX-induced increase in H3K9me2 was prevented (Figure 2.4A and 2.4B) when endoplasmic reticulum calcium reuptake was blocked by thapsigargin (Lee et al., 2013).

To identify Ca^{2+} -dependent signaling pathways upstream of H3K9me2, we pharmacologically blocked CaMK signaling. Previous studies showed that chronic network suppression reduced CaMKIV- and CaMKK-mediated phosphorylation due to decreased intracellular calcium (Thiagarajan et al., 2005; Ibata et al., 2008). We used STO-609 to block CaMKK, which in turn inhibits CaMKIV (Ibata et al., 2008). STO-609 treatment increased H3K9me2 comparable to TTX treatment (Figure 2.4A and 2.4B), suggesting that TTX reduces CaMKK/CaMKIV signaling, and this pathway directly contributes to increased H3K9me2 during synaptic scaling up. Collectively, these experiments indicate that chronically increased or decreased neuronal activity bidirectionally alters H3K9me2 levels in cortical neurons.

EHMT1 is required for the TTX-dependent increase in neuronal H3K9me2

Since EHMT1 catalyzes H3K9 dimethylation, we focused on the role of EHMT1 in synaptic scaling up. We first evaluated whether EHMT1 is required for the TTX-dependent increase in

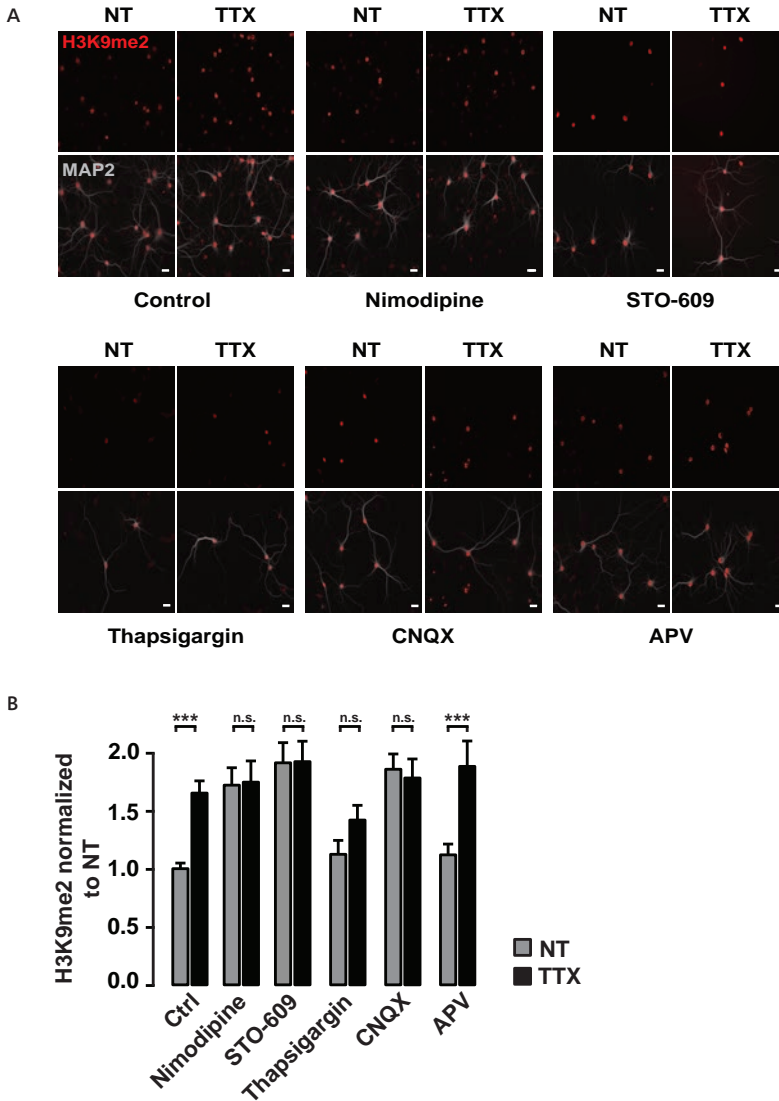


Figure 2.4. H3K9me2 respond dynamically to chronic variations in intracellular Ca^{2+} concentration. **A)** Representative images of H3K9me2 immunoreactivity levels in neurons treated with: TTX, nimodipine, STO-609, thapsigargin, APV and CNQX. Scale bars, 20 μm . **B)** Quantitative analysis of H3K9me2 levels in conditions as indicated. Data are represented as mean \pm SEM, fold change from NT cultures. ***, $p < 0.001$; $n = 28-50$; n.s., non significant; two-way ANOVA.

H3K9me2 by designing GFP-expressing constructs to encode shRNA sequences (Ehmt1#1-4) that specifically knockdown EHMT1 in neurons (Figure 2.5A, 2.5B and 2.5C).

We sparsely transfected cortical cultures with either control vector or shRNA-expressing vectors (Ehmt1#1 or Ehmt1#2) at DIV 0. Cultures were then treated at DIV 11 with TTX for 48h. H3K9me2 fluorescence was measured in transfected (GFP+) and untransfected (GFP-) neurons

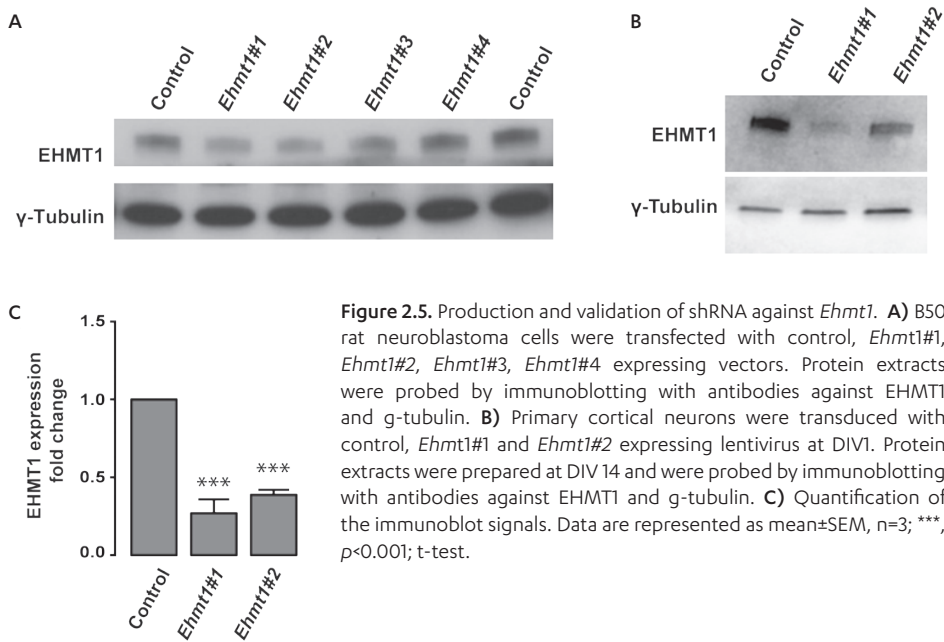


Figure 2.5. Production and validation of shRNA against *Ehmt1*. **A)** B50 rat neuroblastoma cells were transfected with control, *Ehmt1*#1, *Ehmt1*#2, *Ehmt1*#3, *Ehmt1*#4 expressing vectors. Protein extracts were probed by immunoblotting with antibodies against EHMT1 and g-tubulin. **B)** Primary cortical neurons were transduced with control, *Ehmt1*#1 and *Ehmt1*#2 expressing lentivirus at DIV1. Protein extracts were prepared at DIV 14 and were probed by immunoblotting with antibodies against EHMT1 and g-tubulin. **C)** Quantification of the immunoblot signals. Data are represented as mean±SEM, n=3; ***, $p < 0.001$; t-test.

and compared to untreated neurons. As expected, we found that TTX increased H3K9me2 in GFP- and GFP+ neurons treated with the control vector. Conversely, TTX did not increase H3K9me2 in neurons transfected with either of the *Ehmt1* hairpins (Figure 2.6A and 2.6C). Moreover, we observed that basal H3K9me2 fluorescence, before adding TTX, was significantly lower in neurons transfected with the *Ehmt1* hairpins (Figure 2.6A and 2.6C). Importantly, co-transfection of *Ehmt1*#1, which targets the 3' UTR of the endogenous *Ehmt1* mRNA, together with a construct that over-expresses mouse *Ehmt1* cDNA (*Ehmt1*-OE) restored both basal H3K9me2 levels and the TTX-induced increase (Figure 2.6A and 2.6C).

Next, we pharmacologically blocked the methyltransferase activity of EHMT1 and EHMT2 with UNC0638 (Vedadi et al., 2011). We treated neurons with UNC0638 in the presence or absence of TTX and measured the immunofluorescence intensity of H3K9me2. UNC0638 blocked the increase in H3K9me2 by TTX (Figure 2.6B and 2.6C). We also found that UNC0638 alone reduced the basal H3K9me2 levels, similar to *Ehmt1*#1 and *Ehmt1*#2 (Figure 2.6A, 2.6B and 2.6C). These results suggest that EHMT1, through activity-dependent dimethylation of H3K9, functions as an epigenetic regulator of homeostatic synaptic scaling up.

EHMT1 is required for the TTX-dependent increase in mEPSC amplitude

To determine if EHMT1 is required for homeostatic synaptic scaling up, we recorded miniature excitatory postsynaptic currents (mEPSCs) from untreated and TTX-treated neurons that were transfected with *Ehmt1*#1, *Ehmt1*#2 or control vector. Consistent with previous observations, TTX significantly increased mEPSC amplitudes recorded from untransfected and control neurons (Figure 2.7A and 2.7B) but not mEPSC frequency (Figure 2.8) (Hou et al., 2008; Kim and Ziff, 2014; Wierenga et al., 2006).

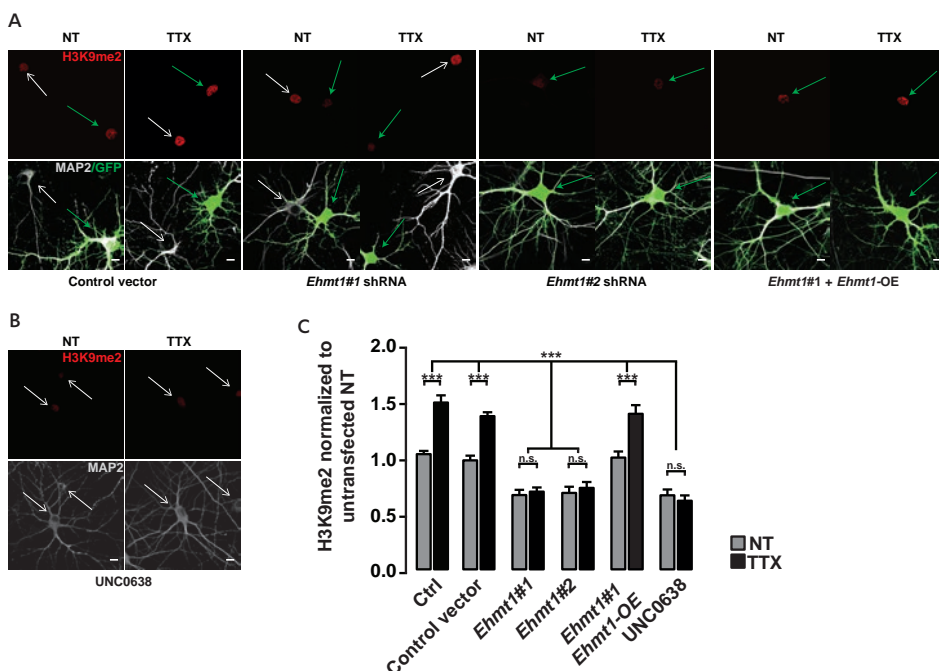


Figure 2.6. Neuronal H3K9me2 levels increase after TTX treatment depend on EHMT1 function. **A)** Representative images of H3K9me2 immunofluorescence levels in neurons transfected with control vector; *Ehmt1#1*, *Ehmt1#2*, *Ehmt1#1 + Ehmt1-OE*, in untreated (NT) and neurons treated with TTX for 48h. Scale bars 5 μ m. **B)** Representative images of H3K9me2 immunofluorescence levels of untreated or TTX-treated neurons (48h) with UNCO638 (48h). Scale bars 5 μ m. **C)** Quantitative analysis of H3K9me2 levels in neurons transfected with control vector; *Ehmt1#1*, *Ehmt1#2*, *Ehmt1#1 + Ehmt1-OE*, UNCO638, in untreated (NT) and neurons treated with TTX for 48h. Data are represented as mean \pm SEM, fold change from NT. *, $p < 0.05$; ***, $p < 0.001$; n=21-41; n.s., non significant; two-way ANOVA.

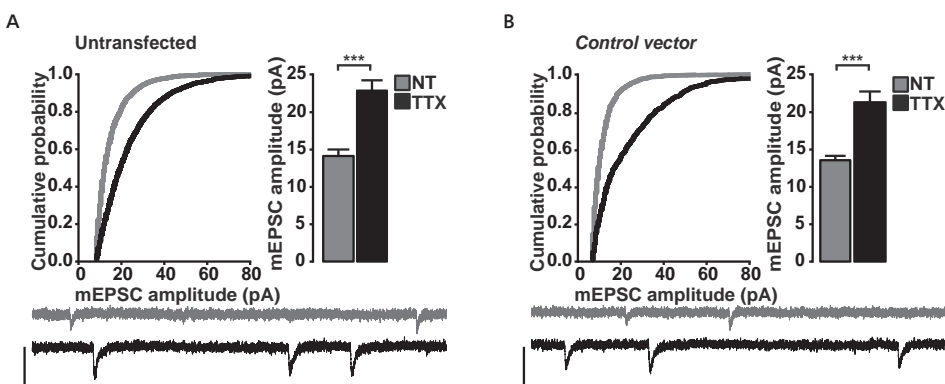


Figure 2.7. TTX treatment induce an increase in mEPSC amplitudes in WT neuronal cultures. Representative mEPSC traces, cumulative plots and mean \pm SEM amplitude bar graphs of cortical neurons, untreated (NT) or TTX-treated (TTX) (48h). **A)** Untransfected neurons NT, TTX, n=9-11, **B)** neurons transfected with a Control vector, NT, TTX, n=10-11. Vertical scale 25pA and horizontal scale 50ms.

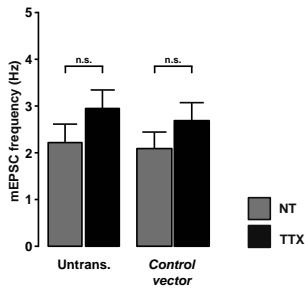


Figure 2.8. mEPSC frequencies in untransfected and control transfected neurons. Quantification of mEPSC frequency in indicated conditions. Data are represented as mean±SEM, untransfected NT, TTX, n=9-11; control vector NT, TTX, n=10-10. Data are represented as mean±SEM; n.s., non significant; two-way ANOVA.

However, when EHMT1 was knocked down, mEPSC amplitudes did not increase in response to chronic TTX treatment (Figure 2.9A and 2.9B). We also found that neurons co-transfected with *Ehmt1#1* and *Ehmt1*-OE had increased mEPSC amplitudes after TTX treatment, similar to control neurons (Figure 2.9C). Therefore, specific knock down of EHMT1 appears to prevent synaptic scaling up. We then recorded mEPSCs from neurons treated with either UNC0638 alone or in combination with TTX. Inhibiting EHMT1/2 with UNC0638 alone for 48h had no effect on either mEPSC amplitude or frequency compared to untreated neurons, whereas synaptic scaling up was impeded in neurons co-treated with UNC0638 and TTX (Figure 2.9D, 2.9E and 2.9F). Collectively, these findings provide further evidence that EHMT1 is required for homeostatic scaling up of synapses.

Interestingly, we found that pharmacological inhibition or genetic knock down of *Ehmt1*, despite reducing basal H3K9me2 fluorescence (Figure 2.6A and 2.6C), did not affect basal mEPSC amplitude or frequency (Figure 2.9A, 2.9B, 2.9D, 2.9E and 2.9F). To investigate whether increasing H3K9me2 levels was sufficient to scale up synapses, we used the class-I HDAC inhibitor MS-275. When used in combination with cocaine, MS-275 was shown to enhance *Ehmt1/2* expression and subsequently raise H3K9me2 levels in the nucleus *Accumbens* (Kennedy et al., 2013). Treating neurons with MS-275 alone for 48h significantly increased H3K9me2 fluorescence (Figure 2.10A); however, it did not increase mEPSC amplitude (Figure 2.10B). We therefore propose that EHMT1 acts as an epigenetic regulator which represses a genetic program required but not sufficient for homeostatic synaptic scaling up.

EHMT1 is required for surface AMPA receptor expression upon TTX-induction

Previous studies have shown that neurons increase their mEPSC amplitudes by increasing the surface expression of AMPA receptors GluA1 and GluA2 (Diering et al., 2014; Gainey et al., 2009). We performed live-cell fluorescent labeling of surface GluA1 and GluA2 and compared the signal between control and TTX-treated neurons (Wierenga et al., 2005). TTX caused a significant increase in fluorescent puncta in control neurons but not in *Ehmt1#2* transfected neurons (Figure 2.11). We conclude that *Ehmt1* knock down prevents increased surface expression of AMPA receptors during synaptic scaling up, which supports our notion that EHMT1 protein is required for this process.

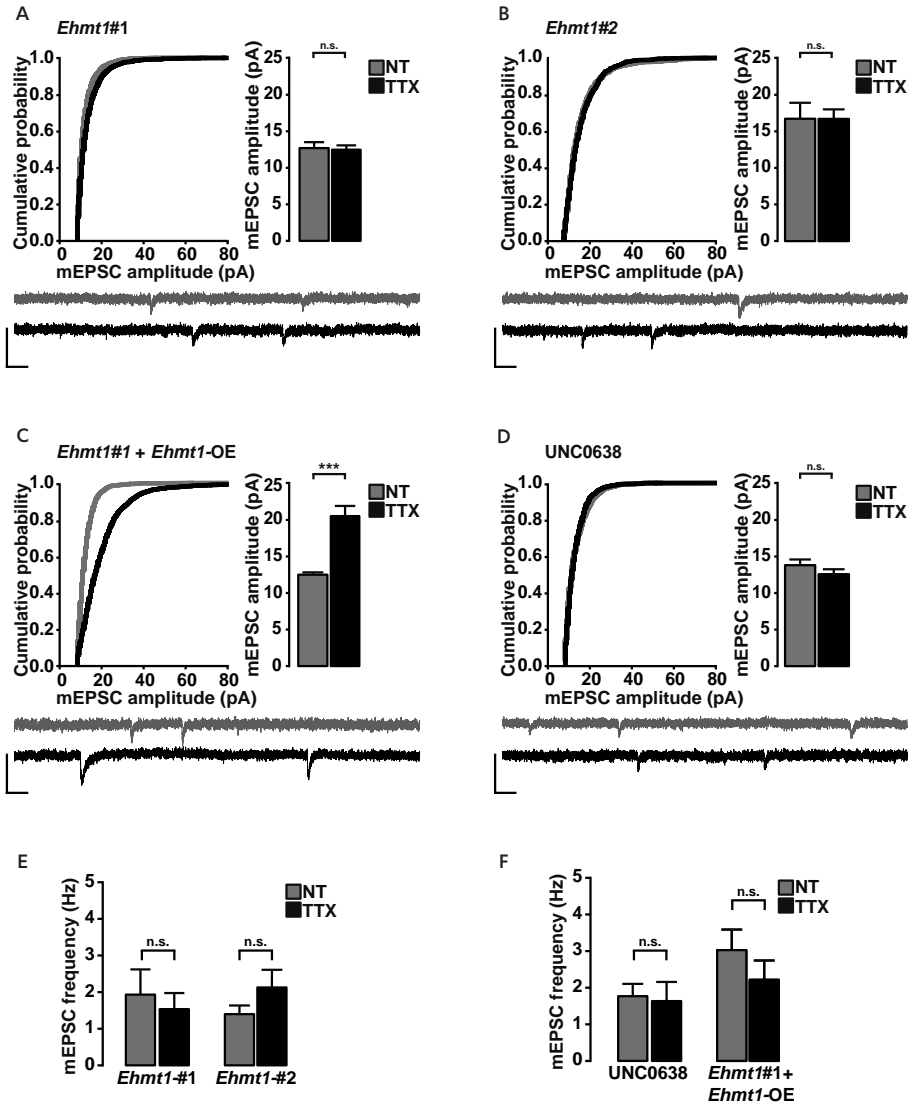


Figure 2.9. EHMT1 is required to increase the mEPSC amplitude without altering mEPSC frequency in response to chronic network deprivation. Representative traces and quantification of mEPSC amplitudes from neurons transfected with **A)** shRNA *Ehmt1#1*, NT, TTX, n=10-11, **B)** shRNA *Ehmt1#2*, NT, TTX, n=8-8, **C)** co-transfected with shRNA *Ehmt1#1+Ehmt1-OE* neurons, NT, TTX, n=11-14, **D)** UNC0638 treated neurons NT, TTX, n=10-10. ***, $p < 0.001$; n.s., non significant; two-way ANOVA. Vertical scale 25pA and horizontal scale 50ms. Quantification of mEPSC frequency in **E)** *Ehmt1#1* NT, n=10-11 and *Ehmt1#2* NT, TTX n=8-8 and **F)** *Ehmt1#1+Ehmt1-OE* NT, TTX, n=11-14 and UNC0638 NT, TTX n=10-10. Data are represented as mean \pm SEM; n.s., non significant; two-way ANOVA.

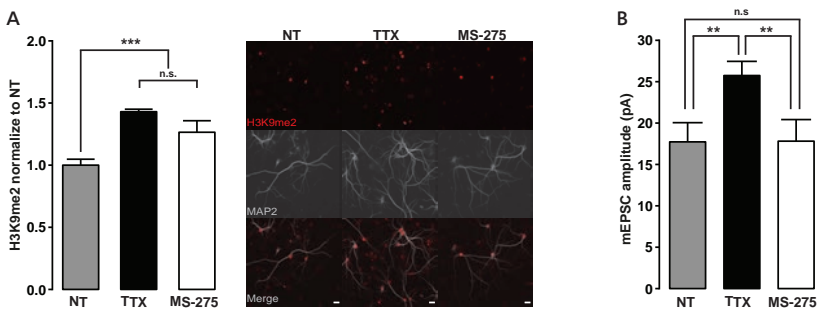


Figure 2.10. Effect of HDAC class-1 inhibitor, MS-275, on H3K9me2 levels and synaptic transmission. **A)** Representative images of H3K9me2 immunoreactivity (red) levels in neurons (MAP2 positive cells, gray) untreated or treated with TTX or MS-275. Scale bars 20µm. Quantitative analysis of H3K9me2 levels in untreated or TTX and MS-275 treated neurons. Data are represented mean±SEM fold change from NT cultures; n=34-55, ***, $p<0.001$; n.s., non significant; one-way ANOVA. **B)** mEPSC amplitude bar graphs from untreated neurons, TTX and MS-275 treated neurons. Data are represented mean±SEM; n=8; **, $p<0.01$; n.s., non significant; one-way ANOVA.

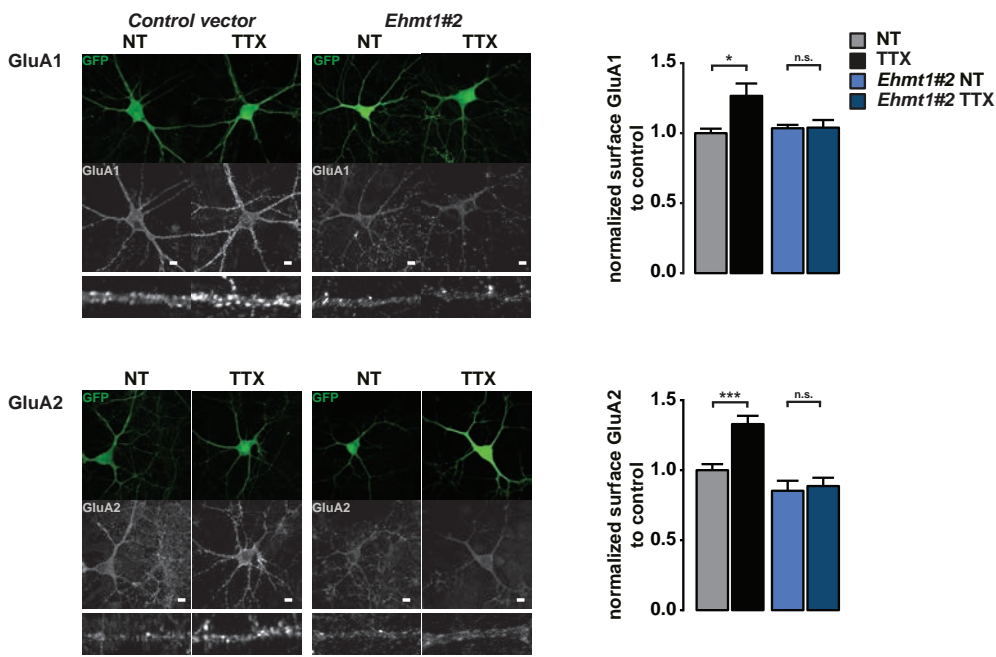


Figure 2.11. EHMT1 is required to increase surface AMPA receptor expression in response to TTX. Representative images of GluA1 and GluA2 surface immunoreactivity in control vector and *Ehmt1#2* transfected neurons, untreated (NT) or TTX-treated (TTX) (48h). Scale bar 5µm. Immunoreactivity intensity quantification analysis expressed as fold change from NT. *, $p<0.05$; ***, $p<0.001$; n.s., non significant. GluA1: Control vector NT, TTX n=8-10; *Ehmt1#2* NT, TTX, n=8-8. GluA2: Control vector NT, TTX n=8-8; *Ehmt1#2* NT, TTX, n=8-8; two-way ANOVA.

EHMT1/EHMT2 complex is required for synaptic scaling up

EHMT1 interacts with EHMT2 to form a functional complex that catalyzes H3K9 dimethylation (Tachibana et al., 2008; 2005). Thus, the TTX-mediated increase in H3K9me2 may be caused by the modulation of gene or protein expression levels of EHMT1, EHMT2 or both. Alternatively, neuronal activity could change the subcellular distribution of EHMT1/2, similar to histone deacetylases such as HDAC4 (Sando et al., 2012). To assess these possibilities, we analyzed the distribution of EHMT1 and EHMT2 after TTX treatment. EHMT1 and EHMT2 were primarily expressed in the nucleus under normal conditions, and TTX treatment did not change their subcellular localization (Figure 2.12A and 2.12B).

Next, we examined EHMT1 and EHMT2 protein and mRNA levels before and after TTX treatment. TTX caused a significant increase in both the short and long isoforms and total EHMT2 protein levels, but EHMT1 protein levels were unaffected (Figure 2.13A and 2.13B). Consistent with previous studies (Bateup et al., 2013a; Shepherd et al., 2006), we found that ARC protein levels were significantly reduced after TTX treatment (Figure 2.13A and 2.13B).

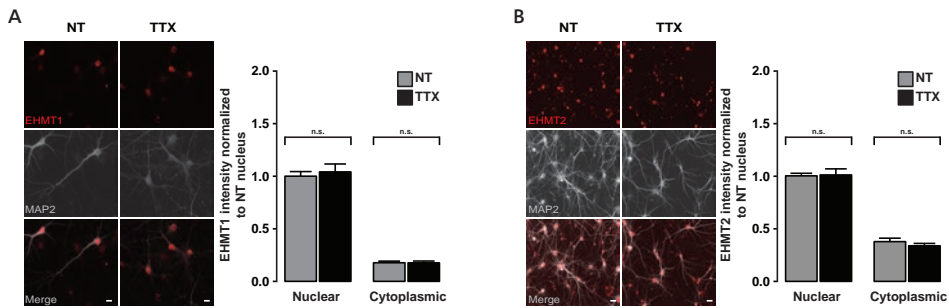


Figure 2.12. Subcellular expression of EHMT1 and EHMT2. **A, B)** Representative images of EHMT1 and EHMT2 immunostainings in primary cortical neurons and quantification of relative EHMT1 and EHMT2 levels in the cytoplasm versus nucleus in untreated and TTX-treated neurons. Data are represented as mean \pm SEM; n=22-23; n.s., non significant; t-test. Scale bars 20 μ m.

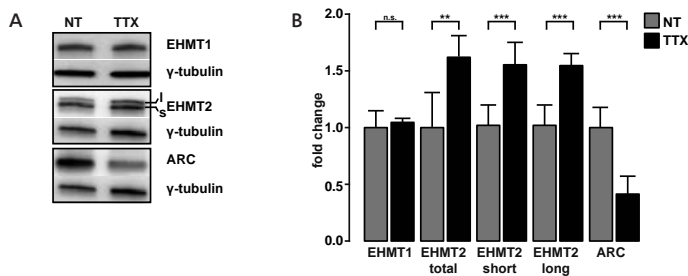


Figure 2.13. EHMT1 and EHMT2 protein levels dynamics after synaptic scaling up induction. **A)** Representative immunoblot images of EHMT1, EHMT2 short and long isoform (s and l) and ARC in untreated and TTX-treated neurons (48h). **B)** Quantification of protein levels of EHMT1, EHMT2 (s, l and total bands) and ARC in untreated and TTX-treated neurons expressed as mean \pm SEM fold change from NT cultures. **, $p < 0.01$; ***, $p < 0.001$; n.s., non significant; n=3-5; t-test.

Transcriptional regulation has been shown to occur as early as 4h after TTX treatment (Ibata et al., 2008). To determine when changes in EHMT1/2 occur, we profiled *Ehmt1* and *Ehmt2* mRNA expression at two time points after TTX treatment (4h and 48h). *Ehmt2* mRNA levels were significantly increased after 48h but not after 4h. *Ehmt1* expression, however, did not change and was comparable to untreated neurons at both time points (Figure 2.14).

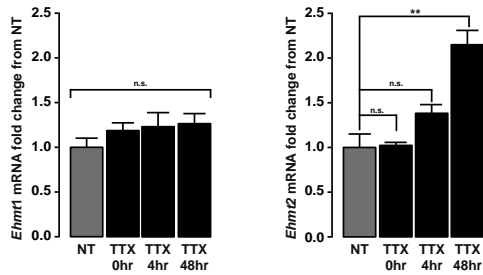


Figure 2.14. EHMT1 and EHMT2 transcript levels dynamics after synaptic scaling up induction. Analysis of time course expression of *Ehmt1* and *Ehmt2* mRNA in neurons after 0h, 4h and 48h after treating neurons with TTX. Changes in mRNA levels are expressed as mean±SEM fold change from untreated neurons. n=3; **, $p<0.01$; n.s., non significant; one-way ANOVA.

Since EHMT1 dimerizes with EHMT2 to form a functional complex (Tachibana et al., 2005; 2008), we hypothesized that the TTX-dependent increase in H3K9me2 levels may result from an enhanced interaction leading to higher enzymatic activity. First, we measured enzymatic activity using an ELISA-based assay for histone methyltransferase (HMT) and found increased HMT activity in nuclear extracts from TTX-treated neurons (Figure 2.15A). Next, using nuclear protein lysates, we co-immunoprecipitated EHMT2 with an EHMT1 antibody. Similar to previous findings (Tachibana et al., 2005), EHMT2 co-immunoprecipitated with EHMT1 (Figure 2.15B). Interestingly, Western blot analysis showed that TTX treatment significantly increased the interaction between EHMT1 and EHMT2 (Figure 2.15B).

Based on these results, we hypothesized that EHMT2 is also required for the functional expression of homeostatic scaling up. We designed and validated two independent shRNAs (*Ehmt2#1* and *Ehmt2#3*) to downregulate endogenous EHMT2 (Figure 2.16).

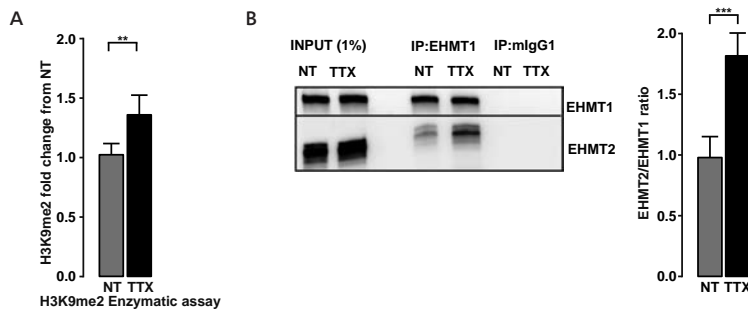


Figure 2.15. EHMT1 interacts with EHMT2 during synaptic scaling up. **A)** H3K9 dimethyltransferase enzymatic assay expressed as mean±SEM fold change from NT cultures. **, $p<0.01$; n=3; t-test. **B)** Western blot of EHMT1 and EHMT2 input (1%) and after co-immunoprecipitation of nuclear cell lysates with antibody against EHMT1 and a mouse IgG, from NT or TTX-treated (48h) cortical cultures. Quantification of EHMT2/EHMT1 ratio expressed as mean±SEM. ***, $p<0.001$; n=7; t-test.

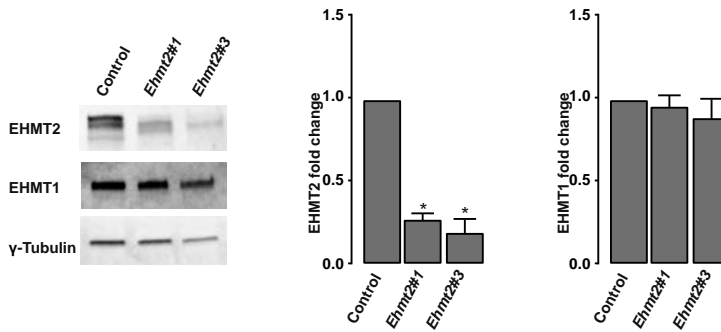


Figure 2.16. Validation of *Ehmt2* knockdown. Cortical neurons were transduced with *Ehmt2#1*, *Ehmt2#3* and control neurons. Western blot showing EHMT1, EHMT2 and γ -tubulin expression. Data are represented as mean \pm SEM, $n=3$; *, $p<0.05$; t-test.

Chronic TTX treatment failed to increase H3K9me2 levels and scale up in neurons transfected with either *Ehmt2#1* or *Ehmt2#3* (Figure 2.17A, 2.17B, 2.17C and 2.17D).

Interestingly, we found that knocking down *Ehmt2* specifically reduced mEPSC frequency but did not affect amplitude in basal conditions (Figure 2.17E), suggesting a specific function for EHMT2 in early synapse formation. Indeed, EHMT2- but not EHMT1-deficient cortical neurons showed fewer juxtaposing PSD-95/VGLUT puncta and hence fewer synapses (Figure 2.18A). However, neither *Ehmt1* nor *Ehmt2* knock down affected neurite outgrowth (Figure 2.18B). Collectively, our data suggest that chronic network deprivation activates a repressive program whereby upregulated EHMT1-EHMT2 complex increases H3K9me2 and scales up synapses.

EHMT1 is required for TTX-induced gene repression

Next, we sought to decipher the genetic program that is associated with synaptic scaling up. We generated strand-specific RNA-Seq libraries from WT and *Ehmt1#2*-transduced neuronal cultures, with and without TTX-treatment. In *Ehmt1#2* neurons, *Ehmt1* transcript was significantly down-regulated (DEseq2, $p<0.026$, $\log_2(fc)=-0.61$), whereas *Ehmt2* transcript remained unaffected (DEseq2, $p<0.43$, $\log_2(fc)=-0.21$). In the absence of TTX treatment, *Ehmt1#2* exhibited differential expression of a relative small number of genes, with an equal amount of down and upregulated genes (89 upregulated genes, and 88 down-regulated genes, DEseq2 $p<0.01$, Figure 2.19A). TTX-treatment of WT neurons induced a larger change in the number of genes and Spearman correlations sharply segregated the untreated and TTX-treated conditions (301 genes, Figure 2.19B).

TTX-treatment of WT neurons mostly triggered gene repression, since the number of DOWN-regulated genes was approximately 7-fold higher than UP-regulated ones (263 against 38, Figure 2.20A). Also, TTX treatment of *Ehmt1#2* neurons led to a significant down-regulation, but only a partial overlap was found with the genes down-regulated in WT neurons (Figure 2.20A left, 2.20B and 2.20C). UP-regulated genes were few in both conditions and the overlap was low (Figure 2.21A right).

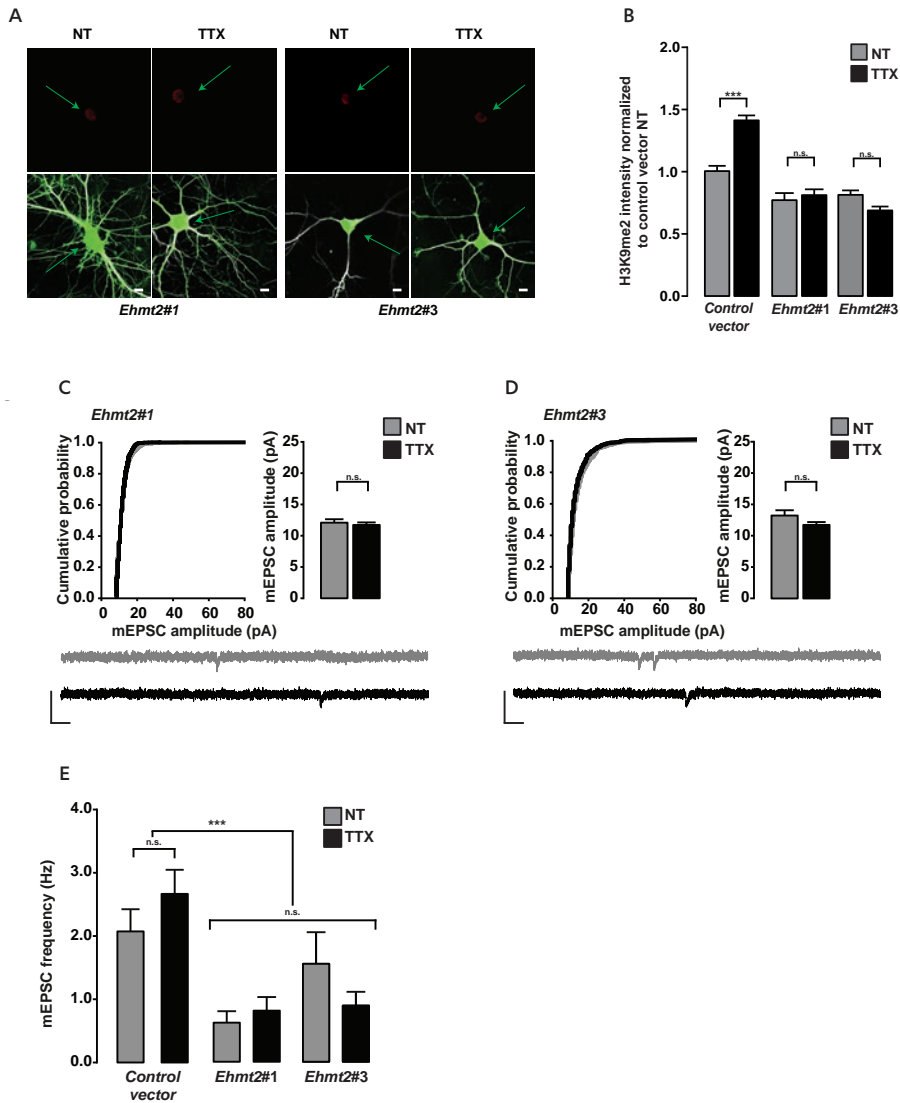


Figure 2.17. EHMT2 is required for synaptic scaling up. **A)** Representative images of H3K9me2 immunofluorescence levels in transfected neurons with hairpins *Ehmt2#1* and *Ehmt2#3*. Scale bars 5µm. **B)** Quantitative analysis of H3K9me2 levels in indicated conditions, expressed as mean±SEM fold change from NT cultures. ***, $p < 0.001$; n.s., non significant; control vector NT, TTX, $n = 41-41$; *Ehmt2#1* NT, TTX, $n = 30-34$; *Ehmt2#3* NT, TTX, $n = 49-50$; two-way ANOVA. **C, D)** Representative mEPSC traces (1s), cumulative plots and mEPSC amplitude bar graphs expressed as mean±SEM from *Ehmt2#1* and *Ehmt2#3* transfected neurons, untreated (NT) or TTX-treated (TTX) (48h). Vertical scale, 25pA, and horizontal scale, 50ms. Control vector NT, TTX, $n = 10-10$ (Figure 2B); *Ehmt2#1* NT, TTX, $n = 10-10$; *Ehmt2#3* NT, TTX, n.s., non significant; $n = 9-8$; two-way ANOVA. **E)** mEPSC frequency bar graphs from transfected with shRNA *Ehmt2#1* and *Ehmt2#3*. Data are represented as mean±SEM; $n = 9-10$; ***, $p < 0.001$; n.s., non significant; two-way ANOVA.

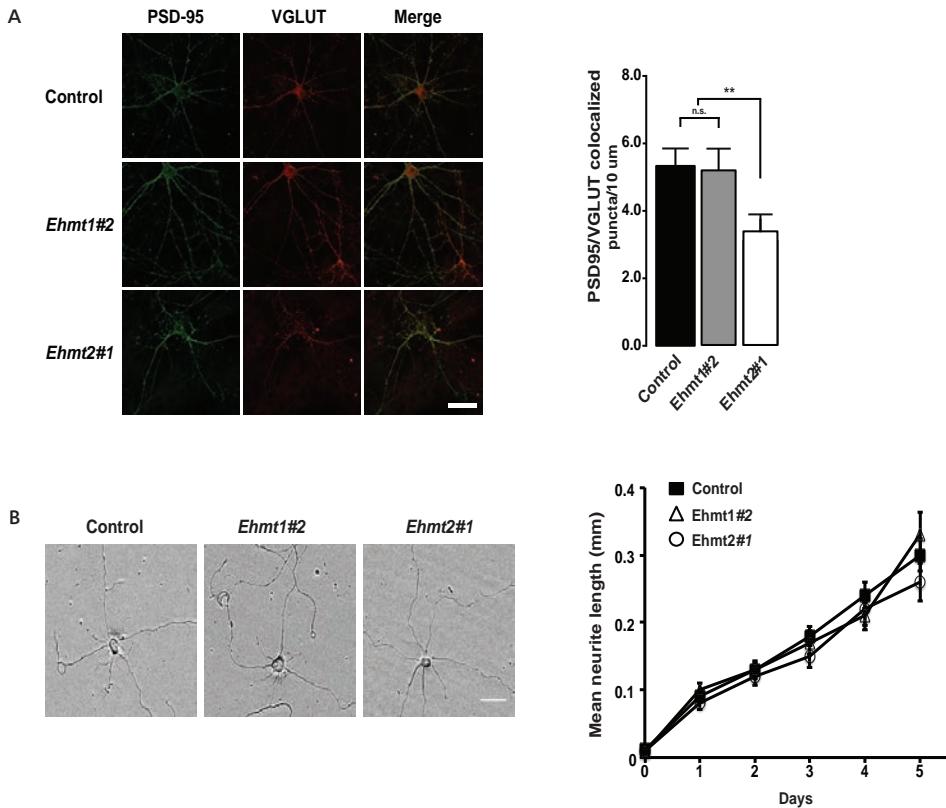
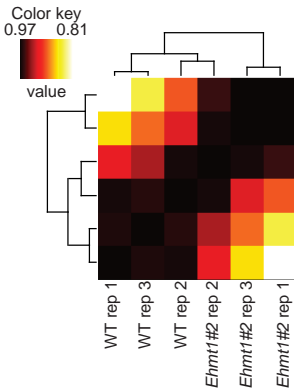


Figure 2.18. EHMT2 is required for synaptogenesis but does not affect neurite outgrowth. **A)** Representative images of VGLUT and PSD-95 colocalizing punctae immunolabeling in control and *Ehmt1#2* and *Ehmt2#1* transduced neuronal. Data are represented as mean \pm SEM colocalized PSD-95/VGLUT punctae on a stretch of 10 μ m of dendritic length. $n=20-23$ neurons; **, $p<0.01$; one-way ANOVA. **B)** Mean neurite length was determined from data obtained by live cell imaging (Incucyte) and plotted as a function of time. *Left*, representative images at DIV 4 of cortical neurons transfected with control, *Ehmt1#2* or *Ehmt2#1* shRNA. *Right*, quantification of mean neurite length per neuron. Mean neurite length is not significantly different between conditions. $n=42-53$ neurons, 3 independent experiments, multiple t-test. Scale bar represent 10 μ m.

Interestingly, we found a significant reduction in the global TTX-induced repression of *Ehmt1#2* neurons as compared to control neurons ($p<5.8e-13$, Figure 2.21A). Moreover, in *Ehmt1#2* neurons, the TTX responsive genes showed significantly higher basal expression level (Figure 2.21B), suggesting that these genes are directly or indirectly controlled by EHMT1. Overall, these data indicate that in *Ehmt1#2* neurons the TTX-induced repression is impaired, and suggests that a subset of TTX-responsive genes is EHMT1-dependent.

When looking in greater detail at individual genes, we found that ~30 % of the genes normally repressed in WT neurons by TTX were not repressed in EHMT1-deficient neurons (Figure 2.22A and 2.22C). This subset of genes can therefore be categorized as EHMT1-dependent. We performed GO enrichment analysis to gain insights into the functional properties of TTX responsive genes (Figure 2.22B). Genes down-regulated by TTX treatment are implicated in

A *Ehmt1#2* effect on WT (177 genes, $p<0.01$)



B TTX effect on WT (301 genes, $p<0.01$)

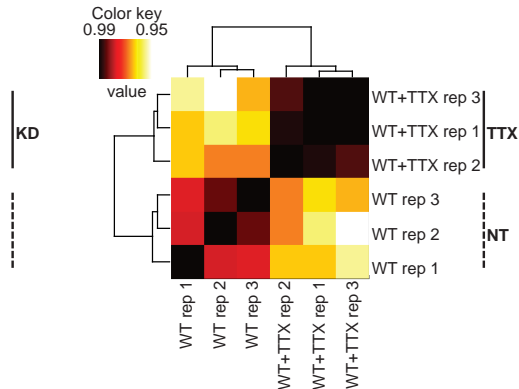
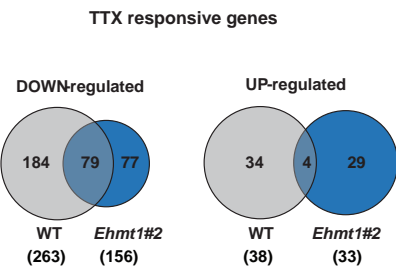


Figure 2.19. EHMT1-dependent gene repression program associated with synaptic scaling up. **A)** Clustering of Spearman correlations (complete linkage) partially segregates *Ehmt1#2* samples from WT samples. A total of 177 dysregulated genes (89 UP-regulated and 88 DOWN-regulated) are determined by use of the DEseq2 algorithm, which models the sequencing noise with a negative binomial distribution ($n=3$ biological replicates, $p<0.01$). Color code represents Spearman correlation. **B)** Clustering of Spearman correlations (complete linkage) segregates for the TTX samples (48h) from NT samples in WT neurons. A total of 301 differentially regulated genes (38 UP-regulated and 263 DOWN-regulated) are determined by use of the DEseq2 algorithm ($n=3$ replicates, $p<0.01$). Color code represents Spearman correlation.

A



B

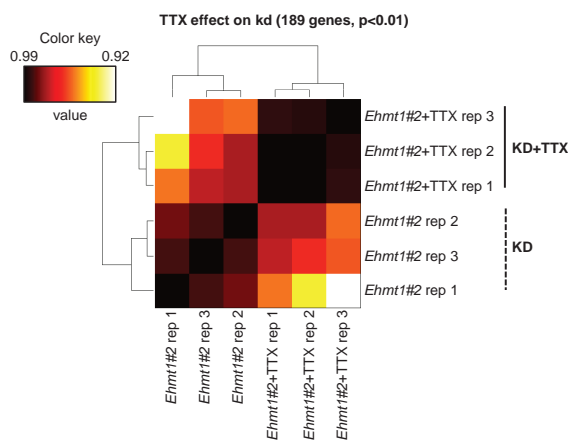
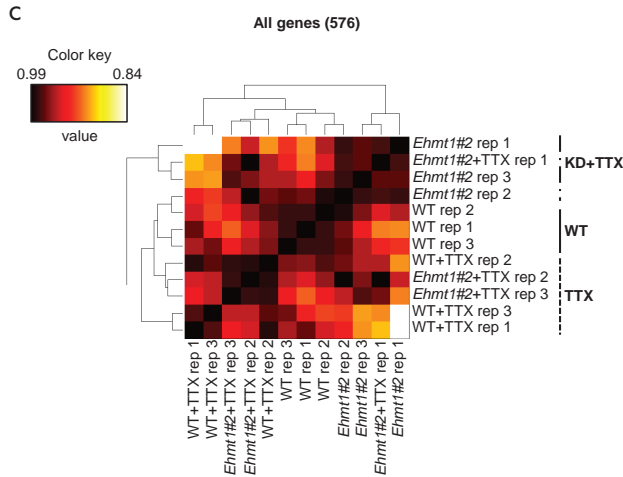


Figure 2.20. EHMT1 knock down gene repression profile respond differently to network activity deprivation. **A)** Venn diagrams of differentially expressed genes at 48h following TTX treatment in WT and *Ehmt1#2* transduced neurons, as determined by RNA-seq, $n=3$ replicates, $p<0.01$. Left, amount of downregulated genes: in gray WT, 263 genes (184+79), and in blue *Ehmt1#2*, 156 genes (77+79). The intersection consists of 79 common genes. Right, number of upregulated genes: in gray WT, 38 genes (34+4), and in blue *Ehmt1#2*, 33 genes (29+4). **B)** The intersection consists of 4 common genes. Clustering of Spearman correlations (Complete linkage) segregates untreated *Ehmt1#2* neurons from TTX-treated *Ehmt1#2* neurons ($n=3$ samples per condition, $p<0.01$). **C)** Clustering of Spearman correlations (Complete linkage) for the complete RNA-seq dataset and the complete set of responsive genes (576 genes associated with either of the treatments/conditions). The main division splits TTX treated from untreated neurons. ►



- Exception is the TTX treated *Ehmt1#2*-rep1 sample, which is clustered together with the untreated ones because of a stronger impairment of the TTX effect. Beyond the division in treated and untreated samples segregations are less clear mainly because the impact of *Ehmt1#2* over the basal transcriptome is mild.

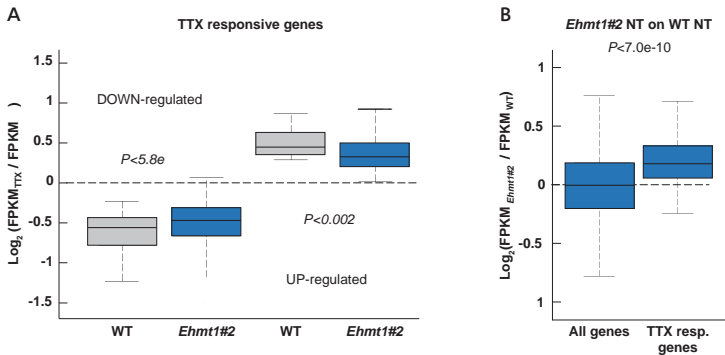


Figure 2.21. EHMT1 is required for the repression of a subset of genes after chronic TTX treatment. **A)** Boxplot representing the distribution of the $\log_2(fc)$ for TTX DOWN- and UP-regulated genes in WT and *Ehmt1#2* neurons. Wilcoxon signed-rank test, $n=3$, downregulation $p < 5.8e-13$ and upregulation $p < 0.002$. The upregulation p -value is lower because of the much smaller size of the gene set (38 vs. 263). Center line: median value; box limits: 25th and 75th percentile values; whiskers: maximum and minimum data points excluding the outliers; data points that are higher or lower than the 1.5 times the quartile (25th and 75th) values. **B)** Boxplot comparing the distribution of the $\log_2(fc)$ caused by *Ehmt1#2* transduction. The distributions show the genome-wide (all genes) and the subset of TTX-responsive genes (301 genes) effect in *Ehmt1#2* transduced neurons. One-way ANOVA, $n=3$, $p < 7.0e-10$.

a number of processes including: cholesterol biosynthesis ($p < 2e-6$), potassium ion channels ($p < 6e-7$), calcium signaling ($p < 4e-6$), and synaptic transmission ($p < 4e-7$). Interestingly, EHMT1-dependent and EHMT1-independent genes segregated in different functional groups. More precisely, *Ehmt1#2* neurons were unable to properly repress genes linked to ion channels ($p < 1.5e-5$), synaptic-vesicle ($p < 1.4e-4$) and calcium signaling ($p < 1.4e-5$). On the other end,

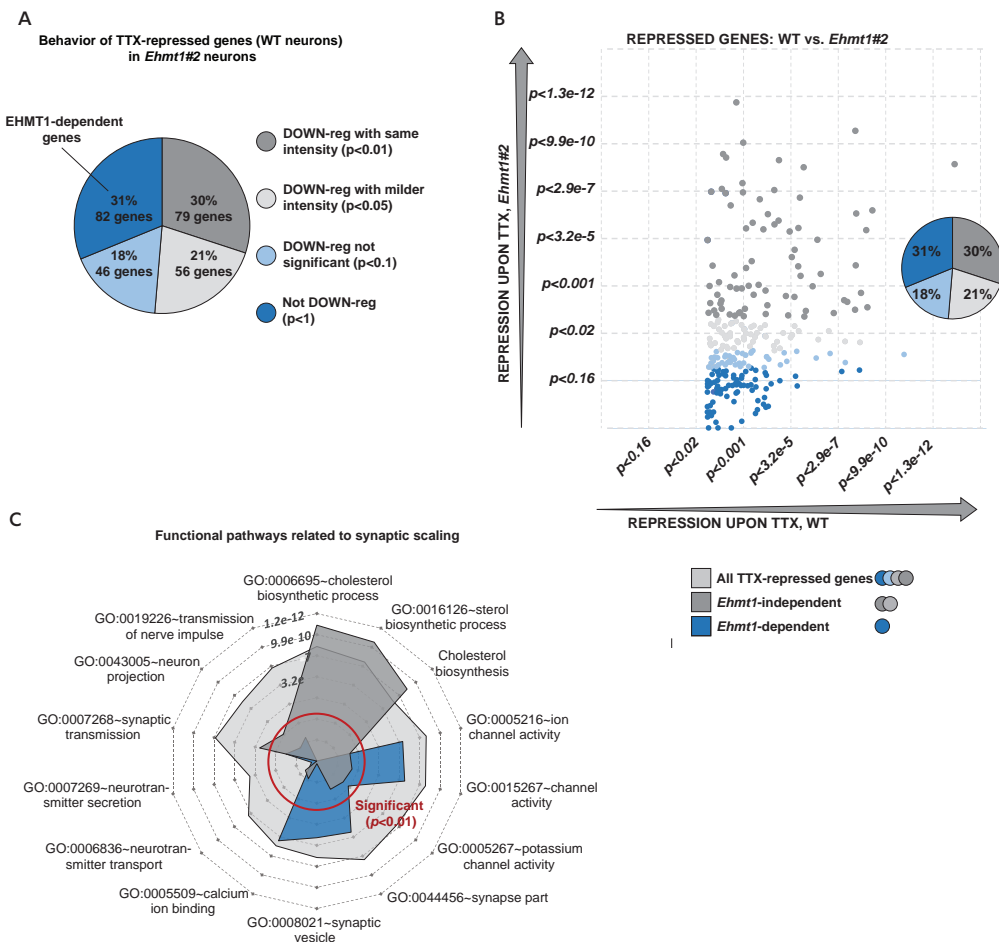


Figure 2.22. Behavior of EHMT1-dependent and independent repressed genes. **A)** Behavior of TTX-repressed genes (WT neurons) in *Ehmt1#2* neurons. The pie chart represents all the genes (263, $p < 0.01$) that are DOWN-regulated by TTX in WT neurons and divided in groups according to their DOWN-regulation in *Ehmt1#2* neurons (based on their p -value). Dark gray group encompasses those genes that in *Ehmt1#2* neurons are downregulated by TTX with the same strength as in WT neurons ($p < 0.01$). Bright gray area features genes that are downregulated in *Ehmt1#2*, but with milder strength ($p < 0.05$). Light blue delimits an intermediate area with uncertain behavior. Dark blue area isolates those genes that in *Ehmt1#2* neurons are not downregulated after TTX treatment. **B)** Scatter plots comparing the strength of transcriptional repression induced by TTX in WT and *Ehmt1#2* neurons. Each dot represents a gene. P -values ($n = 3$ samples per condition) on the axes are represented in Z score scale and decreasing numbers indicate stronger repression. Genes have been divided in four groups, associated with progressively impaired repression in *Ehmt1#2* conditions as compared to WT conditions. Essentially, 50% of the genes (pie chart, dark gray and light gray) seem significantly repressed also in *Ehmt1#2* conditions whereas 31% show (dark blue) a lack of repression. **C)** EHMT1-dependent and independent functional pathways related to homeostatic plasticity. The radar plot shows GO enrichment main terms and scores (Benjamini-adjusted p -values, represented in Z-score scale) for the 263 genes DOWN-regulated by TTX. Outer rings correspond to higher enrichment. Threshold for $p < 0.01$ is indicated by the red circle.

the modulation of the cholesterol biosynthesis was normal in *Ehmt1#2* neurons ($p < 5.7 \times 10^{-11}$), suggesting that this specific pathway does not seem to be dependent on EHMT1.

Chronic neuronal deprivation induces EHMT1/2-mediated repression of BDNF

Our RNA-Seq analysis revealed that *Bdnf* is misregulated in *Ehmt1#2*-transduced neurons. BDNF is a growth factor secreted from excitatory neurons that bidirectionally modulates homeostatic synaptic scaling and *Bdnf* (exon IX) repression is known to be required for synaptic scaling up (Rutherford et al., 1998; Desai et al., 1999; Lindskog et al., 2010). We therefore validated *Bdnf* IX mRNA expression, which is the most common *Bdnf* splicing variant (Aid et al., 2007) (Figure 2.23A). Together with *Bdnf* IX, we analyzed a set of EHMT1-dependent and -independent TTX-responsive genes, by performing real-time quantitative PCR (qPCR), including *Arc*, *Rab3b* and *Prnp* (Figure 2.23B). We were intrigued to find that in *Ehmt1#2* transduced neurons, basal *Bdnf* IX mRNA was high and it was not repressed by TTX (Figure 2.23A), indicating that EHMT1 is required for TTX-mediated repression of BDNF. Furthermore, UNC0638 also prevented *Bdnf* mRNA repression in neurons that were co-treated with TTX (Figure 2.23C).

Previous studies have shown that BDNF decreases in response to chronic network deprivation (Castrén et al., 1992; Karpova et al., 2010) and exogenous BDNF can block synaptic scaling up in pyramidal neurons (Desai et al., 1999; Rutherford et al., 1998). In addition, scavenging BDNF with TrkB-Ig was sufficient to induce synaptic scaling up in neuronal cultures. We therefore hypothesized that scavenging excess BDNF from *Ehmt1#2* transduced neurons with a soluble form of TrkB receptor (TrkB-FC) could restore plasticity. First, we confirmed that BDNF blocked synaptic scaling up when neurons were co-treated with TTX, whereas BDNF

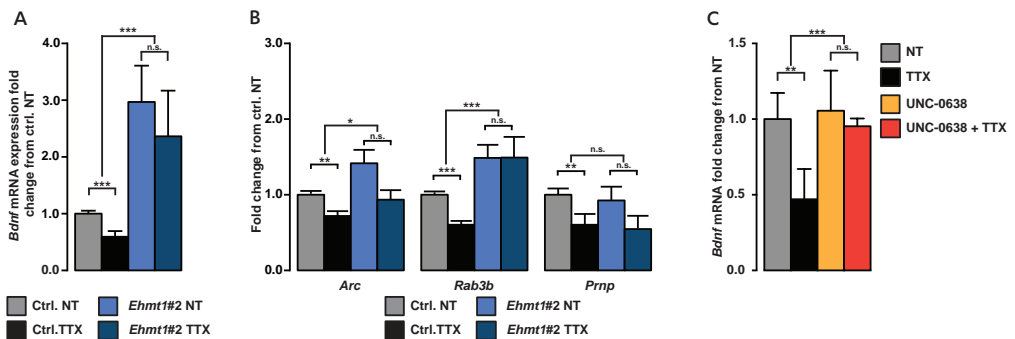


Figure 2.23. EHMT1-dependent BDNF mRNA repression in response to chronic TTX treatment. **A**) qPCR analysis of *Bdnf* exon IX mRNA levels in control vectors and *Ehmt1#2* transduced neurons treated with TTX (48h) and untreated. Data are represented as mean±SEM. ***, $p < 0.001$; n.s., non significant; $n = 6$; two-way ANOVA. **B**) Transcript levels analysis with quantitative PCR of *Arc*, *Rab3b* and *Prnp* genes from primary neuronal cultures transduced with control and *Ehmt1#2* vectors and treated or untreated with TTX. Data are represented as mean±SEM fold change from control NT; $n = 6$; *, $p < 0.05$; **, $p < 0.01$; ***, $p < 0.001$; $p < 0.01$; n.s., non significant; two-way ANOVA. **C**) *Bdnf* transcription levels in primary neurons treated with UNC0638 and/or TTX. Data are represented as mean±SEM; $n = 3$; *, $p < 0.01$; ***, $p < 0.001$; n.s., non significant; two-way ANOVA.

alone did not have any effect on mEPSC amplitudes (Rutherford et al., 1998) (Figure 2.24A). Applying TrkB-FC alone to the neuronal cultures was sufficient to augment mEPSC amplitudes (Figure 2.24A). Synaptic scaling up was restored in *Ehmt1* shRNA#2 transduced neurons when co-treated with TTX and TrkB-FC (Figure 2.24B). These results strongly suggested that synaptic scaling up is achieved at least in part through H3K9me2-mediated repression of BDNF.

Previous studies have shown that BDNF expression is regulated by H3K9me2 occupancy at *Bdnf* promoter IV in the nucleus *Accumbens* when stimulated by cocaine (Maze et al., 2010) and

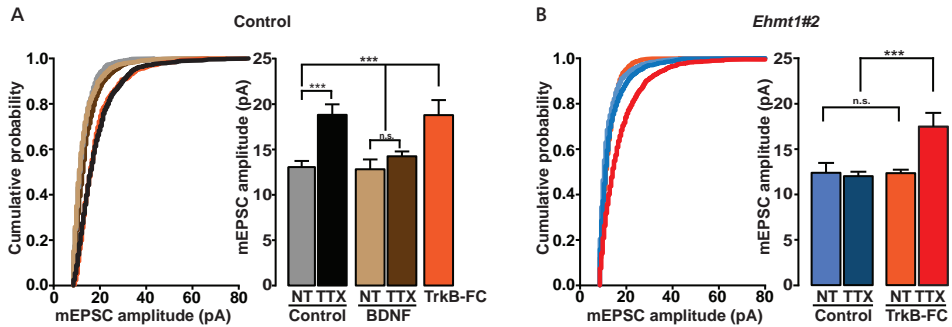


Figure 2.24. EHMT1 and EHMT2 repress BDNF expression to scale up synapses. **A)** Cumulative plots and mEPSC amplitude bar graphs of control neurons in conditions as indicated: untreated (NT), TTX, BDNF (25 ng/ml), BDNF+TTX or TrkB-FC (500 ng/ml). All drugs were added for 48h. Data are represented as mean±SEM. ***, $p<0.001$; n.s., non significant; $n=10$; one-way ANOVA. **B)** Cumulative plots and mEPSC amplitude bar graphs of *Ehmt1*#2 transduced neurons, in conditions as indicated: untreated (NT), TTX or TrkB-FC (500ng/ml) (48h). Data are represented as mean±SEM. ***, $p<0.001$; n.s., non significant; $n=10$; two-way ANOVA.

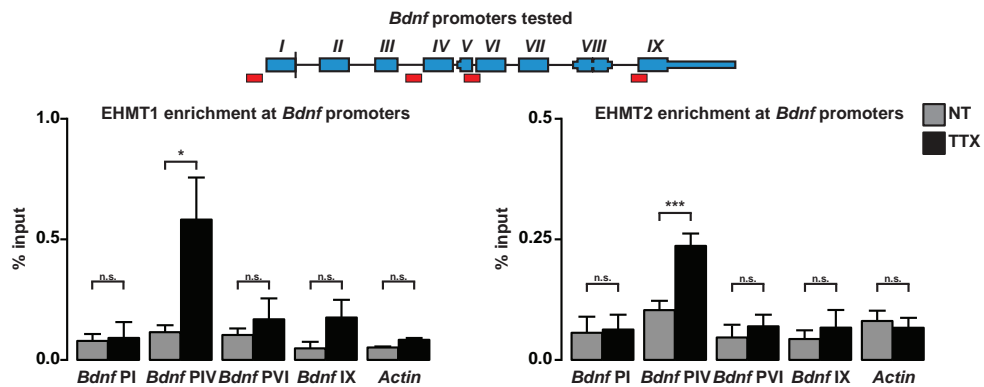


Figure 2.25. EHMT1 and EHMT2 are specifically enriched at *Bdnf* promoter IV in response to chronic network deprivation. Chromatin immunoprecipitation with EHMT1 and EHMT2 antibody and qPCR analysis of the specified *Bdnf* promoter I, IV, VI, exon IX and *Actin* promoter from WT neurons treated with TTX (48h) and not, expressed as EHMT1 or EHMT2 % input recovery. Data are represented mean as mean±SEM, $n=4-4$; *, $p<0.05$; ***, $p<0.001$; n.s., non significant; t-test. Above the bar graphs, *Bdnf* gene structure is depicted. Each blue box represents an exon, while the red boxes indicate the promoter sequences analyzed and their position within the rat *Bdnf* gene.

at *Bdnf* promoters I, IV and IXa in primary rat cortical neurons when stimulated by nicotine (Chase and Sharma, 2013). We immunoprecipitated chromatin (ChIP) with EHMT1 and EHMT2 antibodies, separately, and analyzed their enrichment at four *Bdnf* promoter regions. EHMT1 and EHMT2 occupancy was specifically enriched at *Bdnf* promoter IV after TTX treatment (Figure 2.25).

Next, we performed H3K9me2 ChIP-qPCR and confirmed that in TTX-treated WT neurons H3K9me2 occupancy was also increased at BDNF promoter IV, with no significant changes in other *Bdnf* promoter regions (Figure 2.26A). In contrast, H3K9me2 enrichment at the *Bdnf* promoter regions in *Ehmt1#2* transduced neurons was significantly lower compared to untreated WT neurons and lacked any kind of regulation after TTX treatment (Figure 2.26A). Accordingly, TTX did not alter H3K9me2 enrichment in either EHMT2-deficient or UNCO638-treated neurons (Figure 2.26B). Together, these results suggest that the EHMT1/2 complex modifies chromatin specifically at *Bdnf* promoter IV by increasing H3K9me2 during synaptic scaling up.

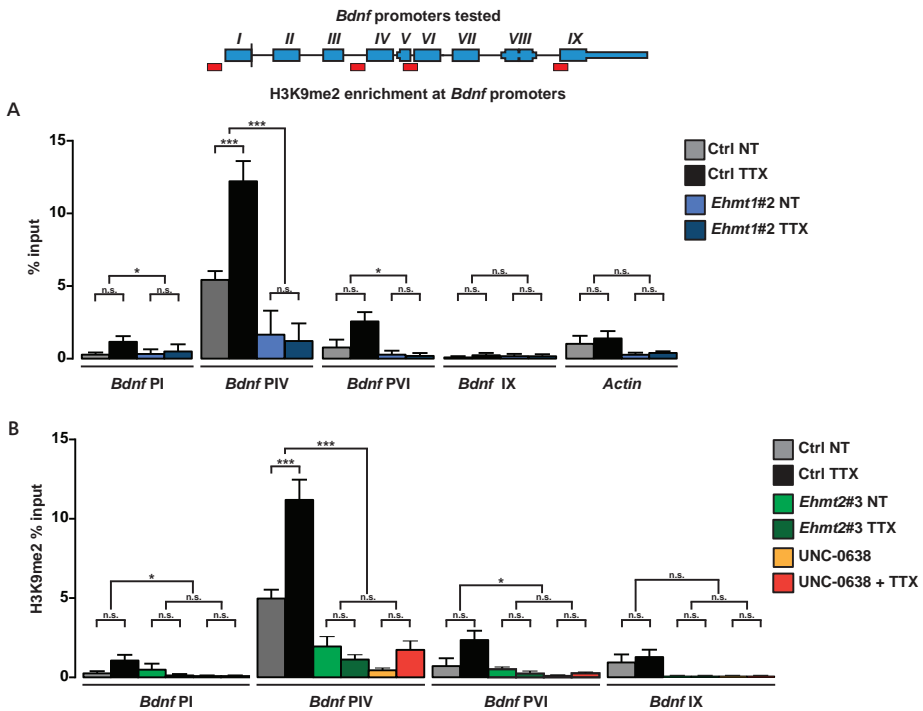


Figure 2.26. EHMT1 and EHMT2 are required to specifically catalyze H3K9me2 enrichment at *Bdnf* promoter IV after chronic TTX treatment. **A)** Chromatin immunoprecipitation with H3K9me2 and qPCR analysis of the specified *Bdnf* promoter I, IV, VI, exon IX and *Actin* promoter from WT and transduced with *Ehmt1#2* neuronal cultures, untreated (NT) or TTX-treated (48h), expressed as H3K9me2 % input recovery. n=8-8 **B)** Chromatin immunoprecipitation with H3K9me2 and qPCR analysis of the specified *Bdnf* promoter I, IV, VI, exon IX promoter from primary neuronal cultures transduced with control vector, *Ehmt2#3* or treated with UNCO638 in untreated (NT) or TTX-treated condition, expressed as H3K9me2 % input recovery. n=8-4-4 Data are represented as mean±SEM; *, $p<0.05$; ***, $p<0.001$; n.s., non significant; two-way ANOVA. Above the bar graphs, *Bdnf* gene structure is depicted. Each blue box represents an exon, while the red boxes indicate the promoter sequences analyzed and their position within the rat *Bdnf* gene.

EHMT1 is required for homeostatic synaptic scaling *in vivo*

Synaptic scaling can be induced in mice by ≥ 2 days of light deprivation (Desai et al., 2002; Goel et al., 2011; Maffei and Turrigiano, 2008). Light deprivation paradigms cause scaling up at glutamatergic synapses of layer II/III pyramidal neurons in the primary visual cortex (V1) of p21 and adult mice (Goel and Lee, 2007). This suggests that synaptic scaling plays a critical role in experience-dependent development. We evaluated H3K9me2 fluorescence and mEPSCs in V1 after 3 days of light deprivation (dark-reared (DR)), comparing wild type (WT) to *Ehmt1*^{-/-} mice, since the *Ehmt1*^{-/-} mouse recapitulates core features of Kleefstra syndrome (Balemans et al., 2013; 2014; 2010). H3K9me2 fluorescence was significantly higher in NeuN-positive V1 layer II/III cells of WT DR mice (Figure 2.27A and 2.27B). In contrast, H3K9me2 was not significantly different between normal reared (NR) and DR *Ehmt1*^{-/-} mice (Figure 2.27A and 2.27B).

In addition, basal H3K9me2 levels were significantly lower in *Ehmt1*^{-/-} mice, compared to WT. These data support our observations in primary cortical neurons, where chronic activity deprivation induces an EHMT1-dependent increase in neuronal H3K9me2.

To evaluate the effect of light deprivation on synaptic strength, we recorded mEPSCs in layer II/III pyramidal neurons from acute slices of V1. As previously shown (Desai et al., 2002; Goel et al., 2011; Maffei and Turrigiano, 2008), mEPSC amplitudes increased significantly in WT DR mice (Figure 2.28A and 2.28B). However, DR *Ehmt1*^{-/-} mice did not show an increase in mEPSC amplitudes compared to NR *Ehmt1*^{-/-} mice (Figure 2.28A and 2.28B). The basal amplitude of the mEPSCs was not different between the genotypes nor did we find any differences in the frequency of mEPSCs between the genotypes or between the treatments (Figure 2.28C).

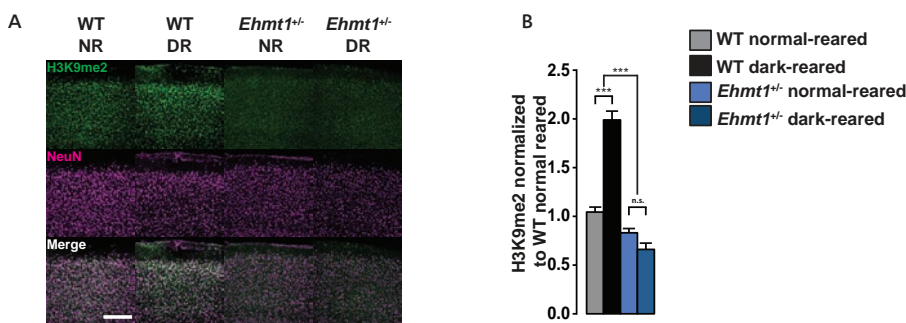


Figure 2.27. H3K9me2 levels increase in the primary visual cortex of light deprived mice. **A)** Representative confocal images of primary visual cortex showing H3K9me2 immunostaining and NeuN immunoreactive neurons from WT and *Ehmt1*^{+/-} dark-reared (DR) and normal-reared (NR) WT and *Ehmt1*^{+/-} mice. Scale bar, 200 μ m, lower panel. **B)** Quantification of H3K9me2 immunofluorescence in the primary visual cortex layer II/III expressed as mean \pm SEM fold change. WT and *Ehmt1*^{+/-} normal-reared (NR) and dark-reared (DR), 4 animals each, n=16 frames each. Data are represented as mean \pm SEM; lower and top-most ***, $p < 0.001$; n.s., non significant; two-way ANOVA.

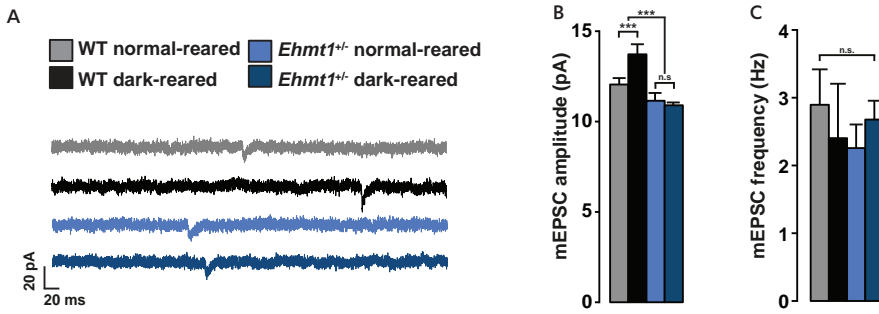


Figure 2.28. EHMT1 is required for synaptic scaling up *in vivo* in response to light deprivation in the mouse primary visual cortex. **A, B)** Mean mEPSC amplitude bar graph from whole-cell patch clamp recordings in the layer II/III in the primary visual cortex and representative traces (1s) from dark-reared (DR) and normal-reared (NR) WT and *Ehmt1*^{-/-} mice, n=11-16. Vertical scale 20pA, horizontal scale 20ms; Data are represented as mean±SEM; lower and top-most ***, *p*<0.001; n.s., non significant; two-way ANOVA. **C)** Mean mEPSC frequency bar graph from whole-cell patch clamp recordings in the layer II/III in the primary visual cortex from dark-reared and normal-reared WT and *Ehmt1*^{-/-} mice, n=11-16; Data are represented as mean±SEM; *, *p*<0.05; n.s., non significant; two-way ANOVA.

We showed *in vitro* that EHMT1 is required for synaptic scaling up and increases H3K9me2 at *Bdnf* promoter IV (Figure 2.25 and 2.26). We next tested whether this was also the case *in vivo*. To this end, we measured mRNA expression (qPCR) and H3K9me2 enrichment (ChIP-qPCR) in V1 from NR or DR WT and *Ehmt1*^{-/-} mice (Figure 2.29A and 2.29B). Dark rearing did not affect *Ehmt1* mRNA expression in WT mice, which was significantly lower in the *Ehmt1*^{-/-} mice (Figure 2.29A). Instead, *Ehmt2* mRNA expression increased significantly in DR WT mice (Figure 2.29A). Importantly, we found that dark rearing downregulated *Bdnf* mRNA expression in WT mice, confirming previous observations (Karpova et al., 2010). *Bdnf* mRNA downregulation was also associated with an increase in H3K9me2 at *Bdnf* promoter IV (Figure 2.29B). In contrast, DR *Ehmt1*^{-/-} mice were unable to repress *Bdnf* expression (Figure 2.29B) and did not show an increase in H3K9me2 at *Bdnf* promoters I, IV and VI (Figure 2.29D). In accordance with our *in vitro* data (Figure 2.23), *Rab3b* and *Arc* mRNA were significantly downregulated in DR WT mice but not in DR *Ehmt1*^{-/-} mice (Figure 2.29C). In contrast, *Prnp* expression was significantly downregulated irrespective of the genotype, indicating that *Prnp* regulation is independent of EHMT1 activity (Figure 2.29C). Similar to *Bdnf*, we found that *Rab3b* mis-repression in *Ehmt1*^{-/-} mice correlated with insufficient H3K9me2 enrichment at the *Rab3b* promoter (Figure 2.29D), suggesting that *Rab3b* expression depends on H3K9me2. This was not the case for *Arc* (Figure 2.29D). Finally, we did not find any significant changes in H3K9me2 levels at the *Actin* promoter, confirming the specificity of our results (Figure 2.29D).

These results provide evidence that EHMT1 is required for homeostatic scaling up after sensory deprivation *in vivo* and suggest that the increase in mEPSC amplitudes parallels the rise in H3K9me2 levels, which represses *Bdnf* expression.

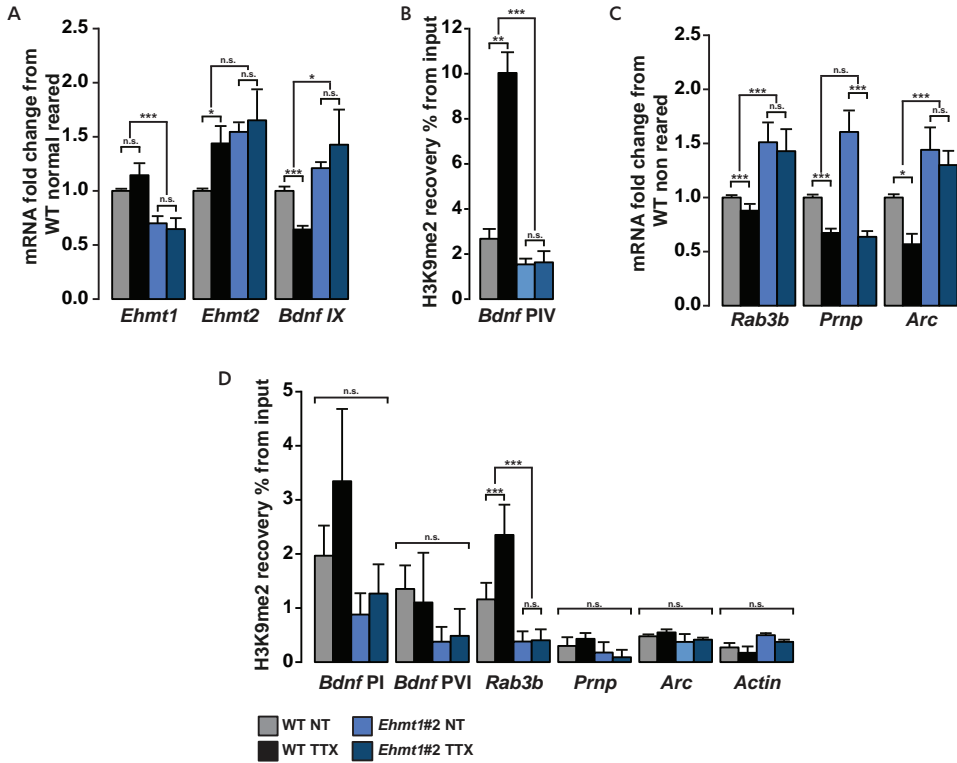


Figure 2.29. EHMT1-mediated gene expression and H3K9me2 levels regulation after light deprivation in the mouse primary visual cortex. **A**) mRNA expression analysis in the primary visual cortex from dark-reared (DR) and normal-reared (NR) WT and *Ehmt1*^{-/-} mice (n=6-6) of *Ehmt1*, *Ehmt2*, and *Bdnf IX*. Data are represented as mean±SEM; lower and top-most *, *p*<0.05, **, *p*<0.01, ***, *p*<0.001; n.s., non significant; n=6-6; two-way ANOVA. **B**) Chromatin immunoprecipitation with H3K9me2 and qPCR analysis of the specified *Bdnf* promoter IV from WT and *Ehmt1*^{-/-} mice, dark-reared (DR) and normal-reared (NR), expressed as H3K9me2 % input recovery. Data are represented as mean±SEM, n=6-6; lower and top-most *, *p*<0.05; ***, *p*<0.001; n.s., non significant; two-way ANOVA. **C**) mRNA expression analysis in the primary visual cortex from dark reared and non WT and *Ehmt1*^{-/-} mice of *Rab3b*, *Prnp*, and *Arc*. Data are represented as mean±SEM, n=6-6; *, *p*<0.05, **, *p*<0.01, ***, *p*<0.001; n.s., non significant; two-way ANOVA. **D**) Chromatin immunoprecipitation with H3K9me2 and qPCR analysis of the specified *Bdnf* promoter I, VI, *Rab3b*, *Prnp*, *Arc* and *Actin* promoters from WT and *Ehmt1*^{-/-} mice, dark reared (DR) and non reared (NR), expressed as H3K9me2 % input recovery. Data are represented as mean±SEM, n=6-6; *, *p*<0.05; ***, *p*<0.001; two-way ANOVA.

DISCUSSION

Role of EHMT1 and EHMT2 in homeostatic plasticity

In this study, we provide several lines of evidence for the requirement of EHMT1 and EHMT2 for synaptic scaling up. First, sustained chronic deprivation or activation in primary cortical neurons increased or decreased H3K9me2 levels, respectively. Similarly, chronic visual deprivation resulted in increased H3K9me2 levels in layer II/III of the mouse visual cortex. Second, the changes in H3K9me2 were pivotal for the functional expression of synaptic scaling since

genetic or pharmacological blockade of EHMT1/2 *in vitro* prevented the increases in H3K9me2, mEPSC amplitudes and synaptic expression of AMPA receptors. Furthermore, visual deprivation did not cause synaptic scaling up in *Ehmt1*^{-/-} mice. Third, EHMT1 and EHMT2 occupancy as well as H3K9me2 deposition were increased at *Bdnf* promoter IV after chronic activity suppression. Consequently, loss of EHMT1 or EHMT2 prevented *Bdnf* repression during synaptic scaling up. Together our data indicate that EHMT1 and EHMT2 comprise a repressive epigenetic complex that is engaged during synaptic scaling up.

Specifically, we found that chronic activity suppression upregulated EHMT2 protein levels, leading to more EHMT1/2 complex. Previous studies showed that H3K9me2 is catalyzed by the EHMT1-EHMT2 heteromer and is enriched at the promoters of silenced genes (Tachibana et al., 2002). A direct correlation between EHMT1/2 expression, H3K9me2 and gene repression was shown in studies where chronic cocaine abuse decreased EHMT1 and EHMT2 levels in the nucleus *Accumbens* and this correlated with reduced H3K9me2 (Maze et al., 2010; Feng et al., 2014). Conversely, they also showed that increasing EHMT1 and EHMT2 expression by pharmacologically inhibiting HDAC1/2 with MS-275 in combination with cocaine treatment or by site-directed targeting zinc finger proteins fused with EHMT2 at the *ΔfosB* promoter, caused an increase in global and site specific H3K9me2 levels, respectively (Kennedy et al 2013; Heller et al., 2014). Unlike other repressive marks, H3K9me2 does not correlate with a terminally repressed state. Rather it functions as a permissive tag to recruit a machinery that adds more stable repressive markers such as H3K9me3, H3K27me3 and DNA methylation through HP1 recruitment (Mozzetta et al., 2014; Rothbart and Strahl, 2014; Yearim et al., 2015). Taken together a picture is emerging in which H3K9me2 could act as an epigenetic mark that represents the activity state of a neuronal network and could serve as a general mechanism for poising a state in the genome in a “ready to repress” mode. The H3K9me2 can thus be viewed as a dynamic regulatory histone mark as opposed to only a mark for heterochromatin.

EHMT1 contributes to a genomic repressive program required for scaling up synapses

Consistent with previous studies, we found that 48h of activity suppression mainly resulted in gene repression (Bateup et al., 2013b). Interestingly, in EHMT1-deficient neurons, the set of genes implicated in synaptic scaling showed aberrantly high basal expression and misregulated expression after TTX treatment. Essentially, there were fewer repressed genes compared to control neurons. GO analysis showed that the misregulated genes clustered in functional groups related to ion channel activity, potassium channel activity, synaptic vesicles and calcium ion binding, suggesting that EHMT1 regulates these synaptic-scaling related pathways. BDNF is a central mediator of homeostatic excitatory synaptic plasticity *in vitro* and *in vivo* (Rutherford et al., 1998; Desai et al., 1999). Although *Bdnf* repression has been linked to synaptic scaling up, its transcriptional and epigenetic regulation has not been resolved (Rutherford et al., 1998; Yu et al., 2015). We show that EHMT1 and EHMT2 are both required to repress *Bdnf* expression during synaptic scaling up. Furthermore, we show that both are recruited specifically to *Bdnf* promoter IV after TTX treatment, leading to increased H3K9me2 at this promoter region,

in vitro and *in vivo*. EHMT1 and EHMT2 are recruited to chromatin via their ankyrin repeats and anchor to histone H3 N-terminals containing H3K9me1-2 (Collins et al., 2008). Interestingly, EHMT1 has a higher affinity for H3K9me1 compared to EHMT2. Since we found that only EHMT2 but not EHMT1 protein levels increased after TTX, we propose a model in which EHMT1 serves as a scaffold, and during chronic network inactivity, EHMT1 may increase its association with EHMT2. Using co-IP experiments, we found that EHMT1 interacts significantly more with EHMT2 after TTX, supporting the above scenario. However, we cannot exclude that other mechanisms, including PTMs, contribute to enhanced EHMT1/2 activity.

An interesting finding from our studies is that scavenging BDNF excess in conditions of network deprivation restored the ability to scale up synapses in EHMT1-lacking cortical neurons. However, in contrast to controls, we could not increase mEPSC amplitudes by scavenging BDNF from untreated *Ehmt1* knockdown neurons. This may be caused by disengagement of parallel signaling pathways normally recruited in conditions of lowered intracellular calcium concentration, therefore leading to a failure in synaptic scaling up in the *Ehmt1* knockdown neurons. In addition, *Bdnf* levels are likely affected by other epigenetic mechanisms, such as DNA methylation and the activity of DNA methylation binding proteins, both of which rely on histone modifications (Yu et al., 2015). This might explain why *Bdnf* upregulation was less pronounced in normally reared *Ehmt1*^{-/-} mice compared to neurons *in vitro*, and might function as a compensatory mechanism to keep *Bdnf* expression within a normal range during development.

Another intriguing possibility is that EHMT1/2 cooperates with the Rett syndrome related protein MECP2 to repress gene transcription (Noh et al., 2012; Subbanna et al., 2014). MECP2 is also required for synaptic scaling (Blackman et al., 2012; Chao et al., 2007 and Qiu et al., 2012). A recent study suggests that MeCP2 is involved in the repression of long genes, >100 Kb. Interestingly, the same authors showed an overlap in the long genes that were misregulated in DNMT3A and MeCP2 knock-down mice (Gabel et al., 2015; Guo et al., 2014). Elucidation of a parallel action would be interesting to trace a potential cooperation between EHMT1/2 and MeCP2 in the repression of genes required for synaptic scaling up based on their gene body length.

Other genes that deserve attention are *Arc* and *Rab3b*. Both genes were repressed during synaptic scaling up, but not in EHMT1 lacking conditions. Although *Arc* mRNA levels failed to be repressed in EHMT1-deficient neurons, our experiments did not show any regulation of H3K9me2 levels at the promoter region of *Arc*. This suggests that *Arc* is only indirectly regulated by EHMT1, potentially via BDNF (Bateup et al., 2013b; Ji et al., 2010; Shepherd et al., 2006). On the contrary and similar to *Bdnf*, the changes in H3K9me2 at the *Rab3b* promoter were in line with a direct regulation of *Rab3b* by EHMT1, during synaptic scaling. Interestingly, at the *Drosophila* neuro muscular junction (NMJ), *Rab3b* has been suggested to facilitate homeostatic up-regulation of presynaptic strength at a late stage of synaptic vesicle exocytosis by relieving an inhibitory control over homeostatic changes (Müller et al., 2011). In mammals *Rab3b* is enriched presynaptically at inhibitory synapses where it is required for LTD of hippocampal inhibitory synapses (Tsetsenis et al., 2011) and thus could potentially be involved in scaling of gabaergic synapses during homeostatic plasticity.

Further studies should be addressed to characterize the full complement of epigenetic events that characterize synaptic scaling. In this regard sequencing for multiple histone modifications by analyzing in parallel different histone markers at different gene regulatory elements could provide further information of how the genome rearranges gene transcription in conditions of chronic deprivation in order to scale up synapses (Sun et al. 2012; Feng et al., 2014).

Role of EHMT1 in Kleeftsa syndrome

Although loss of function of EHMT1 has directly been associated to Kleefstra syndrome, the nature of the synaptic deficits underlying the neurological symptoms has remained unclear. Previously we found that LTP was unaffected in *Ehmt1*^{+/-} mice. We showed that pyramidal CA1 hippocampal neurons of *Ehmt1*^{+/-} mice had significant reductions in spine density, number of mature spines and dendritic arborization, indicating a post-synaptic deficit (Balemans et al., 2013). Decreased mEPSC frequency and increased paired-pulse facilitation indicated a presynaptic locus of action for EHMT1. In our current study, we found normal basal synaptic transmission in primary cortical neurons after EHMT1 knockdown and in layer II/III neurons from acute slices of *Ehmt1*^{+/-} mouse primary visual cortex. The discrepancies may derive from altered homeostatic regulation during development and/or could be attributable to brain region differences (Gupta-Agarwal et al., 2012; 2014).

Unlike Hebbian plasticity, homeostatic plasticity has not been shown to directly influence learning and memory. However, the inability of a neuronal network to adapt to long-lasting changes in activity might lead to imbalances during development. In this way, loss of EHMT1/2 function could dynamically alter the responsiveness of a neuronal network to certain stimuli (Kennedy et al., 2013; Maze et al., 2010) and affect a wide range of cognitive functions.

MATERIAL AND METHODS

Electrophysiology

Whole-cell voltage clamp recordings were performed as previously described (Nadif Kasri et al., 2011). In brief, for acute slices, mice (p23, *Ehmt1*^{+/-} and *Ehmt1*^{-/-}) of both genotypes were anesthetized with isoflurane prior decapitation. 350 μ m thick coronal slices were cut using a microtome (HM650V, Thermo Scientific) in ice cold artificial cerebrospinal fluid (ACSF) containing: NaCl 87 mM; Glucose 11 mM; Sucrose 75 mM; KCl 2.5 mM; NaH₂PO₄ 1.25 mM; CaCl₂ 0.5 mM; MgCl₂ 7 mM; NaHCO₃ 26 mM continuously oxygenated with O₂ 95%/CO₂ 5% and incubated for 1h at 32°C after which they were allowed to cool down to room temperature (RT). For recordings, acute slices or primary cortical neurons attached to glass coverslips were transferred to the recording setup and incubated in recording ACSF containing: NaCl 124 mM, NaH₂PO₄ 1.25 mM, KCl 3 mM, NaHCO₃ 26 mM, Glucose 10 mM, CaCl₂ 2 mM, MgCl₂ 1 mM at continuously oxygenated with O₂ 95%/CO₂ 5% at 30°C. Cells were visualized with an upright microscope (Olympus). Patch pipettes (5-7 M Ω) were made from borosilicate glass capillaries and filled with intracellular solution containing: CsMeSO₃ 115 mM; CsCl 20 mM; HEPES 10 mM; MgCl₂ 2.5 mM; Na₂ATP 4 mM; NaGTP 0.4 mM; Na-Phosphocreatine 10 mM; EGTA 0.6 mM (pH 7.2-7.3, 285-295 mOsm).

Neuronal cultures and treatments

Low-density primary cortical neuronal cultures were prepared from embryonic day 18 (E18) rat pups as previously described (Nadif Kasri et al., 2011). Cell cultures were incubated in Neurobasal media (GIBCO-Invitrogen) supplemented with B27, penicillin, streptomycin, and L-glutamine at 37°C in CO₂ 5%. Medium was half refreshed with unconditioned culturing medium every third day until treatment, which coincided with last medium renewal. At days *in vitro* 11 (DIV 11) low-density primary cortical neuronal cultures were treated for 48h (unless specified differently), with TTX (1 µM, Tocris 1069), PTX (10 µM, Tocris 1128), nimodipine (5 µM, Tocris 0600), STO-609 (2 µM, Tocris, 1551), thapsigargin (1 µM, Tocris 1138), CNQX (40 µM, Tocris 0190), APV (100 µM, Tocris 0106), UNCO638 (85 nM, Sigma-Aldrich U4885), MS-275 (5 µM, Sigma-Aldrich EP-S002) TrkB-FC (500 ng/ml, R&D systems 688-TK) and BDNF (25 ng/ml, PeproTech 450-02). Amaxa Rat Nucleofector kit (Lonza, VSPI-1003) was used to transfect primary neurons with shRNAs prior plating (DIV 0) as described by manufacturer. In different set of experiments neurons were transduced with lentiviruses co-expressing GFP and shRNAs.

Immunocytochemistry

Primary neurons were fixed with paraformaldehyde 4%/ sucrose 4% in phosphate buffered saline (PBS 1X, Sigma Aldrich, P5493-1L) at 37°C for 15min. After fixation cells were washed and permeabilized with PBS 1X and Triton 0.1%. Cells were blocked in normal goat serum (NGS) 10% and triton 0.05%. Primary antibodies were incubated in PBS 1X with NGS 5% and Triton 0.01% overnight at 4°C. Secondary antibody incubation was done the next day with Alexa-488 and Alexa-568 (Molecular Probes) for 1h at room temperature. Cells were washed in PBS 1X to remove secondary antibody excess and finally mounted using DAKO (DAKO, S3023) fluorescent mounting medium and stored at 4°C. Signal intensity was measured with ImageJ and data was normalized to untreated condition (NT). Primary antibodies: H3K9me2 (1:500, Millipore 07-441); H3K4me3 (1:500, Abcam ab8580); H3K4me1 (1:500, Diogenode CS-037-100); H3K27me3 (1:500, Millipore 07-449); MAP2 (1:2000, Sigma-Aldrich M4403); EHMT1 (1:100, Abcam ab41969); EHMT2/EHMT2 (1:100, Cell Signaling Technology 3306); PSD-95 (1:50, Thermo Scientific MA1-045); VGLUT (1:2000, Synaptic Systems 135302). Secondary antibodies: Goat anti-Mouse Alexa Fluor® 488 (1:2000, Invitrogen A11029), Goat anti-Mouse Alexa Fluor® 568 (1:2000, Invitrogen A11031), Goat anti-Mouse Alexa Fluor® 647 (1:2000, Invitrogen A21236), Goat anti-Rabbit alexa fluor 488 (1:2000, Invitrogen A11034), Goat anti-Rabbit Alexa Fluor® 568 (1:2000, Invitrogen A11031).

Surface AMPA receptor labeling and quantification

GluA1 (1:50, Millipore MAB2263) and GluA2 (1:50, Millipore MAB397) antibodies were diluted in culturing medium and incubated to primary neurons for 10 min in the incubator at 37°C and CO₂ 5% (Zhou et al., 2008). Cells were fixed and stained as described above. Data was acquired from confocal images, analyzed by using ImageJ plug-in Foci picker 3D and 2D (Du et al., 2011), and normalized to untreated control vector. Two-way ANOVA with Bonferroni comparison

was used to compare between genotypes (control and EHMT1 knockdown) and the treatment (NT vs. TTX).

Neurite outgrowth assay

Neurons were prepared and electroporated at DIV 0 with constructs expressing shRNA against *Ehmt1* or *Ehmt2*. Neurons were imaged every 4h for 5 days using the Incucyte live cell imaging system (Essen Bioscience). Phase contrast images of the GFP positive neurons were analyzed online using a custom neurite outgrowth detection program, Neurotrack (Essen Bioscience).

Immunohistochemistry

Dark-reared and normal-reared mice were anaesthetized with Isofluran and transcardially perfused with PFA 4%/sucrose 4% in PBS 1X. Brains were removed and kept overnight in PFA 4%/sucrose 4% in PBS 1X at 4 °C. 60 µm thick coronal slices in correspondence of primary visual cortex were derived using a vibratome V1000S (Leica) in ice-cold PBS. Free-floating slices were stored in PBS with 0.01% sodium-azide 0.01% at 4 °C prior IHC procedure. Slices were washed and permeabilized in TBS 1X with Triton 0.1% and blocked with 10% NGS 10%, NDS 10% for 2h at RT. Primary antibodies H3K9me2 (1:200, Millipore 07-441) and NeuN (1:300, Millipore ABN91) in TBS 1X-Triton 0.1% with NGS 5% and NDS 5% were incubated for 3 days at 4 °C on a horizontal shaker. Tissue was washed and incubated with secondary antibodies (Goat anti-Rabbit Alexa fluor 568; 1:1000, Invitrogen A11031 and Donkey anti-Chicken; 1:300, Jackson Immuno Research Laboratories 703-545-155) in NGS 5%, NDS 5% in TBS 1X-Triton 0.1% for 2h on a horizontal shaking plate at RT in darkness. Free-floating slices were then washed with TBS 1X and mounted on a glass slide for imaging. Intensity signals were measured from confocal images. Two-way ANOVA with Bonferroni comparison was used to compare between genotypes (*Ehmt1*^{+/+} and *Ehmt1*^{+/-}) and visual manipulation.

DNA constructs and virus production

For RNAi knockdown experiments, DNA fragments encoding short hairpin RNAs (shRNAs) directed against mouse/rat *Ehmt1* mRNA (*Ehmt1*#1: 5'-GGTGATTGAGATGTTTAA-3'; *Ehmt1*#2: 5'-GCCTCTTACTGGTGTCTTCT-3'; *Ehmt2*#1: 5'-GGGTGGACTCTGACAGCAA-3', *Ehmt2*#2: 5'-CCCAGAGGACTATAAGTA-3'; *Ehmt2*#3: 5'-CGAAGCTCTAGCTGAACAG-3' and control shRNA (*src*#1: 5'-GCTCACCCTTCTACTCTC-3') were cloned into the pSuper vector (Oligoengine) and pTRIPAU3-EF1α-EGFP lentiviral vector (Janas et al., 2006; Kasri et al., 2008). Empty vector was used as control vector. Mouse *Ehmt1* cDNA over-expression was produced by combining two overlapping mRNA clones: D430022D24 containing mRNA AK084994 and IRAKp961B18195Q containing mRNA BC089302 under the control of a CMV promoter. Lentiviral supernatants were prepared, concentrated, and tittered as described (Janas et al. 2006; Kasri et al. 2008). Briefly, lentiviruses were generated by co-transfecting the transfer vector, the HIV-1 packaging vector Δ8.9, and the VSVG envelope glycoprotein vector into HEK293T cells, using calcium phosphate precipitation. Supernatants of culture media were collected 48h after transfection and centrifuged at 100,000x g to concentrate the viral vector. Viral particles were then stored at -80 °C until use.

Western blot and co-immunoprecipitation

Proteins extracts were separated by SDS-PAGE, transferred on nitrocellulose membranes (BioRad, 170-4158) and probed with antibodies against EHMT1 (1:7000, Abcam AB41969), EHMT2 (1:500, Cell Signaling C6H3), Arc (1:500, Synaptic systems 156003), H3K9me2 (1:1500, Millipore 07-441), Histone 3 (D1H2) (1:4000, Cell signaling 4499) and g-Tubulin (1:10000, Sigma-Aldrich T-5326). Proteins were then detected with horseradish peroxidase-conjugated goat anti-Mouse (1:8000, Jackson ImmunoResearch Laboratories 115-035-062) and goat anti-Rabbit (1:8000, Invitrogen G21234). Proteins were revealed with Super Signal West Femto and Pico ECL (Thermo Scientific, 34095 and 34080) and visualized with ChemiDoc Touch Imaging system (BioRad). Histone protein extraction was performed by using EpiQuick™ Total Extraction Kit (Epigentek, OP-0006-100). Nuclear and Cytoplasmic protein fractions were extracted EpiQuick™ Nuclear Extraction Kit I (Epigentek, OP-0002). Densitometric measures were acquired with Image lab 2.0 (Bio-Rad) and intensity signals were normalized to untreated condition. Unpaired student t-test was used to compare the two treatments (NT vs. TTX).

For co-immunoprecipitation experiments EHMT1 (5 µg, Abcam AB41969) or mlgG1k (5 µg, BD Pharmingen, 557273) antibodies were coupled to Protein A/G Plus-Agarose (12.5 µl beads, Santa Cruz Biotechnologies sc-2003) for 2h rotating at 4 °C. Whole protein extract from primary neurons were first obtained by cell lysis with lysis buffer (NaCl 300 mM; HEPES 50 mM pH=8; IGEPAL CA-630 1%; Sodium-Deoxycholate 0.1%; DTT 1 mM; protease inhibitors EDTA-free 1 mM, Roche) while coupling beads and antibodies. Coupled Ab-beads were extensively washed with Protein binding buffer (PBB) (NaCl 150 mM; HEPES 50 mM pH=8.0; IGEPAL CA-630 0.25%; DTT 1 mM) to remove unbound antibody in excess. Salt and IGEPAL concentration was reduced from protein extract with Low salt buffer (NaCl 150 mM, HEPES 50 mM pH=8.0, IGEPAL CA-630 0.25%; DTT 1 mM; protease inhibitors EDTA-free 1 mM). Subsequently, whole protein extract and Ab-beads complex were coupled and incubated overnight at 4 °C on a rotating wheel. After the beads-Ab-protein complex was extensively washed with PBB and washing buffer (NaCl 150 mM, HEPES 50 mM pH=8.0; DTT 1 mM), resuspended in Laemni buffer. Half of the sample was used for Western blot against EHMT1, the other half for Western blot against EHMT2.

Densitometric measures were acquired with Image lab 2.0 (Bio-Rad) and intensity signals were normalized to untreated condition. Unpaired student T-test was used to compare the two treatments (NT vs. TTX).

RNA-isolation primary cortical cultures

Total RNA was isolated from cultured neurons with NucleoSpin RNA (Macherey-Nagel 740955.50) according to the supplied protocol. Concentration and purity of the RNA samples was determined using Nano drop ND1000. Total RNA (500 ng) was reverse transcribed (RT) with iScript™ Reverse Transcription Supermix for RT-qPCR (Bio-Rad 170-8840) according to manufacturer instructions.

RNA-isolation from primary visual cortices

For qPCR in vitro and in vivo total RNA was obtained from either primary neuronal cultures or from biopsies of primary visual cortices by using QiAzol (Qiagen, 79306), followed by Phenol/Chloroform RNA extraction. Subsequently RNA was purified with RNeasy Lipid Tissue Mini Kit (Qiagen, 74804) and DNA digested with DNase (Qiagen, 79254). Retrotranscription was performed to obtain cDNA with iScript™ Reverse Transcription Supermix for RT-qPCR (Bio-Rad 170-8840) according to manufacturer instructions.

Whole genome RNA sequencing and analysis

2000 ng of Total RNA were treated with the Ribo-Zero rRNA Removal Kit (Human/Mouse/Rat; Illumina MRZH11124). Depleted RNA was precipitated 1h at -80 °C in three volumes of ethanol plus 1 µg of glycogen. RNA was then washed and resuspended in 36 µl of RNase free water. RNA fragmentation buffer (NEBNext® Magnesium RNA Fragmentation Module, E6150S) was added to the solution and the RNA was fragmented by incubation at 95 °C for 3min. Reverse transcription: cDNA first strand synthesis was performed with random examer primers. cDNA second strand synthesis was performed with dNTPs, to ensure strand specificity.

The RNA-seq library was synthesized with KAPA Hyper prep kit (KK8504): a treatment with USER enzyme (NEB, M5505L) was added to digest the unspecific strand. The libraries were pooled (4/lane) and sequenced on the illumina HiSeq, which yielded approximately 40 million single-end reads per sample. The RNA-seq libraries were mapped with GSNAP, gene expression counts were calculated with a custom C++ script and DEseq2 was used to call the dysregulated genes. The GO enrichments were calculated in the gene David website (<http://david.abcc.ncifcrf.gov/>) The Z-scores of Figure 2.22C were calculated by fitting the local distribution of the variable $\log_2(TTX_i/\text{untreated}_i)$ against the variable $\log_2(TTX_i+\text{untreated}_i)$, where TTX_i and untreated_i represent the number of tag counts for the i -th transcript. RNA-Seq data are deposited in GEO ID: GSE68960. <http://www.ncbi.nlm.nih.gov/geo/query/acc.cgi?acc=GSE68960>.

GEO data: Excel tables including the normalized read counts for all the samples, as well as the DEseq2 p -values for each of the comparisons. The normalized counts are found in the columns. The values in these columns represent the DEseq-normalized counts multiplied by 42 (bp coverage of one tag). Therefore, they represent the normalized total number of bp sequenced for each transcript. There are 5 pair-wise comparisons of expression and each has its table. WT_ttx and shrna_ttx for the study of ttx effect in WT samples or transduced samples. Startpoint_WT_shrna_VS_WT for the effect of shrna alone on WT neurons. Endpoint_ttx_shrna_VS_ttx for the effect of shrna on the TTX treated samples. Rattus_shrna_total_6vs_6_effect for the effect of shrna regardless to the TTX treatment. Gene David GO enrichments for the TT down-regulated genes (Down-reg), their shrna blocked subset (Blocked_shrna) and shrna independent subset (Common).

Chromatin immunoprecipitation (ChIP)

Cell cultures and primary visual cortices were cross-linked with formaldehyde to immunoprecipitate H3K9me2 at a final concentration of 1% for 9min at room temperature. For

EHMT1 and EHMT2 chromatin immunoprecipitation primary neuronal cultures were cross-linked priory with disuccinimidyl glutarate (DSG) 2 mM for 45min room temperature and followed by formaldehyde 1% for 9min at RT. Glycine 125 mM, was added to stop crosslink reaction. Cells were washed and harvested in PBS 1X with 1 mM protease inhibitors EDTA-free. Cells were then lysed in lysis buffer (Tris HCl 10 mM, pH=7.5; NaCl 10 mM; IGEPAL-CA630 0.2%; Triton 0.2%; EDTA 1 mM, pH=8.0; EGTA 0.5 mM, pH=8.0; protease inhibitors EDTA-free 1 mM) for 10min rotating at 4 °C. Pelleted nuclei were washed in buffer C (NaCl 150 mM; EDTA 1mM, pH=8.0; HEPES 50 mM, pH=7.6; protease inhibitors EDTA-free 1 mM) for 10min rotating at 4 °C and resuspended in sonication buffer (HEPES 20 mM, pH=7.6; SDS 1%; protease inhibitors EDTA-free 1 mM) and sonicated with Bioruptor Power-up (Diagenode) to shear DNA into 150-300bp fragments. Chromatin was precleared with Dynabeads Protein A and G (Life Technologies, 10003D and 10001D) for 2h rotating at 4 °C. Immunoprecipitated with H3K9me2 (2 µg/reaction, Abcam ab1220), EHMT1 (5µg/reaction, Abcam Ab41969) and EHMT2 (5 µg, Cell Signaling Technology 3306) overnight rotating at 4 °C. Beads were washed twice in buffer 1 (SDS 0.1%, sodium-Deoxycholate 0.1%; Triton 1.0%; NaCl 150 mM; EDTA 1 mM; EGTA 0.5 mM, pH=8.0; HEPES 20 mM), once in buffer 2 (SDS 0.1%; Sodium-Deoxycholate 0.1%; Triton 1.0%; NaCl 500 mM; EDTA 1 mM, pH=8.0; EGTA 0.5 mM, pH=8.0; HEPES 20 mM), once in buffer 3 (LiCl 250 mM; Sodium-Deoxycholate 0.5%; IGEPAL-CA630 0.5%; EDTA 1 mM, pH=8.0; EGTA 0.5 mM, pH=8.0; HEPES 20 mM), twice in buffer 4 (EDTA 1 mM, pH=8.0; EGTA 0.5 mM, pH=8.0; HEPES 20 mM) and eluted in elution buffer (SDS 1%; NaHCO₃ 0.1M) rotating at RT for 20min. Eluate was de-crosslinked in elution buffer with 24 µg proteinase-K and NaCl 200 mM for 4h at 65 °C and DNA material was cleaned with NucleoSpinâ Gel and PCR Clean-up (Macherey-Nagel) according to manufacturer instructions. DNA was resuspended in water and qPCR was performed. ChIP-qPCR results are expressed as percentage of IP/input signal (% input). Unpaired student T-test was performed to compare the NT and TTX % EHMT1 and EHMT2 recovery from input for each of the promoters separately. Whereas two-way ANOVA was used to compare % H3K9me2 recovery from input to compare between WT and *Ehmt1*#2 transduced neurons untreated and TTX-treated.

List of primers designed to amplify RAT promoter regions (ChIP)

Name	Sequence
<i>Bdnf</i> P I Fw	GTGCCTCTCGCCTAGTCATC
<i>Bdnf</i> P I Rev	CTGAGCCAGTTACGTGACCA
<i>Bdnf</i> P IV Fw	AGGGATTGGGGATAAACTAGACTC
<i>Bdnf</i> P IV Rev	CACGCAAGTCCCTGAACTC
<i>Bdnf</i> P VI Fw	GGAATTAGGGATACCCCAAGG
<i>Bdnf</i> P VI Rev	TTATTTAGCTCTTCGGTTGAGCTTC
<i>Bdnf</i> exon IXa Fw	TGGGTCACAGCGGCAGATAAAAAG
<i>Bdnf</i> exon IXa Rev	TAAGGGCCCGAACATACGATTGG
<i>Actin</i> Fw	CTCGAGCCATAAAAGGCAACT
<i>Actin</i> Rev	AAAATGCTGCACTGTGCGG

List of primers designed to amplify MOUSE promoter regions (ChIP)

Name	Sequence
<i>Bdnf</i> P I Fw	CAAAATAGGGCAGCGACTCT
<i>Bdnf</i> P I Rev	CTGAGCGAAAAGGTGTAGGC
<i>Bdnf</i> P IV Fw	TGTGGAGGTGGAGAAGAACA
<i>Bdnf</i> P IV Rev	CTCCAATCCCTCCATCTTCA
<i>Bdnf</i> P VI Fw	CTTTGTGTGGACCCTGAGGT
<i>Bdnf</i> P VI Rev	TGCAGTCCCACAACTTCTCA
<i>Rab3b</i> Fw	CAACCCATCTTCAGCCAGAG
<i>Rab 3b</i> Rev	TCGGATAAGAGCTGGCTCAC
<i>Actin</i> Fw	CTCGAGCCATAAAAGGCAACT
<i>Actin</i> Rev	AAAATGCTGCACTGTGCGG
<i>Prnp</i> Fw	GATCAGCAGACCGATTCTGG
<i>Prnp</i> Rev	ACGACGGAAGGCTGAGTG
<i>Arc</i> Fw	GGAGGAGCTTAGCGAGTGTG
<i>Arc</i> Rev	AGCATAAATAGCCGCTGGTG

Quantitative ChIP-qPCR (qPCR) Analysis

Each decrosslinked gDNA immunoprecipitated sample was amplified using SYBR Green (Promega) on the 7500 fast Real-time PCR system (Applied Bio-systems Life Technologies). Every reaction carried 3 μ l gDNA, 0.8 μ M primers in a final volume of PCR mix. Each cycle consisted of denaturation at 95 °C for 15s, annealing and extension at 60 °C for 60s. The primers used for this study are listed in table. For data analysis, the ratio between the dilutions of ChIP-ed material over the input times the amount in μ l loaded of input over ChIP-ed times 100 was used. As control *Actin* was used as a constitutively expressed gene to compare to a gene not regulated by either EHMT1, EHMT2 and H3K9me2. All data are expressed as mean \pm SEM, statistical comparisons were performed by t-test for EHMT1 and EHMT2 separately, and H3K9me2 two-way ANOVA was used to compare the treatments and the genetic manipulations used for this study. Below list of primers used for ChIP-qPCR to amplify rat and mouse promoter regions.

Quantitative PCR (qPCR) Analysis

Each cDNA sample was amplified using SYBR Green (Promega) on the 7500 fast Real-time PCR system (Applied Bio-systems Life Technologies). Every reaction carried 5 μ l cDNA, 0.8 μ M primers in a final volume of PCR mix. Each cycle consisted of denaturation at 95 °C for 15s, annealing and extension at 60 °C for 60s. The primers used for this study are listed in table. For data analysis Livak Method was used (Livak and Schmittgen, 2001), PPIA was used as an endogenous control (housekeeping gene) to normalize each sample. All data are expressed as mean \pm SEM, statistical comparisons were performed by two-way ANOVA. Below list of primers used for qPCR to amplify rat and mouse gene regions.

List of primers designed for qPCR experiments targeting RAT gene regions

Gene name	sequence
<i>Ehmt1</i> Fw	CTTGGACGCAGTGAAGTACC
<i>Ehmt1</i> Rev	CGTCATAGTGGCCTTTCTTG
<i>Ehmt2</i> Fw	ACGCGTACTCTGTGGATGAG
<i>Ehmt2</i> Rev	TCAGCTAGAGCTTCGACTTCAG
<i>Bdnf</i> exon IXa Fw	GAGAAGAGTGATGACCATCCT
<i>Bdnf</i> exon IXa Rev	TCACGTGCTCAAAAGTGTCAG
<i>Arc</i> Fw	ACGACACCAGGTCTCAAGC
<i>Arc</i> Rev	AGGCAGCTTCAAGAGAGGAG
<i>Rab3b</i> Fw	GCAGAGCAACTTGGGTTTGA
<i>Rab3b</i> Rev	TCTTATCGCAGATGGCGTCC
<i>Prnp</i> Fw	CCAAGCCGACTATCAGCCAT
<i>Prnp</i> Rev	GCTTTTTGCAGAGGCCAACA
<i>Ppia</i> Fw	AAGGGTTCCTCTTTCACAG
<i>Ppia</i> Rev	CCATTATGGCGTGTGAAGTC

List of primers designed for qPCR experiments targeting MOUSE gene regions

Gene name	sequence
<i>Ehmt1</i> Fw	AAGAGACCAAGCAGGATTGC
<i>Ehmt1</i> Rev	TGTGGAACCTTCATCAGCAG
<i>Ehmt2</i> Fw	CATGTCCAAACCTAGCAACG
<i>Ehmt2</i> Rev	GAAGTCACCTTCCCCAGATG
<i>Bdnf</i> exon IXa Fw	GCGCCCATGAAAGAAGTAA
<i>Bdnf</i> exon IXa Rev	TTCGATGACGTGCTCAAAAG
<i>Arc</i> Fw	ACCAGTGAAGAAGAGCAGAGC
<i>Arc</i> Rev	CCTTGAGACCTGGTGTCATTC
<i>Rab3b</i> Fw	TGGCCCCAGCTACAGATACT
<i>Rab3b</i> Rev	GTAGGAGGAGGGGCTTGTA
<i>Prnp</i> Fw	CCAAGGAGGGGGTATCCATA
<i>Prnp</i> Rev	CCCAGTCGTTGCCAAATGG
<i>Ppia</i> Fw	AAGGGTTCCTCTTTCACAG
<i>Ppia</i> Rev	CCATTATGGCGTGTGAAGTC

Histone methyltransferase enzymatic assay

Histone H3 lysine 9 methyltransferase activity of EHMT1/2 on H3K9me2 was measured using EpiQuik Histone Methyltransferase Activity/Inhibition Assay Kit (H3K9) (EpiGentek P-3003-1) following manufacturer instructions. An ELISA plate reader at 450 nm (Perkin Elmer Victor™

X3) was used to read the methyltransferase activity. The results were normalized against NT neurons and analyzed by unpaired student t-test.

Animals, genotyping and dark rearing.

For cell cultures, female Wistar Rat were used as described (Watabe-Uchida et al., 2006). For visual experience deprivation experiments we used *Ehmt1*^{+/-} heterozygous and *Ehmt1*^{+/+} wild type mice backcrossed in C57Bl6/J background (Balemans et al., 2010). P21 heterozygous and WT littermate mice were dark-reared in complete darkness for 3 days and compared to both genotypes normal-reared animals. All procedures involving animal experimentation were approved by the Animal Care Committee of the Radboudumc, The Netherlands, conforming to the guidelines of the Dutch Council for Animal Care and the European Communities Council Directive of 24 November 1986 (86/609/EEC).

Imaging

Confocal images were acquired using a Fluoview FV1000 confocal microscope (Olympus). Epifluorescent images were taken with Zeiss Imager 2.1. All histone methylation intensity data and Western Blot intensity signal measures were generated by using ImageJ and Image Lab 2.0 (Bio-Rad), respectively. All conditions were acquired with the same settings (laser power % and/or exposure time) in order to compare signal intensities between the different experimental conditions.

Electrophysiology acquisition and analysis

mEPSC traces were recorded using a Multiclamp 700B amplifier (molecular devices), sampled at 10 kHz and filtered at 2 kHz. Cells were excluded from analysis if the access resistance exceeded 20 MΩ. mEPSCs were recorded in the presence of TTX (1 μM) and PTX (100 μM). Miniature recordings were analyzed using Mini Analysis Program (Synaptosoft, <http://www.synaptosoft.com/MiniAnalysis/>). mEPSC amplitudes and frequencies were statistically tested against untreated control vector or normal-reared *Ehmt1*^{+/-} by using two-way ANOVA with Bonferroni comparison.

Data acquisition and statistical analysis

Comparisons between immunohistochemical, immunocytochemical, western blotting, qPCR, mEPSC amplitudes and frequencies, were performed based on the number of means to compare. The H3K9me2 immunohistochemical intensity signal in WT and *Ehmt1*^{+/-} mice dark and normal-reared were acquired by dividing the layer II/III primary visual cortical column in 16 frames. The intensity signals were measured from every frame and averaged across n=3 animals within the same genotype and treatment. A Two-way ANOVA was used to test differences between the genotypes and the treatment in H3K9me2 immunostaining intensity, therefore yielding to n=64 in the F-value. Analysis of two sets of measurements were performed by using unpaired Student t-Test. Multiple sets of measurements were analyzed by one-way ANOVA and further analyzed with Bonferroni post-hoc comparisons. Unpaired two-way ANOVA

comparison was used when two independent variables (e.g. genotype and treatment) were considered in the analysis of only one dependent variable, with Bonferroni post-hoc test. All data is expressed as mean±SEM. Statistical significance: (*, $p<0.05$; **, $p<0.01$, ***, $p<0.001$). For RNA-sequencing t-test and negative binomial (DESeq2) were used.

ACKNOWLEDGEMENTS

The research is supported by grants from the Hypatia fellowship (Radboudumc) [to N.N.K.]; the “FP7-Marie Curie International Reintegration Grant” [to N.N.K. grant number 277091]; the Jerome Lejeune Foundation [to N.N.K.]; the Netherlands Organization for Scientific Research (open ALW ALW2PJ/13082 to HvB/NNK) and GENCODYS, an EU FP7 large-scale integrating project grant [Grant number 241995] [to HvB].

CONFLICT OF INTEREST

The authors declare that there is no conflict of interest.

AUTHOR CONTRIBUTION

Conceptualization, M.B. and N.N.K.; Investigation, M.B, N.N.K., G.I., W.B., M.S., R.M., E.L., and A.O; Writing - original draft, M.B. and N.N.K; Writing – review & editing, H.v.B., J.K., M.F., T.K., H.Z., G.I., and H.S; Supervision, N.N.K and H.v.B; Funding acquisitions, N.N.K and H.v.B.

REFERENCES

- Aid, T., Kazantseva, A., Piirsoo, M., Palm, K., Timmusk, T. (2007). Mouse and rat BDNF gene structure and expression revisited. *J Neurosci Res* 85, 525–535.
- Balemans, M.C.M., Ansar, M., Oudakker, A.R., van Caam, A.P.M., Bakker, B., Vitters, E.L., van der Kraan, P.M., de Bruijn, D.R.H., Janssen, S.M., Kuipers, A.J., et al. (2014). Reduced Euchromatin histone methyltransferase 1 causes developmental delay, hypotonia, and cranial abnormalities associated with increased bone gene expression in Kleefstra syndrome mice. *Dev Biol* 386, 395–407.
- Balemans, M.C.M., Huijbers, M.M.H., Eikelenboom, N.W.D., Kuipers, A.J., van Summeren, R.C.J., Pijpers, M.M.C.A., Tachibana, M., Shinkai, Y., van Bokhoven, H., and Van der Zee, C.E.E.M. (2010). Reduced exploration, increased anxiety, and altered social behavior: Autistic-like features of euchromatin histone methyltransferase 1 heterozygous knockout mice. *Behav Brain Res* 208, 47–55.
- Balemans, M.C.M., Kasri, N.N., Kopanitsa, M.V., Afinow, N.O., Ramakers, G., Peters, T.A., Beynon, A.J., Janssen, S.M., van Summeren, R.C.J., Eeftens, J.M., et al. (2013). Hippocampal dysfunction in the Euchromatin histone methyltransferase 1 heterozygous knockout mouse model for Kleefstra syndrome. *Hum Mol Genet* 22, 852–866.
- Bateup, H.S., Deneff, C.L., Johnson, C.A., Saulnier, J.L., and Sabatini, B.L. (2013a). Temporal dynamics of a homeostatic pathway controlling neural network activity. *Front Mol Neurosci* 6, 28.
- Bateup, H.S., Johnson, C.A., Deneff, C.L., Saulnier, J.L., Kornacker, K., and Sabatini, B.L. (2013b). Excitatory/inhibitory synaptic imbalance leads to hippocampal hyperexcitability in mouse models of tuberous sclerosis. *Neuron* 78, 510–522.
- Béique, J.-C., Na, Y., Kuhl, D., Worley, P.F., and Huganir, R.L. (2011). Arc-dependent synapse-specific homeostatic plasticity. *Proc Natl Acad Sci USA* 108, 816–821.
- Blackman, M.P., Djukic, B., Nelson, S.B., and Turrigiano, G.G. (2012). A critical and cell-autonomous role for MeCP2 in synaptic scaling up. *J Neurosci* 32, 13529–13536.
- Boulle, F., Massart, R., Stragier, E., Paizanis, E., Zaidan, L., Marday, S., Gabriel, C., Mocaer, E., Mongeau, R., and Lanfumey, L. (2014). Hippocampal and behavioral dysfunctions in a mouse model of environmental stress: normalization by agomelatine. *Transl Psychiatry* 4, e485.
- Castrén, E., Zafra, F., Thoenen, H., and Lindholm, D. (1992). Light regulates expression of brain-derived neurotrophic factor mRNA in rat visual cortex. *Proc Natl Acad Sci USA* 89, 9444–9448.
- Chang, J., Zhang, B., Heath, H., Galjart, N., Wang, X., and Milbrandt, J. (2010). Nicotinamide adenine dinucleotide (NAD)-regulated DNA methylation alters CCCTC-binding factor (CTCF)/cohesin binding and transcription at the BDNF locus. *Proc Natl Acad Sci USA* 107, 21836–21841.
- Chao, H.-T., Zoghbi, H.Y., Rosenmund, C., 2007. MeCP2 controls excitatory synaptic strength by regulating glutamatergic synapse number. *Neuron* 56, 58–65.
- Chase, K.A., and Sharma, R.P. (2013). Nicotine induces chromatin remodelling through decreases in the methyltransferases GLP, G9a, Setdb1 and levels of H3K9me2. *Int J Neuropsychopharmacol* 16, 1129–1138.
- Collins, R. E., Northrop, J. P., Horton, J. R., Lee, D. Y., Zhang, X., Stallcup, M. R., & Cheng, X. (2008). The ankyrin repeats of G9a and GLP histone methyltransferases are mono- and dimethyllysine binding modules. *Nature Struct & Mol Biol* 15, 245–250.
- Cortés-Mendoza, J., de León-Guerrero, S.D., Pedraza-Alva, G., and Pérez-Martínez, L. (2013). Shaping synaptic plasticity: The role of activity-mediated epigenetic regulation on gene transcription. *Int J Dev Neurosci* 31, 359–369.
- Covington, H.E., Maze, I., Sun, H., Bomze, H.M., DeMaio, K.D., Wu, E.Y., Dietz, D.M., Lobo, M.K., Ghose, S., Mouzon, E., et al. (2011). A role for repressive histone methylation in cocaine-induced vulnerability to stress. *Neuron* 71, 656–670.
- De Rubeis, S. et al., (2014). Synaptic, transcriptional and chromatin genes disrupted in autism. *Nature* 515, 209–215.
- Desai, N.S., Rutherford, L.C., and Turrigiano, G.G. (1999). BDNF regulates the intrinsic excitability of cortical neurons. *Learn Mem* 6, 284–291.
- Desai, N.S., Cudmore, R.H., Nelson, S.B., and Turrigiano, G.G. (2002). Critical periods for experience-dependent synaptic scaling in visual cortex. *Nat Neurosci* 5, 783–789.
- Diering, G.H., Gustina, A.S., and Huganir, R.L. (2014). PKA-GluA1 Coupling via AKAP5 Controls AMPA Receptor Phosphorylation and Cell-Surface Targeting during Bidirectional Homeostatic Plasticity. *Neuron* 84, 790–805.

- Du, G., Drexler, G.A., Friedland, W., Greubel, C., Hable, V., Krücken, R., Kugler, A., Tonelli, L., Friedl, A.A., and Dollinger, G. (2011). Spatial dynamics of DNA damage response protein foci along the ion trajectory of high-LET particles. *Radiat. Res.* 176, 706–715.
- Feng, J., Wilkinson, M., Liu, X., Purushothaman, I., Ferguson, D., Vialou, V., Maze, I., Shao, N., Kenedy, P., Koo, J., Dias, C., Laitman, B., Stockman, V., LaPlant, Q., Cahill, M.E., Nestler, E.J. and Shen, L. (2014). Chronic cocaine-regulated epigenomic changes in mouse nucleus accumbens. *Genome Biology* 15:R65
- Gabel, H.W., Kinde, B., Stroud, H., Gilbert, C.S., Harmin, D.A., Kastan, N.R., Hemberg, M., Ebert, D.H., Greenberg, M.E. (2015). Disruption of DNA-methylation-dependent long gene repression in Rett syndrome. *Nature* 522, 89–93.
- Gainey, M.A., Hurvitz-Wolff, J.R., Lambo, M.E., and Turrigiano, G.G. (2009). Synaptic scaling requires the GluR2 subunit of the AMPA receptor. *J Neurosci* 29, 6479–6489.
- Gao, M., Sossa, K., Song, L., Errington, L., Cummings, L., Hwang, H., Kuhl, D., Worley, P., and Lee, H.-K. (2010). A specific requirement of Arc/Arg3.1 for visual experience-induced homeostatic synaptic plasticity in mouse primary visual cortex. *J. Neurosci* 30, 7168–7178.
- Goel, A., and Lee, H.-K. (2007). Persistence of experience-induced homeostatic synaptic plasticity through adulthood in superficial layers of mouse visual cortex. *J Neurosci* 27, 6692–6700.
- Goel, A., Xu, L.W., Snyder, K.P., Song, L., Goenaga-Vazquez, Y., Megill, A., Takamiya, K., Huganir, R.L., and Lee, H.-K. (2011). Phosphorylation of AMPA receptors is required for sensory deprivation-induced homeostatic synaptic plasticity. *PLoS ONE* 6, e18264.
- Goold, C.P., and Nicoll, R.A. (2010). Single-cell optogenetic excitation drives homeostatic synaptic depression. *Neuron* 68, 512–528.
- Guo, J.U., Shin, J.H., Shin, J., Li, H., Xie, B., Zhong, C., Hu, S., Le, T., Fan, G., Zhu, H., Chang, Q., Gao, Y., Ming, G.L., Song, H. (2014) Distribution, recognition and regulation of non-CpG methylation in the adult mammalian brain. *Nat. Neurosci.* 17, 215–22
- Gupta, S., Kim, S.Y., Artis, S., Molfese, D.L., Schumacher, A., Sweatt, J.D., Paylor, R.E., and Lubin, F.D. (2010). Histone methylation regulates memory formation. *J Neurosci* 30, 3589–3599.
- Gupta-Agarwal, S., Franklin, A.V., Deramus, T., Wheelock, M., Davis, R.L., McMahon, L.L., and Lubin, F.D. (2012). G9a/GLP Histone Lysine Dimethyltransferase Complex Activity in the Hippocampus and the Entorhinal Cortex Is Required for Gene Activation and Silencing during Memory Consolidation. *J Neurosci* 32, 5440–5453.
- Gupta-Agarwal, S., Jarome, T.J., Fernandez, J., and Lubin, F.D. (2014). NMDA receptor- and ERK-dependent histone methylation changes in the lateral amygdala bidirectionally regulate fear memory formation. *Learn Mem* 21, 351–362.
- Han, E.B., and Stevens, C.F. (2009). Development regulates a switch between post- and presynaptic strengthening in response to activity deprivation. *Proc Natl Acad Sci USA* 106, 10817–10822.
- Heller, E.A., Cates, H.M., Peña, C.J., Sun, H., Shao, N., Feng, J., Golden, S.A., Herman, J.P., Walsh, J.J., Mazei-Robison, M., et al. (2014). Locus-specific epigenetic remodeling controls addiction- and depression-related behaviors. *Nat Neurosci* 17, 1720–1727.
- Hou, Q., Zhang, D., Jarzylo, L., Huganir, R.L., and Man, H.-Y. (2008). Homeostatic regulation of AMPA receptor expression at single hippocampal synapses. *Proc Natl Acad Sci USA* 105, 775–780.
- Ibata, K., Sun, Q., and Turrigiano, G.G. (2008). Rapid synaptic scaling induced by changes in postsynaptic firing. *Neuron* 57, 819–826.
- Janas, J., Skowronski, J., and van Aelst, L. (2006). Lentiviral delivery of RNAi in hippocampal neurons. *Meth Enzymol* 406, 593–605.
- Ji, Y., Lu, Y., Yang, F., Shen, W., Tang, T.T.-T., Feng, L., Duan, S., and Lu, B. (2010). Acute and gradual increases in BDNF concentration elicit distinct signaling and functions in neurons. *Nat Neurosci* 13, 302–309.
- Karpova, N.N., Rantamäki, T., Di Lieto, A., Lindemann, L., Hoener, M.C., and Castrén, E. (2010). Darkness reduces BDNF expression in the visual cortex and induces repressive chromatin remodeling at the BDNF gene in both hippocampus and visual cortex. *Cell Mol Neurobiol* 30, 1117–1123.
- Kasri, N.N., Govek, E.-E., and van Aelst, L. (2008). Characterization of oligophrenin-1, a RhoGAP lost in patients affected with mental retardation: lentiviral injection in organotypic brain slice cultures. *Meth Enzymol* 439, 255–266.
- Kennedy, P.J., Feng, J., Robison, A.J., Maze, I., Badimon, A., Mouzon, E., Chaudhury, D., Damez-Werno, D.M., Haggarty, S.J., Han, M.-H., et al. (2013). Class I HDAC inhibition blocks cocaine-induced plasticity by targeted changes in histone methylation. *Nat Neurosci* 16, 434–440.

- Kim, S., and Ziff, E.B. (2014). Calcineurin mediates synaptic scaling via synaptic trafficking of Ca²⁺-permeable AMPA receptors. *PLoS Biol.* 12, e1001900.
- Kirov, G., Pocklington, A.J., Holmans, P., Ivanov, D., Ikeda, M., Ruderfer, D., Moran, J., Chambert, K., Toncheva, D., Georgieva, L., et al. (2012). De novo CNV analysis implicates specific abnormalities of postsynaptic signalling complexes in the pathogenesis of schizophrenia. *Mol Psychiatry* 17, 142–153.
- Kleefstra, T., van Zelt-Stams, W.A., Nillesen, W.M., Cormier-Daire, V., Houge, G., Foulds, N., van Dooren, M., Willemsen, M.H., Pfundt, R., Turner, A., et al. (2009). Further clinical and molecular delineation of the 9q subtelomeric deletion syndrome supports a major contribution of EHMT1 haploinsufficiency to the core phenotype. *J Med Genet* 46, 598–606.
- Kleefstra, T., Brunner, H.G., Amiel, J., Oudakker, A.R., Nillesen, W.M., Magee, A., Geneviève, D., Cormier-Daire, V., van Esch, H., Fryns, J.-P., et al. (2006). Loss-of-function mutations in euchromatin histone methyl transferase 1 (EHMT1) cause the 9q34 subtelomeric deletion syndrome. *Am J Hum Genet* 79, 370–377.
- Kleefstra, T., Kramer, J.M., Neveling, K., Willemsen, M.H., Koemans, T.S., Vissers, L.E.L.M., Wissink-Lindhout, W., Fencikova, M., van den Akker, W.M.R., Kasri, N.N., et al. (2012). Disruption of an EHMT1-Associated Chromatin-Modification Module Causes Intellectual Disability. *Am J Hum Genet* 91, 73–82.
- Kleefstra, T., Schenck, A., Kramer, J., and van Bokhoven, H. (2014). The genetics of cognitive epigenetics. *Neuropharmacology* 80, 83–94.
- Kramer, J.M., Kochinke, K., Oortveld, M.A.W., Marks, H., Kramer, D., de Jong, E.K., Asztalos, Z., Westwood, J.T., Stunnenberg, H.G., Sokolowski, M.B., et al. (2011). Epigenetic regulation of learning and memory by *Drosophila* EHMT/G9a. *PLoS Biol.* 9, e1000569.
- Lee, K.J., Queenan, B.N., Rozeboom, A.M., Bellmore, R., Lim, S.T., Vicini, S., and Pak, D.T.S. (2013). Mossy Fiber-CA3 Synapses Mediate Homeostatic Plasticity in Mature Hippocampal Neurons. *Neuron* 77, 99–114.
- Levenson, J.M., Roth, T.L., Lubin, F.D., Miller, C.A., Huang, I.-C., Desai, P., Malone, L.M., and Sweatt, J.D. (2006). Evidence that DNA (cytosine-5) methyltransferase regulates synaptic plasticity in the hippocampus. *J Biol Chem* 281, 15763–15773.
- Lindskog, M., Li, L., Groth, R.D., Aakalu, G., poburko, D., Thiagarajan, T.C., Xue, H., Tsien, R.W., 2010. Postsynaptic GluA1 enables acute retrograde enhancement of presynaptic function to coordinate adaptation to synaptic inactivity. *Proc Natl Acad Sci USA* 107, 21806–21811.
- Livak, K.J., and Schmittgen, T.D. (2001). Analysis of relative gene expression data using real-time quantitative PCR and the 2(-Delta Delta C(T)) Method. *Methods* 25, 402–408.
- Lubin, F.D., Roth, T.L., and Sweatt, J.D. (2008). Epigenetic regulation of BDNF gene transcription in the consolidation of fear memory. *J Neurosci* 28, 10576–10586.
- Maffei, A., and Turrigiano, G.G. (2008). Multiple modes of network homeostasis in visual cortical layer 2/3. *J Neurosci* 28, 4377–4384.
- Martinowich, K., Hattori, D., Wu, H., Fouse, S., He, F., Hu, Y., Fan, G., and Sun, Y.E. (2003). DNA methylation-related chromatin remodeling in activity-dependent BDNF gene regulation. *Science* 302, 890–893.
- Maze, I., Covington, H.E., Dietz, D.M., LaPlant, Q., Renthal, W., Russo, S.J., Mechanic, M., Mouzon, E., Neve, R.L., Haggarty, S.J., et al. (2010). Essential role of the histone methyltransferase G9a in cocaine-induced plasticity. *Science* 327, 213–216.
- McCarthy, S.E., Gillis, J., Kramer, M., Lihm, J., Yoon, S., Berstein, Y., Mistry, M., Pavlidis, P., Solomon, R., Ghiban, E., et al. (2014). De novo mutations in schizophrenia implicate chromatin remodeling and support a genetic overlap with autism and intellectual disability. *Mol Psychiatry* 19, 652–658.
- Mozzetta, C., Pontis, J., Fritsch, L., Robin, P., Portoso, M., Proux, C., Margueron, R., and Ait-Si-Ali, S. (2014). The histone H3 lysine 9 methyltransferases G9a and GLP regulate polycomb repressive complex 2-mediated gene silencing. *Mol Cell* 53, 277–289.
- Müller, M., Pym, E.C.G., Tong, A., Davis, G.W., 2011. Rab3-GAP controls the progression of synaptic homeostasis at a late stage of vesicle release. *Neuron* 69, 749–762.
- Nadif Kasri, N., Nakano-Kobayashi, A., and van Aelst, L. (2011). Rapid synthesis of the X-linked mental retardation protein OPHN1 mediates mGluR-dependent LTD through interaction with the endocytic machinery. *Neuron* 72, 300–315.
- Noh, K.-M., Hwang, J.-Y., Follenzi, A., Athanasiadou, R., Miyawaki, T., Grealley, J.M., Bennett, M.V.L., and Zukin, R.S. (2012). Repressor element-1 silencing transcription factor (REST)-

dependent epigenetic remodeling is critical to ischemia-induced neuronal death. *Proc Natl Acad Sci USA* 109, E962–E971.

Pozo, K., and Goda, Y. (2010). Unraveling mechanisms of homeostatic synaptic plasticity. *Neuron* 66, 337–351.

Pozzi, D., Lignani, G., Ferrea, E., Contestabile, A., Paonessa, F., D'Alessandro, R., Lippiello, P., Boido, D., Fassio, A., Meldolesi, J., et al. (2013). REST/NRSF-mediated intrinsic homeostasis protects neuronal networks from hyperexcitability. *Embo J* 32, 2994–3007.

Qiu, Z., Sylwestrak, E.L., Lieberman, D.N., Zhang, Y., Liu, X.Y., and Ghosh, A. (2012). The Rett Syndrome Protein MeCP2 Regulates Synaptic Scaling. *J Neurosci* 32, 989–994.

Rothbart, S.B., and Strahl, B.D. (2014). Interpreting the language of histone and DNA modifications. *Biochim Biophys Acta* 1839, 627–643.

Rutherford, L.C., Nelson, S.B., and Turrigiano, G.G. (1998). BDNF has opposite effects on the quantal amplitude of pyramidal neuron and interneuron excitatory synapses. *Neuron* 21, 521–530.

Sando, R., Gounko, N., Pieraut, S., Liao, L., Yates, J., and Maximov, A. (2012). HDAC4 governs a transcriptional program essential for synaptic plasticity and memory. *Cell* 151, 821–834.

Schaefer, A., Sampath, S.C., Intrator, A., Min, A., Gertler, T.S., Surmeier, D.J., Tarakhovskiy, A., and Greengard, P. (2009). Control of cognition and adaptive behavior by the GLP/G9a epigenetic suppressor complex. *Neuron* 64, 678–691.

Shepherd, J.D., Rumbaugh, G., Wu, J., Chowdhury, S., Plath, N., Kuhl, D., Hugarir, R.L., and Worley, P.F. (2006). Arc/Arg3.1 mediates homeostatic synaptic scaling of AMPA receptors. *Neuron* 52, 475–484.

Soden, M.E., and Chen, L. (2010). Fragile X protein FMRP is required for homeostatic plasticity and regulation of synaptic strength by retinoic acid. *J Neurosci* 30, 16910–16921.

Subbanna, S., Nagre, N.N., Shivakumar, M., Umaphathy, N.S., Psychoyos, D., and Basavarajappa, B.S. (2014). Ethanol induced acetylation of histone at G9a exon1 and G9a-mediated histone H3 dimethylation leads to neurodegeneration in neonatal mice. *Neuroscience* 258, 422–432.

Sun, H., Maze, I., Dietz, D.M., Scobie, K.N., Kennedy, P.J., Damez-Werno, D., Neve, R.L., Zachariou, V., Shen, L. and Nestler, E.J. (2012). Morphine Epigenomically Regulates Behavior through Alterations in Histone H3 Lysine 9 Dimethylation in the Nucleus Accumbens. *J. Neurosci.* 32, 17454–17464

Sutton, M.A., Ito, H.T., Cressy, P., Kempf, C., Woo, J.C., and Schuman, E.M. (2006). Miniature neurotransmission stabilizes synaptic function via tonic suppression of local dendritic protein synthesis. *Cell* 125, 785–799.

Tachibana, M., Matsumura, Y., Fukuda, M., Kimura, H., and Shinkai, Y. (2008). G9a/GLP complexes independently mediate H3K9 and DNA methylation to silence transcription. *Embo J* 27, 2681–2690.

Tachibana, M., Sugimoto, K., Nozaki, M., Ueda, J., Ohta, T., Ohki, M., Fukuda, M., Takeda, N., Niida, H., Kato, H., et al. (2002). G9a histone methyltransferase plays a dominant role in euchromatic histone H3 lysine 9 methylation and is essential for early embryogenesis. *Genes Dev* 16, 1779–1791.

Tachibana, M., Ueda, J., Fukuda, M., Takeda, N., Ohta, T., Iwanari, H., Sakihama, T., Kodama, T., Hamakubo, T., and Shinkai, Y. (2005). Histone methyltransferases G9a and GLP form heteromeric complexes and are both crucial for methylation of euchromatin at H3-K9. *Genes Dev* 19, 815–826.

Talkowski, M.E., Rosenfeld, J.A., Blumenthal, I., Pillalammarri, V., Chiang, C., Heilbut, A., Ernst, C., Hanscom, C., Rossin, E., Lindgren, A.M., et al. (2012). Sequencing Chromosomal Abnormalities Reveals Neurodevelopmental Loci that Confer Risk across Diagnostic Boundaries. *Cell* 149, 525–537.

Thiagarajan, T.C., Lindskog, M., and Tsien, R.W. (2005). Adaptation to synaptic inactivity in hippocampal neurons. *Neuron* 47, 725–737.

Tsetsenis, T., Younts, T.J., Chiu, C.Q., Kaeser, P.S., Castillo, P.E., Südhof, T.C., 2011. Rab3B protein is required for long-term depression of hippocampal inhibitory synapses and for normal reversal learning. *Proc Natl Acad Sci USA* 108, 14300–14305.

Turrigiano, G.G., Leslie, K.R., Desai, N.S., Rutherford, L.C., and Nelson, S.B. (1998). Activity-dependent scaling of quantal amplitude in neocortical neurons. *Nature* 391, 892–896.

Turrigiano, G. (2012). Homeostatic synaptic plasticity: local and global mechanisms for stabilizing neuronal function. *Cold Spring Harb Perspect Biol* 4, a005736.

Turrigiano, G.G., and Nelson, S.B. (2004). Homeostatic plasticity in the developing nervous system. *Nat. Rev. Neurosci.* 5, 97–107.

Vedadi, M., Barsyte-Lovejoy, D., Liu, F., Rival-Gervier, S., Allali-Hassani, A., Labrie, V., Wigle, T.J., Dimaggio, P.A., Wasney, G.A., Siarheyeva, A., et al. (2011). A chemical probe selectively inhibits G9a and GLP methyltransferase activity in cells. *Nat Chem Biol* 7, 566–574.

- Wierenga, C.J., Ibata, K., and Turrigiano, G.G. (2005). Postsynaptic expression of homeostatic plasticity at neocortical synapses. *J Neurosci* 25, 2895–2905.
- Wierenga, C.J., Walsh, M.F., and Turrigiano, G.G. (2006). Temporal regulation of the expression locus of homeostatic plasticity. *J Neurophysiol* 96, 2127–2133.
- Willemssen, M.H., Vulto-van Silfhout, A.T., Nillesen, W.M., Wissink-Lindhout, W.M., van Bokhoven, H., Philip, N., Berry-Kravis, E.M., Kini, U., van Ravenswaaij-Arts, C.M.A., Delle Chiaie, B., et al. (2012). Update on Kleeftstra Syndrome. *Mol Syndromol* 2, 202–212.
- Yearim, A., Gelfman, S., Shyevitch, R., Melcer, S., Glaich, O., Mallm, J.P., Nissim-Rafinia, M., Cohen, A.H., Rippe, K., Meshorer, E. and Ast, G. (2015). HP1 is involved in regulating the global impact of DNA methylation on alternative splicing. *Cell Rep.* 10, 1122–34.
- Yu, H., Su, Y., Shin, J., Zhong, C., Guo, J.U., Weng, Y.-L., Gao, F., Geschwind, D.H., Coppola, G., Ming, G.-L., et al. (2015). Tet3 regulates synaptic transmission and homeostatic plasticity via DNA oxidation and repair. *Nat Neurosci* 18, 836–843.
- Zhang, Z., Tao, W., Hou, Y.Y., Wang, W., Kenny, P.J., and Pan, Z.Z. (2014). MeCP2 Repression of G9a in Regulation of Pain and Morphine Reward. *J Neurosci* 34, 9076–9087.
- Zhong, X., Li, H., and Chang, Q. (2012). MeCP2 phosphorylation is required for modulating synaptic scaling through mGluR5. *J Neurosci* 32, 12841–12847.
- Zhou, W., Zhang, L., Guoxiang, X., Mojsilovic-Petrovic, J., Takamaya, K., Sattler, R., Huganir, R., and Kalb, R. (2008). GluR1 controls dendrite growth through its binding partner, SAP97. *J. Neurosci.* 28, 10220–10233.

¹Department of Cognitive Neuroscience, Radboudumc, Donders Institute for Brain, Cognition and Behaviour, Nijmegen, the Netherlands.

²Department of Human Genetics, Radboudumc, 6500 HB Nijmegen, the Netherlands; Department of Molecular Developmental Biology, Faculty of Science, Radboud University, 6500 HB Nijmegen, the Netherlands.

This chapter is in preparation for publication

three

EHMT1 IS REQUIRED FOR SYNAPTIC SCALING IN CORTICAL NEURONS DERIVED FROM HUMAN INDUCED PLURIPOTENT STEM CELLS

Marco Benevento¹, Monica Frega¹, Bas van Gestel^{1,2}, Jon-Ruben van Rhijn¹,
Tjitske Kleefstra³, Willem van Akker², Huiqing Zhou², Hans van Bokhoven¹
and Nael Nadif Kasri¹

ABSTRACT

We recently showed in rodent models that the KS-associated protein EHMT1 plays a critical and cell-autonomous role in synaptic scaling by responding to attenuated neuronal firing or sensory drive. To functionally determine whether EHMT1 is required for homeostatic synaptic scaling in human we investigated cortical neurons from a healthy individual and an individual with KS. For this, we adapted a protocol to rapidly and reliably produce a homogeneous population of upper layer cortical neurons from human induced pluripotent stem cells. We show that also in humans EHMT1 is required for synaptic scaling, indicating that the epigenetic and homeostatic role of EHMT1 is evolutionarily conserved and may contribute to KS.

INTRODUCTION

Haploinsufficiency of the Euchromatic Histone Methyl-Transferase 1 (*EHMT1*) gene is one of the major causes of Kleefstra syndrome (KS) (Kleefstra et al., 2006, 2012), a rare disorder disease associated with intellectual disability (ID) and Autism spectrum disorders (ASD). Recently, genetic interference with *EHMT1* function was shown to give rise to improper neuronal circuitry refinement during cortical neuronal network development (Martens et al., 2016). Circuit refinements depends on synaptic scaling, a homeostatic plasticity mechanism that plays an important role in shaping neuronal connectivity during embryonal and early post-natal periods (Turrigiano et al., 2008). Homeostatic synaptic scaling is a global compensatory mechanism that maintains neuronal excitability within a physiological range of activity, relative to network activity. This is achieved by altering the synaptic strength via regulation of the α -amino-3-hydroxy-5-methyl-4-isoxazolepropionic acid (AMPA) receptor abundance at the post-synaptic terminal (Turrigiano et al., 1998). Several reports describe that synaptic scaling is disrupted in neurodevelopmental disorders like Rett-syndrome, Fragile X and Tuberous sclerosis (Qiu et al., 2012; Soden et al., 2010; Bateup et al., 2013 a; b). In Chapter 2, we showed that *EHMT1* plays an important role in regulating synaptic scaling up in response to neuronal network activity deprivation, in rodent models *in vitro* and *in vivo* (Benevento et al., 2016). In particular, we showed that *EHMT1* reacts to chronic neuronal inactivity by increasing di-methylation of the Lysine 9 of histone H3 (H3K9me₂) levels specifically at gene promoter IV of *Bdnf*, subsequently leading to repression of *Bdnf*. the repression of BDNF was previously shown to be necessary to increase miniature excitatory post-synaptic currents (mEPSCs) amplitudes in response to neuronal network deprivation (Rutherford et al., 1998).

To identify whether this mechanism can also be observed in a human neurons, we generated excitatory cortical neurons from human induced pluripotent stem cells (hiPSCs) of KS patients and healthy individuals. hiPSCs allow to model neurological and neurodevelopmental disorders associated with genetic mutations directly in a human genetic background (Takahashi and Yamanaka, 2006; Yu et al., 2007). Since the advent of neuronal induction from hiPSCs, several research groups have developed protocols to convert hiPSCs into neurons (LaVaute et al., 2009; Chamber et al., 2009). Differentiation into neurons has somewhat lagged behind research of other organs, given the large variability and low efficiency of producing functionally mature neurons, using the initial developed differentiation protocols (Johnson et al., 2007; Hu et al., 2010; Kim et al., 2011; Shi et al., 2012). Recently, two studies from independent research groups showed that overexpressing Neurogenin-2 (*Ngn2*) is sufficient to induce a rapid and reproducible conversion of human upper-layer cortical neurons from hiPSCs (iN-hiPSCs) with nearly 100% efficiency (Zhang et al., 2013; Busskamp et al., 2014). In addition, the authors showed that the neuronal population was homogeneous, and exhibited mature synapses and robust synaptic activity already after 20 days post-neuronal-induction. Here, we refined the fast converting neuron strategy of Zhang and colleagues (Zhang et al., 2013). We transduced hiPSC lines with a lentivirus expressing a tri-cistronic vector encoding for reversed tetracycline-controlled induced activator (*rtTA*), Neurogenin 2 (*Ngn2*) and puromycin (*puro*) (*rtTA/Ngn2-puro*). the transduced hiPSC lines were selected for puromycin and *Ngn2*

expression was induced by doxycycline. This allowed us to increase reproducibility and to have control over the neuronal cell density, which is critical for neuronal network formation (Frega *et al.* 2016). We tested whether the neurons derived directly from hiPSCs of KS patients, bearing a mutation in the *EHMT1* gene, displayed deficits in homeostatic synaptic scaling as we previously reported in the rodent models.

In this chapter, we describe for the first time that iN-hiPSCs exhibit homeostatic plasticity in response to chronic neuronal network activity deprivation. Moreover, we found that this synaptic scaling response was impeded in iN-hiPSCs from KS-patients, corroborating our previous results obtained in rodent models for KS (Benevento *et al.*, 2016)

RESULTS

Generation of mature and functionally active neurons induced from hiPSCs

To establish a reliable and robust neuronal differentiation protocol we first generated a stable hiPSCs cell line, expressing *Ngn2* under a doxycycline-dependent promotor (Frega *et al.*, 2016). To this end, hiPSCs from a healthy volunteer were transduced with a tri-cistronic lentivirus expressing *rtTA/Ngn2-puro*. the transduced cells were subsequently treated with pumomycin to select hiPSC clones in which the *rtTA/Ngn2-puro* was stably integrated into the genome. Next, to derive a homogenous and mature neuronal population, we induced *Ngn2* expression in the hiPSCs with doxycycline through activation of tetracyclin-activated receptor (*rtTA*), as previously described (Zhang *et al.*, 2013; Busskamp *et al.*, 2014). We found that the expression of the neuronal marker MAP2 was already visible 7 days *in vitro* (DIV) after doxycycline induction (Figure 3.1). At DIV 13, we observed the expression of the presynaptic vesicle marker, Synapsin (Südhof *et al.*, 1989). During the following days, the intensity and the amount of

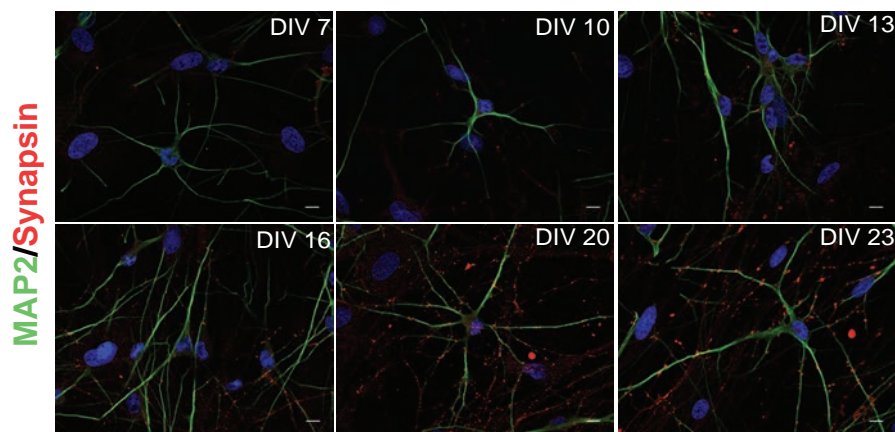


Figure 3.1. hiPSC derived neurons time course characterization after induction. Representative epifluorescent images from induced neurons at different maturative stages. Induced hiPSCs neurons were immunolabeled for: MAP2, green; Synapsin, red; Hoechst, blue. Scale bars: 15µm.

Synapsin *punctae* on MAP2 positive cells increased abundantly. This observation suggests that the induced neurons form critical presynaptic components already at DIV 20 (Figure 3.1).

To investigate, whether iN-hiPSCs make contact to post-synaptic sites, we analysed synapsin *punctae* juxtaposed to the post-synaptic marker PSD-95. We found that the synapsin *punctae* were juxtaposed to PSD-95 *punctae* at DIV 23, indicating the presence of pre- and post-synaptic components (Figure 3.2).

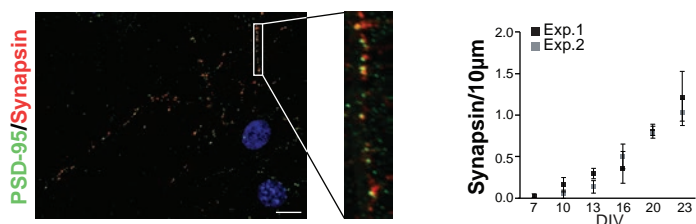


Figure 3.2. hiPSCs induced neurons synapse formation at DIV 23. hiPSC-derived neurons were stained for PSD-95 (green) and Synapsin-1/2 (red) DIV 23 after neuronal induction. Synapsin *punctae* are juxtaposed to PSD-95 *punctae*. Right insert shows a magnification of a 10 μm dendritic stretch depicting juxtaposed PSD-95/Synapsin *punctae*.

To confirm whether the anatomical observed pre-and post-synapse are forming functional synapses, we next performed whole-cell current and voltage patch-clamp recordings on the hiPSCs-induced neurons. At DIV 7, iN-hiPSCs were able to fire action potentials when depolarized. From DIV 7 to DIV 20, the amount of evoked action potentials increased over the time, showing that the iN-hiPSCs acquired mature firing properties (Figure 3.3A). Indeed, at DIV 16, the percentage of neurons showing action potentials reached nearly 100%, and was maintained until DIV 23 (Figure 3.3B).

To investigate the network activity, we recorded spontaneous excitatory post-synaptic currents (sEPSC). We found that the iN-hiPSCs received excitatory synaptic input already at DIV 7, which further increased in both frequency and amplitude of the sEPSC during development (Figure 3.4).

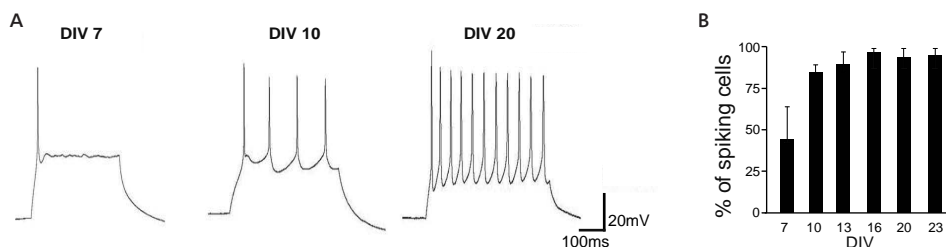


Figure 3.3. Induced hiPSCs neurons show active properties. **A)** Representative current patch-clamp recordings depicting action potential generation induced at three different maturative stages at DIV 7, 10 and 20. **B)** Time course depicting the percentage of spiking neurons at different days after rtTA/Ngn2 hiPSCs induction.

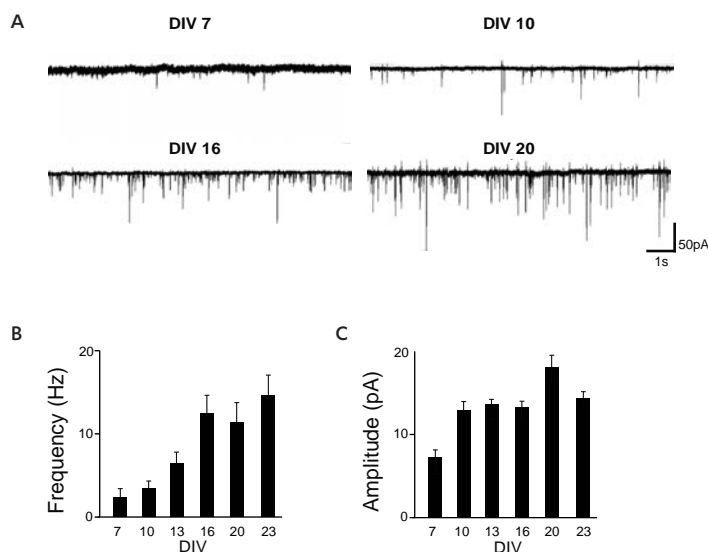


Figure 3.4. Induced hiPSCs neurons display spontaneous excitatory network activity. **A)** Representative traces of excitatory postsynaptic currents (EPSCs) received by hiPSC-derived neurons at different days after differentiation. **B)** and **C)** Frequency and amplitude of spontaneous excitatory postsynaptic currents during development.

These data indicate that we were able to generate iN-hiPSCs, which show mature neuronal intrinsic properties and show high network activity. Importantly, the addition of glial cells as structural and functional support was essential for the proper maturation of the iN-hiPSCs (data not shown).

Synaptic scaling induction in induced neurons from hiPSCs

In the next step, we investigated the impact of synaptic scaling in iN-hiPSCs from KS patients. We generated neurons from a control and a patient affected by KS hiPSCs. The KS iN-hiPSCs were generated from a patient with a heterozygous 132-bp deletion in the *EHMT1* gene, leading to a premature stop codon (c.3181-80_3233del pTyr1061fs, patient 25 in Willemsen et al, 2012) using lentiviral transduction of the Yamanaka factors (Takahashi and Yamanaka, 2006; Warlich et al., 2011). Three different clones resulting from the reprogramming were expanded, stored and validated through a battery of quality control tests including morphological assessment, expression of pluripotent markers measured by RT-qPCR and immunocytochemistry, ability to generate cells from the 3 germ layers when spontaneously differentiated. Karyotype and genomic integrity was assessed by high-density SNP arrays, all to ensure they are suitable for our investigations (data not shown). One validated clone was selected to make a stable cell line, expressing the doxycycline inducible *Ngn2* cassette. No differences were observed between iN-hiPSCs from control and KS patient during the differentiation process. Both lines showed neuronal morphology as assessed with MAP2 staining starting at DIV 7. After DIV 20, we could reliably record sEPSCs from the Kleefstra line and morphological detect synaptic *punctae* (data not shown).

Homeostatic synaptic scaling induction in neurons is dependent on *Bdnf* expression. Previous studies have shown that exogenous application of BDNF to neuronal cultures prevents synaptic scaling up after chronic neuronal network activity deprivation induced by tetrodotoxin (TTX) for 48h (Rutherford et al., 1998). Given that BDNF is one of the supplemented factors used in the medium to maintain iN-hiPSCs, we removed BDNF completely from the culturing medium at DIV 17 after iN-hiPSCs induction. Next, we induced synaptic scaling up by treating DIV 21 iN-hiPSCs for 48h with TTX 1 μ M. After 48h TTX-induction (DIV 23), we found a significant increase in the miniature EPSC (mEPSC) amplitude in the control iN-hiPSCs (Figure 3.5A), but no changes in frequency (Figure 3.5B). These data are similar to what was previously extensively shown by us and others in rodent neuronal preparations (Turrigiano et al., 1998; Benevento et al., 2016) and show that homeostatic synaptic scaling up can reliably be induced in iN-hiPSCs. Next, we performed the same experiment in iN-hiPSCs from the KS patient. Interestingly, the TTX-dependent increase in mEPSC amplitude was absent in these neurons (Figure 3.5A). Also no changes in mEPSC frequency was observed (Figure 3.5B). This is consistent with our previous observations in rodent models for EHMT1 deficiency (Figures 2.7, 2.9, 2.24, and 2.28).

Similar to our previous observations (Benevento et al., 2016), we did not observe any baseline differences between genotypes (non-treated) in the mEPSC amplitudes and frequencies, suggesting that there are no basal differences between control and KS neurons (Figure 3.5A and 3.5B).

DISCUSSION

In this chapter, we have successfully generated active neurons from hiPSCs. By modifying previously established protocols, we converted with nearly 100% efficiency hiPSCs into functionally connected neurons (Zhang et al., 2013; Busskamp et al., 2014). We temporally profiled the development of the neuronal network after doxycycline induction of *rtTA/Ngn2* of hiPSCs at different time points. We found that iN-hiPSCs were expressing synaptic markers (Synapsin

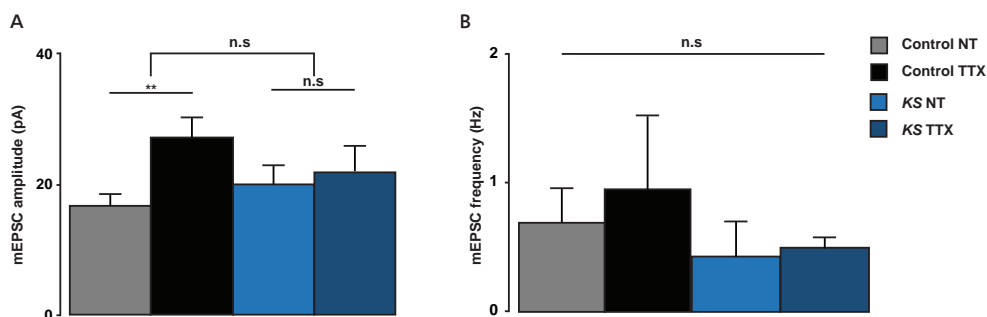


Figure 3.5. EHMT1 is required to increase the mEPSC amplitude but not mEPSC frequency in response to chronic network deprivation in human neurons induced from control and KS hiPSCs. **A)** mEPSC amplitude control (NT, TTX, n=14-15) and KS (NT, TTX, n=10-10), **B)** mEPSC frequency control (NT, TTX, n=14-15) and KS (NT, TTX, n=10-10). Data are represented as mean \pm SEM; **, $p < 0.001$; n.s., non significant; two-way ANOVA.

and PSD-95) as early as DIV 7 after doxycycline induction. the expression of these markers increased over the time course of maturation. Importantly, this was paralleled by an increment in the number of action potentials evoked by depolarization, and in the frequency and amplitude of the spontaneous events (sEPSCs). Together these findings confirmed that the generated iN-hiPSCs showed active membrane properties and formed organized neuronal networks.

The optimized production and synchronization of human neuronal population from control and KS-patients iN-hiPSCs allowed us to functionally use human neurons to validate our previous findings in rodent models for KS (Benevento et al., 2016). We validated the functional requirement of EHMT1 in regulating synaptic scaling directly in iN-hiPSCs. In line with our previous studies, our preliminary experiments indicate that the TTX-dependent rise in the mEPSCs amplitude is blocked in KS iN-hiPSCs. Synaptic scaling defects have been found in rodent models for various neurodevelopmental disorders such as Tuberous-sclerosis, Fragile X and Rett syndrome (Qiu et al., 2012; Soden et al., 2010; Bateup et al., 2013 a; b). However, this is the first demonstration of deficits in synaptic scaling using iN-hiPSCs derived neurons from patient lines.

Importantly, we are the first research group showing that iN-hiPSCs respond homeostatically to chronic neuronal network activity suppression by scaling up glutamatergic synapses. This result suggests that both homeostatic synaptic scaling and EHMT1 function have an important evolutionarily conserved function in regulating the epigenetic mechanisms associated with synaptic plasticity, neuronal circuitry refinement and brain development in humans.

The successful validation of our previous results using rodent models directly in iN-hiPSCs from controls and KS-patients provides us with an *in vitro* human model that can be used to biochemically and genetically study how EHMT1 regulates aspects of neuronal circuitry development in humans. For example, determining whether also in BDNF expression is also misregulated in iN-hiPSCs from KS patients could provide a powerful indication to strategize therapies for phenotype reversion. Moreover, by using genomic editing techniques like CRISPR-Cas9 technology, we could determine during development the temporal window of EHMT1 requirement during neuronal network formation or brain development, and possibly use this information to rescue the phenotype.

However, to finally cross-validate our findings in a human genetic background, more experiments should be conducted by using various isogenic iN-hiPSCs from different healthy individuals and KS patients.

MATERIALS AND METHODS

All experiments on animals were carried out in accordance with the approved animal care and use guidelines of the Animal Care Committee, Radboud University Medical Centre, the Netherlands, (RU-DEC-2011-021, protocol number: 77073).

Glia cell isolation and culture

The protocol is based on the work of McCarthy and de Vellis published in 1980, and a very similar detailed protocol for mouse astrocytes is available (Schlidge et al., 2013). To generate

primary cultures of cortical astrocytes from embryonic (E18) rat brains, a pregnant rat was sacrificed and embryos were collected from the *uterus*, and the brains need to be isolated from the embryos as recently described (Frega et al., 2016). To fill a T75 flask, the cortices from 2 embryonic brains need to be combined.

Generation of puromycin-rtTA/Ngn2-positive hiPSCs

hiPSCs were generated as previously described in (Frega et al., 2016). hiPSCs were plated in 12 well plate and cultured in DMEM/F12 (Gibco; 11320-074) in a humidified incubator at 37 °C with an atmosphere of CO₂ 5%. For hiPSCs transduction the DMEM/F12 was substituted with pre-warmed E8 medium (Gibco; A1517001) supplemented with Penicillin/Streptomycin (Sigma-Aldrich; P4333), ROCK-inhibitor (RevitaCell™, Gibco; A2644501) and polybrene (Sigma-Aldrich; AL-118). hiPSCs were transduced with lentiviruses expressing *puromycin-rtTA/Ngn2*, produced as previously described (Ba et al., 2016; Frega et al. 2016). After transduction, hiPSCs were washed in DPBS (Sigma-Aldrich; D8662) and kept in E8 medium at 37 °C in a humidified incubator with a CO₂ 5% atmosphere. For selecting cells stably integrating the *puromycin-rtTA/Ngn2* lentivirus, hiPSCs were selected with Puromycin 0.5µg/ml (Sigma-Aldrich; P9620-10ML) and G418 50µg/ml (Sigma-Aldrich; G8168-10ML) for 5 days in a humidified 37 °C incubator with an atmosphere of CO₂ 5%.

Neuronal induction of rtTA/Ngn2-positive hiPSCs

For neuronal induction, we used DMEM/F12 medium and E8 supplemented with Penicillin/Streptomycin 1% (v/v), Doxycycline 4 µg/ml (Sigma-Aldrich; D9891-5G) and ROCK inhibitor. Cells after treatment were kept in 24 wells plate in a humidified 37 °C incubator with an atmosphere of CO₂ 5% overnight. the following day, E8 supplemented medium was replaced with DMEM/F12 supplemented with N-2 supplement 1% (v/v) (Gibco; 17502-048), non-essential amino acids 1% (v/v) (Sigma-Aldrich; M7145), Penicillin/Streptomycin 1% (v/v), Neurotrophin-3 (NT-3) 10 ng/ml (Promokine; C66425), human recombinant brain-derived neurotrophic factor (BDNF) 10 ng/ml (Promokine; C66212) and Doxycycline 4 µg/ml. After one day rat astrocytes were added as previously described (Frega et al., 2016). After 4 days of *rtTA/Ngn2* induction medium was replaced with Neurobasal supplemented with B-27 supplement 2% (v/v) (Gibco; 0080085SA), L-alanyl-L-glutamine 1% (v/v) (GLUTAMAX) (Gibco; 35050-038), Penicillin/Streptomycin 1% (v/v), NT-3 10 ng/ml, Doxycycline 4 µg/ml and cytosine β-D-arabinofuranoside (ARA-C) (Sigma-Aldrich; C1768-100MG). iN-hiPSCs were maintained in a humidified 37°C incubator with an atmosphere of CO₂ 5%. At DIV 10 after *rtTA/Ngn2* induction, FBS 2% (v/v) (Sigma-Aldrich; F2442-500ML) was added to Neurobasal supplemented medium. For homeostatic plasticity induction, starting from DIV 17, BDNF was completely removed from Neurobasal supplemented medium. Neurobasal supplemented medium was refreshed every third day from the iN-hiPSCs and maintained in a humidified 37 °C incubator with an atmosphere of CO₂ 5%.

Immunocytochemistry

iN-hiPSCs were fixed with paraformaldehyde 4% / sucrose 4% in phosphate buffered saline (PBS 1X) (Sigma-Aldrich, P5493-1L) at 37 °C for 15min. After fixation cells were washed with PBS 1X.

Cells were blocked in normal goat serum (NGS) 10%. Primary antibodies were incubated in PBS 1X with NGS 5% overnight at 4 °C. Secondary antibody incubation was done the next day with Alexa-488 and Alexa-568 (Molecular Probes) for 1h at room temperature. Cells were washed in PBS 1X to remove secondary antibody excess and nuclei were labeled. Finally, cells were mounted using DAKO (DAKO, S3023) fluorescent mounting medium and stored at 4 °C. Primary antibodies: Synapsin (1:500, Synaptic systems, 106 001); MAP2 (1:2000, Sigma-Aldrich M4403); PSD-95 (1:50, Thermo Scientific MA1-045). Secondary antibodies: Goat anti-Mouse Alexa Fluor® 488 (1:2000, Invitrogen A11029), Goat anti-Mouse Alexa Fluor® 568 (1:2000, Invitrogen A11031), Goat anti-Mouse Alexa Fluor® 647 (1:2000, Invitrogen A21236), Goat anti-Rabbit alexa fluor 488 (1:2000, Invitrogen A11034), Goat anti-Rabbit Alexa Fluor® 568 (1:2000, Invitrogen A11031).

Electrophysiology

Whole-cell voltage- and current-clamp recordings were performed as previously described (Nadif Kasri et al., 2011). In brief, iN-hiPSCs attached to glass coverslips were transferred to the recording setup and incubated in recording (ACSF) containing: NaCl 124 mM, NaH₂PO₄ 1.25 mM, KCl 3 mM, NaHCO₃ 26 mM, Glucose 10 mM, CaCl₂ 2 mM, MgCl₂ 1 mM at continuously oxygenated with O₂ 95% / CO₂ 5% at 30°C. iN-hiPSCs were visualized with an upright microscope (Olympus). Patch pipettes (5-7 MΩ) were made from borosilicate glass capillaries and filled with intracellular solution containing: CsMeSO₃ 115 mM; CsCl 20 mM; HEPES 10 mM; MgCl₂ 2.5 mM; Na₂ATP 4 mM; NaGTP 0.4 mM; Na-Phosphocreatine 10 mM; EGTA 0.6 mM (pH 7.2-7.3, 285-295 mOsm).

hiPSCs-induced neuronal cultures treatments

Low-density 20000 cell/well iN-hiPSCs were used. iN-hiPSCs cultures at DIV 21 were treated for 48h with TTX (1 μM, Tocris 1069). In order to study synaptic scaling BDNF was completely removed from the medium at DIV 17 and hiPSCs-induce neurons were kept in a BDNF-free culturing medium for the reason that BDNF was reported to block synaptic scaling up induction (Rutherford et al., 1998).

Imaging

Images were acquired with an epifluorescent upright Zeiss Axio Imager 2.1 microscope, using a 40X objective, equipped with a camera (AxioCam MRm, Zeiss). Images were processed using Axiovision Rel (V4.6) and analysed using ImageJ (NIH, Bethesda, Maryland, USA). Synapsin and PSD-95 *punctae* were quantified by using ImageJ plug-in Foci picker 3D and 2D (Du et al., 2011).

Electrophysiology acquisition and analysis

Intrinsic electrophysiological properties were recorded in current clamp mode. Only cells showing a resting membrane potential < -50mV and stable passive and active properties during recording were taken into consideration. Passive intrinsic membrane properties were determined via injection of a 0.5s hyperpolarizing current of -25pA at a holding potential of -60mV. At the same holding potential action potential (AP) characteristics were determined

from the first AP elicited by a 0.5s depolarizing current just sufficient to bring the membrane potential of the cell to threshold. the rheobase was determined by the amount of current required to generate this first AP. AP threshold was defined as the voltage at which the slope of the membrane potential strongly increases and exceeds 10mV/ms.

sEPSC and mEPSCs were recorded using a Multiclamp 700B amplifier (molecular devices), sampled at 10kHz and filtered at 2kHz. Cells were excluded from analysis if the access resistance exceeded 20 MΩ. mEPSCs were recorded in the presence of TTX (1 μM). sEPSCs and mEPSCs recordings were analyzed using Mini Analysis Program (Synaptosoft, <http://www.synaptosoft.com/MiniAnalysis/>). mEPSC amplitudes and frequencies were statistically tested against untreated control or KS iN-hiPSCs by using two-way ANOVA with Bonferroni comparison.

Statistics

Student-T-test was used for pair-wise comparisons. Unpaired two-way ANOVA comparison was used when two independent variables (e.g. genotype and treatment) were considered in the analysis of only one dependent variable, with Bonferroni post-hoc test. All data is expressed as mean±SEM. Statistical significance: (**, $p < 0.01$).

REFERENCES

- Ba, W., *et al.* ARHGAP12 functions as a developmental brake on excitatory synapse function. *Cell Rep.* 14 (6), 1355–1368, DOI: 10.1016/j.celrep.2016.01.037 (2016).
- Bateup, H.S., Deneffrio, C.L., Johnson, C.A., Saulnier, J.L., and Sabatini, B.L. (2013a). Temporal dynamics of a homeostatic pathway controlling neural network activity. *Front Mol Neurosci* 6, 28.
- Bateup, H.S., Johnson, C.A., Deneffrio, C.L., Saulnier, J.L., Kornacker, K., and Sabatini, B.L. (2013b). Excitatory/inhibitory synaptic imbalance leads to hippocampal hyperexcitability in mouse models of tuberous sclerosis. *Neuron* 78, 510–522.
- Benevento, M. *et al.* Histone methylation by the Kleefstra syndrome protein EHMT1 mediates homeostatic synaptic scaling. *Neuron*. 91 (2), 341–355, DOI: 10.1016/j.neuron.2016.06.003 (2016).
- Chambers, S.M., Fasano, C.A., Papapetrou, E.P., Tomishima, M., Sadelain, M. and Studer, L., 2009. Highly efficient neural conversion of human ES and iPS cells by dual inhibition of SMAD signaling. *Nature biotechnology*, 27(3), pp.275–280.
- Du, G., Drexler, G.A., Friedland, W., Greubel, C., Hable, V., Krücken, R., Kugler, A., Tonelli, L., Friedl, A.A., and Dollinger, G. (2011). Spatial dynamics of DNA damage response protein foci along the ion trajectory of high-LET particles. *Radiat. Res.* 176, 706–715.
- Frega M, van Gestel S, Linda K, van der Raadt J, Keller J, van Rhijn JR, Schubert D, Albers CA, Nadif Kasri N. Rapid neuronal differentiation of induced pluripotent stem cells for measuring network activity on micro-electrode arrays (2016) *JoVE*, in press.
- Johnson, M. A., Weick, J. P., Pearce, R. A. & Zhang, S. C. Functional neural development from human embryonic stem cells: accelerated synaptic activity via astrocyte coculture. *J Neurosci.* 27 (12), 3069–3077, DOI:10.1523/JNEUROSCI.4562-06.2007 (2007).
- Hu, B. Y. *et al.* Neural differentiation of human induced pluripotent stem cells follows developmental principles but with variable potency. *Proc Natl Acad Sci USA.* 107 (9), 4335–4340, DOI: 10.1073/pnas.0910012107 (2010).
- Kim, H. *et al.* miR-371-3 expression predicts neural differentiation propensity in human pluripotent stem cells. *Cell Stem Cell.* 8 (6), 695–706, DOI: 10.1016/j.stem.2011.04.002 (2011).
- Kleefstra, T., Brunner, H.G., Amiel, J., Oudakker, A.R., Nillesen, W.M., Magee, A., Geneviève, D., Cormier-Daire, V., van Esch, H., Fryns, J.-P., *et al.* (2006). Loss-of-function mutations in euchromatin histone methyl transferase 1 (EHMT1) cause the 9q34 subtelomeric deletion syndrome. *Am J Hum Genet* 79, 370–377.
- Kleefstra, T., Kramer, J.M., Neveling, K., Willemsen, M.H., Koemans, T.S., Vissers, L.E.L.M., Wissink-Lindhout, W., Fencikova, M., van den Akker, W.M.R., Kasri, N.N., *et al.* (2012). Disruption of an EHMT1-Associated Chromatin-Modification Module Causes Intellectual Disability. *Am J Hum Genet* 91, 73–82.
- LaVaute, T.M., Yoo, Y.D., Pankratz, M.T., Weick, J.P., Gerstner, J.R. and Zhang, S.C., 2009. Regulation of neural specification from human embryonic stem cells by BMP and FGF. *Stem Cells*, 27(8), pp.1741–1749.
- Martens, M.B., Frega, M., Classen, J., Epping, L., Benevento, M., van Bokhoven, H., Tiesinga, P.H.E., Schubert, D. and Kasri, N.N., 2016. Euchromatin histone methyltransferase-1 regulates cortical neuronal network development. *Scientific Reports*, 6:35756 DOI: 10.1038/srep35756
- McCarthy, K. D. & de Vellis, J. Preparation of separate astroglial and oligodendroglial cell cultures from rat cerebral tissue. *J Cell Biol.* 85, 890–902 (1980).
- Qiu, Z., Sylwestrak, E.L., Lieberman, D.N., Zhang, Y., Liu, X.Y., and Ghosh, A. (2012). the Rett Syndrome Protein MeCP2 Regulates Synaptic Scaling. *J Neurosci* 32, 989–994.
- Rutherford, L.C., Nelson, S.B. and Turrigiano, G.G., 1998. BDNF has opposite effects on the quantal amplitude of pyramidal neuron and interneuron excitatory synapses. *Neuron*, 21(3), pp.521–530.
- Schildge, S., Bohrer, C., Beck, K. & Schachtrup, C. Isolation and culture of mouse cortical astrocytes. *J. Vis. Exp.* (71), e50079, doi:10.3791/50079 (2013).
- Shi, Y., Kirwan, P., Smith, J., Robinson, H.P. and Livesey, F.J., 2012. Human cerebral cortex development from pluripotent stem cells to functional excitatory synapses. *Nature neuroscience*, 15(3), pp.477–486.
- Soden, M.E., and Chen, L. (2010). Fragile X protein FMRP is required for homeostatic plasticity and regulation of synaptic strength by retinoic acid. *J Neurosci* 30, 16910–16921.
- Südhof TC, Czernik AJ, Kao HT, Takei K, Johnston PA, Horiuchi A, Kanazir SD, Wagner MA, Perin MS, De Camilli P (September 1989). "Synapsins: mosaics of shared and individual domains in a family of

synaptic vesicle phosphoproteins". *Science*. 245 (4925): 1474–80. doi:10.1126/science.2506642

Takahashi, K. and Yamanaka, S., 2006. Induction of pluripotent stem cells from mouse embryonic and adult fibroblast cultures by defined factors. *Cell*, 126(4), pp.663-676.

Turrigiano, G.G., 2008. the self-tuning neuron: synaptic scaling of excitatory synapses. *Cell*, 135(3), pp.422-435.

Warlich, E., Kuehle, J., Cantz, T., Brugman, M.H., Maetzig, T., Galla, M., Filipczyk, A.A., Halle, S., Klump, H., Schöler, H.R. and Baum, C., 2011. Lentiviral vector

design and imaging approaches to visualize the early stages of cellular reprogramming. *Molecular Therapy*, 19(4), pp.782-789.

Willemsen, M.H., Vulto-van Silfhout, A.T., Nillesen, W.M., Wissink-Lindhout, W.M., van Bokhoven, H., Philip, N., Berry-Kravis, E.M., Kini, U., van Ravenswaaij-Arts, C.M.A., Delle Chiaie, B. and Innes, A.M.M., 2012. Update on Kleeftstra syndrome. *Molecular syndromology*, 2(3-5), pp.202-212.

Zhang, Y. et al. Rapid single-step induction of functional neurons from human pluripotent stem cells. *Neuron*. 78 (5), 785-798, DOI: 10.1016/j.neuron.2013.05.029 (2013).

¹Department of Cognitive Neuroscience, Radboudumc, Donders Institute for Brain, Cognition and Behaviour, Nijmegen, the Netherlands.

²Synome Ltd., Babraham Research Campus, Cambridge CB22 3AT, UK.

³Department of Psychology, University of Cambridge, Cambridge, UK.

⁴Behavioural and Clinical Neuroscience Institute, University of Cambridge, Cambridge, UK.

⁵Neuroscience Research Center, Institute of Neuropharmacology, Kerman University of Medical Sciences, Kerman, Iran.

⁶Department of Human Genetics, Radboudumc, Donders Institute for Brain, Cognition, and Behaviour, Nijmegen, the Netherlands.

⁷Centre for Clinical Brain Sciences, Chancellors Building, University of Edinburgh, 49 Little France Crescent, Edinburgh EH16 4SB, UK.

⁸Department of Cell Biology, Radboudumc, Radboud Institute for Molecular Life Sciences, Nijmegen, the Netherlands.

Scientific Reports, 2017 Jan 10;7:40284.

doi: 10.1038/srep40284.

four

HAPLOINSUFFICIENCY OF EHMT1 IMPROVES PATTERN SEPARATION AND INCREASES HIPPOCAMPAL CELL PROLIFERATION

Marco Benevento¹, Charlotte A. Oomen¹, Alexa E. Horner^{2,3,4},
Houshang Amiri^{1,5}, Tessa Jacobs¹, Charlotte Pauwels¹, Monica Frega¹,
Tjitske Kleefstra⁶, Maksym V. Kopanitsa², Seth G. N. Grant⁷, Timothy J. Bussey^{3,4},
Lisa M. Saksida^{3,4}, Catharina E.E.M. Van der Zee⁸, Hans van Bokhoven^{1,6},
Jeffrey C. Glennon¹, Nael Nadif Kasri^{1,6}

ABSTRACT

Heterozygous mutations or deletions of the human Euchromatin Histone Methyltransferase 1 (*EHMT1*) gene are the main causes of Kleefstra syndrome, a neurodevelopmental disorder that is characterized by impaired memory, autistic features and mostly severe intellectual disability. Previously, *Ehmt1*^{+/-} heterozygous knockout mice were found to exhibit cranial abnormalities and decreased sociability, phenotypes similar to those observed in Kleefstra syndrome patients. In addition, *Ehmt1*^{+/-} knockout mice were impaired at fear extinction and novel- and spatial object recognition. In this study, *Ehmt1*^{+/-} and wild-type mice were tested on several cognitive tests in a touchscreen-equipped operant chamber to further investigate the nature of learning and memory changes. Performance of mutant mice in the Visual discrimination and reversal learning, object-location paired-associates learning- and extinction learning tasks was found to be unimpaired. Remarkably, *Ehmt1*^{+/-} mice showed enhanced performance on the location discrimination test of pattern separation. In line with improved location discrimination ability, an increase in BrdU-labelled cells in the subgranular zone of the dentate gyrus was observed. In conclusion, reduced levels of EHMT1 protein in *Ehmt1*^{+/-} mice do not result in general learning deficits in a touchscreen-based battery, but lead to increased adult cell proliferation in the hippocampus and enhanced pattern separation ability.

INTRODUCTION

Haploinsufficiency of the Euchromatic histone methyltransferase 1 (*GLP/EHMT1*) gene is the cause of Kleefstra syndrome (KS; #OMIM 610253) (Kleefstra et al., 2006). The core features of KS are intellectual disability (ID), hypotonia and cranio-facial abnormalities, frequently associated by various other conditions as congenital (heart) defects, epilepsy and Autism Spectrum Disorder (ASD) (Kleefstra et al., 2006; Willemsen et al., 2012). The effects of mutations in the *Ehmt* gene studied in *Drosophila* (EHMT) and in mouse models (*Ehmt1*) at molecular, cellular and behavioral levels recapitulated some core features of the KS (Balemans et al., 2010, 2013, 2014; Benevento et al., 2015; Parkel et al., 2009; Schaefer et al., 2009).

We previously reported that haploinsufficiency of the *Ehmt1* gene can result in altered performance on several classical tests of learning and memory (Balemans et al., 2013). *Ehmt1*^{+/-} mice show reduced novelty preference in both novel object and spatial recognition tests, indicating putative perirhinal cortex- and hippocampus-dependent memory impairments. However, *Ehmt1*^{+/-} mice showed normal performance on a spatial navigation task (Barnes maze) and exhibited increased freezing during acquisition of a cued fear-conditioning paradigm and during the test phase of contextual fear conditioning. Finally, *Ehmt1*^{+/-} mice were impaired at cued fear extinction. These findings may be, in part, explained by putative differences in anxiety- and exploration-related behavior (Balemans et al., 2013; Schaefer et al., 2009). Therefore, a thorough characterization of the learning and memory ability of *Ehmt1*^{+/-} mice in low-aversive and low-stress tests, using positive reinforcers, would improve our insight into the cognitive phenotype of this mouse model of intellectual disability.

Here we tested *Ehmt1*^{+/-} and litter-matched wild-type (WT) mice on several learning and memory tests in a touchscreen-equipped operant chamber (Bussey et al., 2008). This cognitive testing method requires animals to respond to visual stimuli by touching a touch-sensitive screen in order to receive an appetitive reward. It imposes a low demand on the motor ability or innate novelty driven exploration of animals and is relatively non-aversive. Due to the flexible nature of this method, animals can be tested on several cognitive domains within the same setup, allowing for between-task comparison. In this study, six different tests of learning and memory were implemented (Figure 4.1), some of which also assessed executive functions such as response inhibition and behavioral flexibility (Oomen et al., 2013; Horner et al., 2013; Mar et al., 2013). In addition, animals were tested on the Location Discrimination task (Oomen et al., 2013; McTighe et al., 2009) in order to assess spatial learning and, in particular, pattern separation (Gilbert et al., 2001).

Although we could confirm lower levels of spontaneous activity in the *Ehmt1*^{+/-} mice compared to WT mice, learning and memory performance of *Ehmt1*^{+/-} mice was mostly unimpaired. Interestingly however, *Ehmt1*^{+/-} mice performed better on the location discrimination task, in particular when similarity of locations was high. Using the location discrimination task, it has been shown that adult born neurons in the hippocampal dentate gyrus (DG) are involved in pattern separation (Clelland et al., 2009). Furthermore, this touchscreen task was found to be sensitive to changes in adult hippocampal neurogenesis in different animal models, both in the case of increased adult neurogenesis (Creer et al., 2010) and decreased adult neurogenesis

A



B

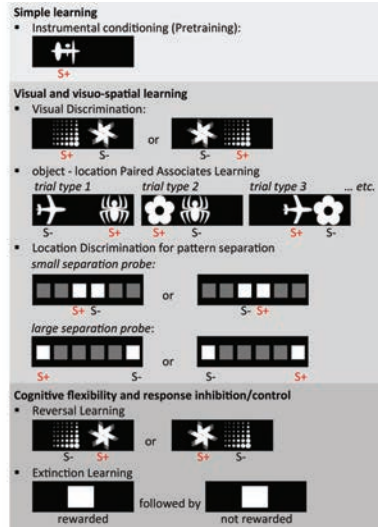


Figure 4.1. Cognitive testing in the touchscreen operant chamber. **A)** Example of a Campden touchscreen operant chamber for mice. **B)** Overview of the cognitive tasks: *Ehmt1*^{+/-} and WT mice were tested on operant conditioning (Pretraining); Visual Discrimination; object-location Paired-Associates Learning; Reversal Learning; Extinction Learning and Location Discrimination for pattern separation. (Panel B; Adapted by permission from Macmillan Publishers Ltd: Nature Neuroscience, copyright (2013) (Nithianantharajah et al., 2013) and Cold Spring Harbor Laboratory Press, copyright (2013) (Oomen et al., 2013))

(Coba et al., 2012). Accordingly, in *Ehmt1*^{+/-} mice, we found that increased location discrimination ability was paralleled by increased neuronal stem cell proliferation in the subgranular zone of the DG as assessed by BrdU incorporation.

RESULTS

Ehmt1^{+/-} mice show reduced activity but normal learning and memory in the touchscreen operant chamber

To test cognitive function of *Ehmt1*^{+/-} mice in low-aversive and low-stress conditions with the use of positive reinforcers, we tested *Ehmt1*^{+/-} and WT mice on several learning and memory tests in touchscreen-equipped operant chambers (for an overview, see Figure 4.1). Cognitive testing was preceded by habituation to the testing chambers, during which activity registration was performed. In accordance with earlier findings (Balemans et al., 2010; Schaefer et al., 2009), *Ehmt1*^{+/-} mice exhibited hypoactivity in the novel environment reflected, in this instance, by a significantly lower number of beam breaks ($U_{\text{Mann-Whitney test}}=149.5, p=0.007$), chamber traversals ($t_{46}=4.383, p<0.001$) and screen touches ($t_{46}=2.635, p=0.011$) compared to their WT counterparts on the first day of habituation (Figure 4.2A, 4.2B and 4.2C). This was replicated in the second cohort of animals tested for behavior in which *Ehmt1*^{+/-} mice made significantly fewer chamber traversals compared to WT mice (WT 36.79 ± 2.17 ; *Ehmt1*^{+/-} 29.39 ± 1.10 ; $p=0.034$).

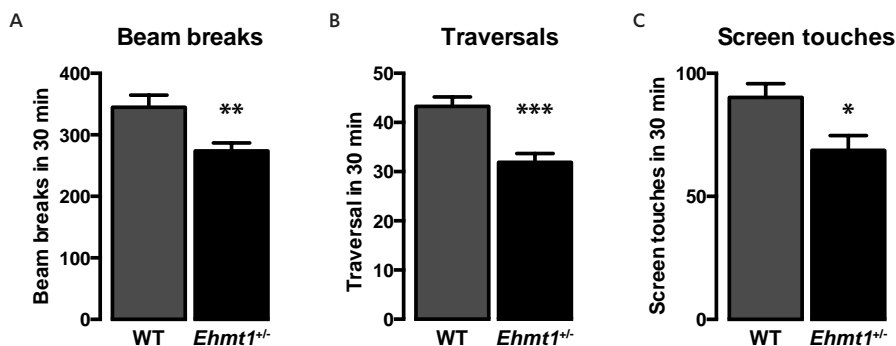


Figure 4.2. Measures of activity during the first exposure of animals to the touchscreen chamber. *Ehmt1*^{+/-} mice (n=23) are hypoactive as they make less. **A)** Beam breaks ($p=0.007$) **B)** Chamber traversals ($p<0.001$) and **C)** Screen touches ($p=0.011$) when compared to WT mice (n=25).

Next, we tested learning and memory abilities of *Ehmt1*^{+/-} mice. Touchscreen testing commenced with instrumental acquisition (pretraining). This was followed by the visual discrimination and reversal-learning task, which was implemented to assess more complex learning and cognitive flexibility. Subsequently, mice were subjected to object-location paired-associates learning task to study their visuospatial learning ability and after this, animals were trained on a simple instrumental response followed by the extinction learning task to study response inhibition. Firstly, *Ehmt1*^{+/-} mice did not differ from WT animals with respect to the average reward collection latency ($p>0.1$) and response latencies ($p>0.1$). As for cognitive performance, *Ehmt1*^{+/-} mice required a similar amount of trials to reach criterion on pretraining, visual discrimination & reversal learning, object-location paired-associates learning and extinction learning tasks (see Table 4.1). During the early phase of reversal learning, *Ehmt1*^{+/-} mice were found to have a higher perseverative index, which may be indicative of reduced cognitive flexibility, however this did not affect the rate of reversal acquisition. Overall, we confirmed that *Ehmt1*^{+/-} mice showed reduced spontaneous activity in a novel environment. Furthermore, *Ehmt1*^{+/-} mice did not exhibit gross impairments in their general learning and memory abilities compared to their WT control counterparts.

Enhanced location discrimination ability in *Ehmt1*^{+/-} mice

In addition to the learning and memory tests described above, a separate cohort of *Ehmt1*^{+/-} mice and WT animals was subjected to the location discrimination task of pattern separation. In this task, animals were required to discriminate and choose between two square response windows. Distance between the locations was varied (i.e. small, intermediate, large), which resulted in increased or decreased similarity of these locations. The rationale behind this is that increased similarity of the to-be-remembered stimuli places a higher demand on resolving confusability between input representations and thus requires, at the network level, increased pattern separation of such inputs (Oomen et al., 2013). Putative impairments of location discrimination at a small distance (but not at a large distance) would be interpreted as a pattern separation

Table 4.1. Outcome-parameters of cognitive testing of *Ehmt1*^{+/-} mice in learning and memory tasks in the touchscreen operant chamber.

Task	Outcome behavioral phenotype	Performance (*)		Significance
Pretraining Visual Discrimination	Normal	WT	8.8±0.5	<i>p</i> >0.1
		<i>Ehmt1</i> ^{+/-}	10.7±0.8	
Pretraining Location Discrimination	Normal	WT	25.0±1.0	<i>p</i> >0.1
		<i>Ehmt1</i> ^{+/-}	23.0±1.1	
Visual Discrimination	Normal	WT	249.2±37.2	<i>p</i> >0.1
		<i>Ehmt1</i> ^{+/-}	234.0±29.6	
Reversal Learning	Normal	WT	549.2±55.6	<i>p</i> >0.1
		<i>Ehmt1</i> ^{+/-}	492.0±63.0	
Reversal Learning early phase	Higher perseverative index (PI) in <i>Ehmt1</i> ^{+/-} mice	WT	3.5±0.2 (PI)	<i>p</i> =0.009
		<i>Ehmt1</i> ^{+/-}	4.9±0.5 (PI)	
Object-location Paired-Associates Learning	Normal	WT	1182±127	<i>p</i> >0.1
		<i>Ehmt1</i> ^{+/-}	1422±128	
Acquisition Instrumental Response	Normal	WT	163.8±7.3	<i>p</i> >0.1
		<i>Ehmt1</i> ^{+/-}	177.0±9.4	
Extinction Instrumental Response	Normal	WT	200.8±18.4	<i>p</i> >0.1
		<i>Ehmt1</i> ^{+/-}	206.7±31.4	

(*) Performance is reported as the average number of trials required to reach the task-criterion for all tests, with the exception of Reversal learning - early phase, in which the perseverative index is reported (PI). PI = total number of errors made/ number of first presentation errors.

impairment. Surprisingly, *Ehmt1*^{+/-} mice outperformed their WT counterparts during location discrimination acquisition at intermediate distance. the *Ehmt1*^{+/-} group required significantly fewer trials and made fewer errors to reach the overall acquisition criterion (Figure 4.3A). Pattern separation probe sessions (using small or large distance between locations) revealed that *Ehmt1*^{+/-} mice required fewer trials to reach the within-session acquisition criterion on such sessions. This seemed to be particularly pronounced on sessions in which animals were required to choose between stimuli at a small separation distance (Figure 4.3B). a main effect of genotype on probe session performance was found ($F_{(1,25)}=6.36$; $p=0.019$), but no genotype × separation interaction ($F_{(1,25)}=1.19$; $p=0.286$). No differences were found in the average reward collection latency (*Ehmt1*^{+/-} mice 1.7±0.2s; WT mice 1.7±0.1s) or response latencies (Correct response latencies: *Ehmt1*^{+/-} mice 7.4±1.3s; WT mice 7.6±0.7s; incorrect response latencies: *Ehmt1*^{+/-} mice 6.7 ± 0.9s; WT mice 6.9±0.6s, all $p>0.1$). To summarize, *Ehmt1*^{+/-} mice showed enhanced acquisition of the location discrimination task and enhanced performance on post-acquisition pattern separation probe sessions. the improvement was most pronounced on sessions in which stimuli were presented at a small or intermediate distance, indicating enhanced pattern separation ability.

Increased neural stem cell proliferation in the subgranular zone of the DG of *Ehmt1*^{+/-} mice

Performance in the location discrimination task, particularly on trials which pose a high demand on pattern separation ability, was previously found to depend on adult neurogenesis

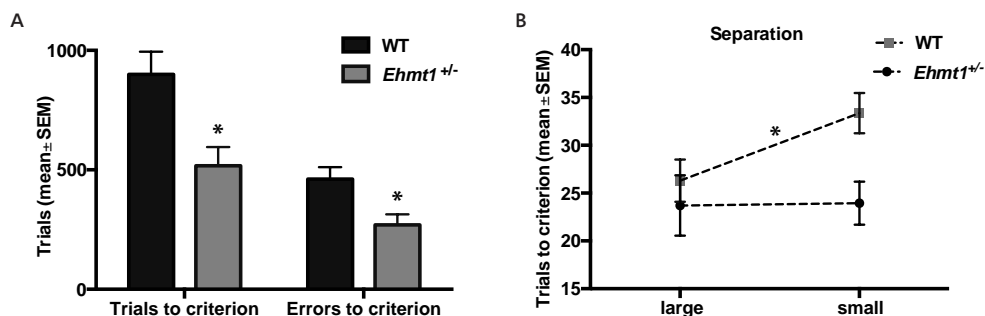


Figure 4.3. Location Discrimination performance. **A)** the number of trials and errors animals required to reach the performance criterion during the initial acquisition phase at an intermediate distance. **B)** Performance on Location Discrimination large separation and small separation probe sessions. *Ehmt1*^{+/-} (n=8) mice outperform WT mice (n=17), as they needed on average fewer trials to reach the within-session criterion of 7 correct out of 8 consecutive responses (main effect $F_{(1,25)}=6.36$; $p=0.019$).

in the DG (Clelland et al., 2009). Additionally, increased location discrimination performance has been correlated with enhanced adult neurogenesis (Creer et al., 2010). Given the better performance of *Ehmt1*^{+/-} mice in this task compared to WT controls, we assessed whether *Ehmt1* haploinsufficiency led to an alteration in the number of proliferating neural stem cells in the DG subgranular zone (SGZ). To do this, we first analyzed the expression pattern of EHMT1 in the DG SGZ (Figure 4.4A). We observed that EHMT1 intensity levels were significantly higher in the subgranular layer compared to the granular cell layer of the DG (Figure 4.4B) (SGZ=68.55±3.20 a.u.; DG=53.85±4.83 a.u.; n=5-5; $t=2.53$, $p=0.035$, t-test). Interestingly, H3K9me2 immunolabeling pattern paralleled the EHMT1 expression pattern (Figure 4.4C), which together with G9a/EHMT2 are responsible for the catalysis of H3K9me2 (Kubicek et al., 2007; Vedadi et al., 2011).

The increase in EHMT1 levels in the SGZ prompted us to test whether EHMT1 is involved in the regulation of cell proliferation in the DG. To this end, we quantified the number of cells in the SGZ that were positive for Ki-67 (Ki-67⁺), a marker of proliferating cells. Although we observed a nominal increase in the amount of Ki67⁺ cells in *Ehmt1*^{+/-} mice, this was not significant (Figure 4.5A), (WT mice 4796±721 cells; *Ehmt1*^{+/-} mice 6296±803 cells; n=8 and 7 animals respectively; $t=1.392$, $p=0.187$, t-test). Ki-67 is a proliferative marker expressed during G1, S and G2 phase of the cell cycle. Although Ki-67 expression is informative, its temporal resolution is not precise enough to give information about the actual pool of cells with replicating DNA. To gain more insight we used BrdU labeling, since this marker only labels the cells that are actively replicating DNA (Kee et al., 2002). WT and *Ehmt1*^{+/-} P70 mice were injected with BrdU (50µg/g) four times every 4h during a 12h period and animals were sacrificed 24h later. BrdU⁺ cells were quantified using serial sections as described previously Hayes and Nowakowski (2002). *Ehmt1*^{+/-} mice had a higher number of BrdU⁺ cells compared to WT animals (Figure 4.5B) (WT 3216±415 cells; *Ehmt1*^{+/-} 4826±361 cells; n=8 and 7 animals respectively; $t=2.882$, $p=0.012$, t-test). Collectively, these experiments suggest that EHMT1 is involved in regulating proliferation of neural stem cells in the DG SGZ.

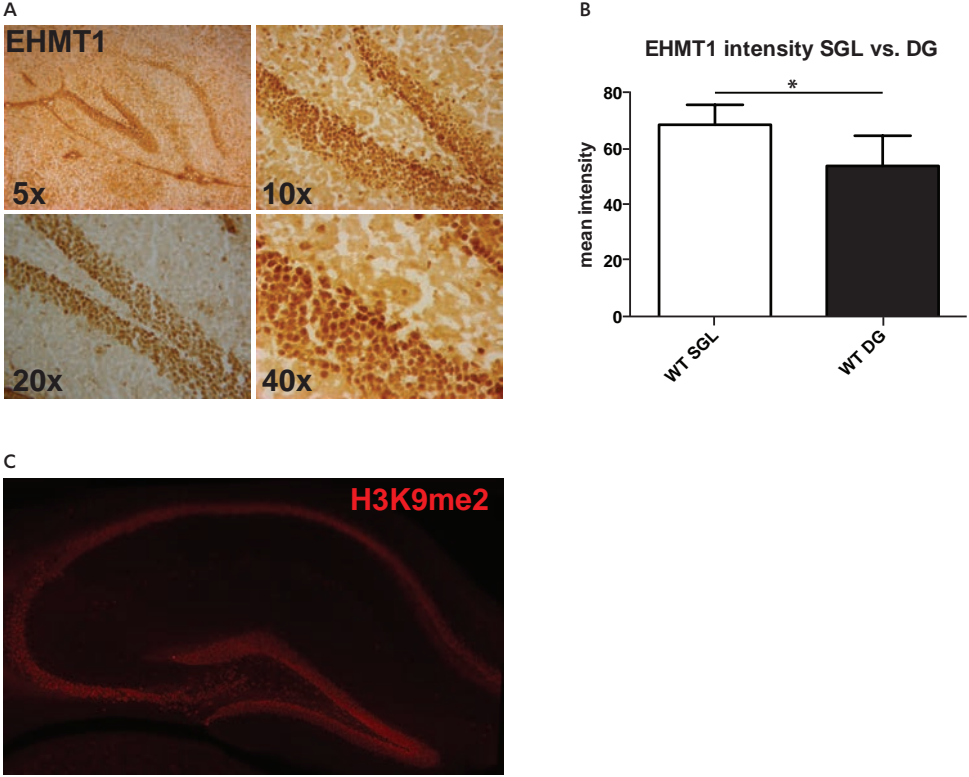
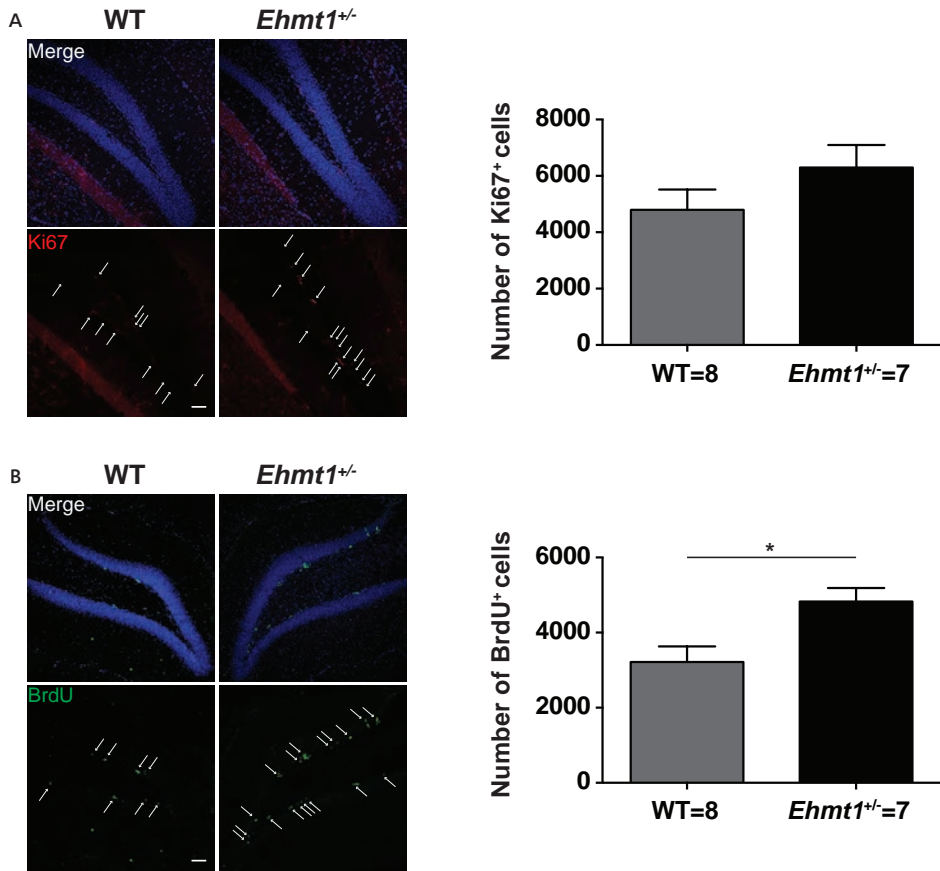


Figure 4.4. EHMT1 expression pattern in the DG. **A)** EHMT1 staining intensity in the DG at different levels of magnification **B)** Quantification of EHMT1 staining intensity in the subgranular zone (SGZ) (n=30 cells) and DG (n=30 cells). **C)** Representative H3K9me2 immunolabeling in a hippocampal section (Scale bar: 100µm).

DISCUSSION

We show here that *Ehmt1* haploinsufficient mice perform normally on several tests of learning and memory in a touchscreen-equipped operant chamber. *Ehmt1*^{+/-} mice acquired visual discrimination and reversal learning, object-location paired-associates learning and extinction learning to the same level and at the same rate as did WT controls. *Ehmt1*^{+/-} mice did show signs of reduced flexibility, as reflected in an increased perseveration index during the early phase of reversal learning. However, this did not impact overall acquisition speed of the reversed contingencies and perseverative behavior did not differ during location discrimination training, which also contains a reversal component. It can therefore be concluded that *Ehmt1*^{+/-} mice are generally unimpaired at learning and memory tasks when tested in a low-stress and unaversive environment, using highly translatable cognitive tests. This is quite remarkable, as patients with KS have in most cases severe intellectual disability (Pagon et al., 1993) and exhibit significant behavioral and psychiatric problems including anxiety (personal communication). It is possible that impairments found earlier in classical learning and memory tests (Balemans et al., 2013) such as novel object (and object in place)



FOUR

Figure 4.5. Increased cell proliferation in the DG of *Ehmt1*^{+/-} mice. **A)** Ki67 immunoreactivity (red) in the DG SGZ. White arrows indicate the Ki67⁺ cells. Below total quantification of Ki67⁺ cells (WT=8; *Ehmt1*^{+/-}=7; $p=0.187$) **B)** BrdU immunolabeling (green) in the DG SGZ. White arrows indicate the BrdU⁺ cells. Total amount of BrdU⁺ cells (WT n=8 animals; *Ehmt1*^{+/-} n=7 animals; $p=0.012$). For all images scale bar: 20 μ m.

recognition memory and fear conditioning, could be partially driven by enhanced anxiety in *Ehmt1*^{+/-} mice (Balemans et al., 2013) and to a lesser extent by impaired cognitive ability. Extended training time during operant conditioning may therefore be beneficial for cognitive performance of *Ehmt1*^{+/-} mice as it ensures thorough habituation to the testing setup. Comparing cognition in mice and humans has traditionally been difficult. the development of touchscreen test for rodents now makes it possible to perform the same test in both species. In a recent study, mice lacking the *Dlg2* gene (*Dlg2*^{-/-}) and individuals with *DLG2* CNV deletions were tested in a touchscreen test for object-location paired-associates task (Nithianantharajah et al., 2015). Interestingly, both mice and humans lacking the *DLG2* gene showed impaired performances. It will therefore be interesting to compare the observations in this study with the results from Cambridge Neuropsychological Test Automated Battery, (CANTAB) performed on KS patients.

As for the enhanced performance of *Ehmt1*^{+/-} mice compared to WT controls on the location discrimination task, this may indicate an improved DG-dependent pattern separation function (McTighe et al., 2009; Oomen et al., 2013). Previously, pattern separation ability (as assessed by location discrimination performance), was shown to be sensitive to disruptions in adult hippocampal neurogenesis (Clelland et al., 2009; Coba et al., 2007), whereas enhanced performance was found to correlate with increased neural stem cell (nsc) proliferation in mice housed with a running wheel (Creer et al., 2010). In line with this, we found that adult *Ehmt1*^{+/-} mice have higher levels of cell proliferation in the DG, as measured by the number of BrdU⁺ cells in the SGZ. Although this was not paralleled by a significant increase in the number of Ki67⁺ cells, there was a nominal trend for a higher number of cells in *Ehmt1*^{+/-} mice. While both Ki67 and BrdU are considered *bona fide* markers of cell proliferation (Kee et al., 2002), Ki67 is expressed during most cell cycle phases, potentially giving a less precise estimation of the actual pool of cells that are replicating the DNA. This is in contrast with BrdU, which is only incorporated into DNA during the S-phase (Gitlin et al., 2014). Enhanced proliferation levels in the *Ehmt1*^{+/-} mice are in line with the fact that EHMT1 likely restricts proliferation of neural stem cells in the SGZ and with its higher expression in the SGZ demonstrated in this study. Several lines of evidences suggest that EHMT1, together with its partner EHMT2, is required to restrict developmental genetic programs for correct cell proliferation and cell differentiation (Ogawa et al., 2002; Chen et al., 2014; Zylitz et al., 2015). Interestingly, the lack of EHMT1/EHMT2 was shown to result in a failure of cells to undergo cell commitment and increased proliferation of human hematopoietic stem cells, brown adipose cells and retinal layering (Chen et al., 2012; Katoh et al., 2012; Schones et al., 2014; Ohno et al., 2013). Moreover, EHMT1/2 interacts with PRC2 (Polycomb complex) to repress and prevent re-expression of time developmental genes (Mozzetta et al., 2015). In this regard, it is interesting to note that *Ezh2*^{-/-} homozygous mice, a known component of PRC2 complex, showed a higher number of BrdU⁺ cells in the developing cerebral cortex (Pereira et al., 2010). Further studies are needed to clarify the role of EHMT1 in the generation of new neurons in the DG, and whether this histone methyltransferase is involved in regulating the balance between self-renewal and differentiation of neurons or glial cells. Furthermore, this would provide valuable information about the cellular mechanisms that underlie KS.

MATERIALS & METHODS

Animals

For the experiments presented in this study, mice heterozygous for a targeted loss-of-function mutation in the *Ehmt1* gene (*Ehmt1*^{+/-} mice) and their WT littermates on C57BL/6 background were used, as previously described (Balemans et al., 2010). Animal experiments were performed at two sites, the Radboudumc (Nijmegen, the Netherlands) and the University of Cambridge (Cambridge, UK). Each test was done entirely at one site or completely at both sites, when done in duplicate. Mice used in experiments executed at the Radboudumc (Nijmegen, the Netherlands) were bred in-house. For behavioral experiments performed at the University of Cambridge,

male mice from Radboudumc (Nijmegen, the Netherlands) were re-derived into the Biological Services Unit of the Babraham Research Campus (Cambridge, UK) on a C57BL/6^{Babcr} background. Males bearing the mutation were then crossed with C57BL/6^{Babcr} WT females to generate the mice used in the present study. These mice were transferred to the animal facility of the University of Cambridge (Cambridge, UK) for behavioral testing around 8 weeks of age. Only males were used for all the experimental procedures here described. Male mice were housed in standard size cages (396mm w × 215mm d × 172mm h) containing a plastic shelter and enrichment material in a temperature and humidity-controlled room under a 12h light/dark cycle (lights off at 7:00 am). All procedures involving animal experimentation and experimental protocols were carried out in accordance and were approved by the Animal Care Committee of the Radboudumc, the Netherlands, conforming to the guidelines of the Dutch Council for Animal Care and the European Communities Council Directive of 24 November 1986 (86/609/EEC) or were executed in accordance with the United Kingdom Animals (Scientific Procedures) Act (1986).

Cognitive testing in the touchscreen operant chamber

Experimental design: *Ehmt1*^{+/-} mice and their WT littermates were tested using touchscreen-equipped operant chambers, which make use of positive reinforcement (liquid or food reward). Two cohorts of mice were used, which were tested during daily, 1h sessions (4-7 times per week) for several months. the first cohort was tested at the University of Cambridge and was composed of WT n=25 and *Ehmt1*^{+/-} n=23 mice that were 12 weeks of age when testing began. Mice were first subjected to a simple measure of activity registration, which occurred during the first habituation session. Following this, 13 WT and 10 *Ehmt1*^{+/-} mice were given further testing. After pretraining, these mice were subjected to the following learning and memory tasks: Visual Discrimination and Reversal learning, object-location paired-associates learning and extinction learning, consecutively. a second cohort of mice was tested at the Radboudumc (Nijmegen, Netherlands). This cohort was composed of 19 WT and 10 *Ehmt1*^{+/-} mice that were 11 weeks old at the start of testing. Similar to the first cohort, mice were first tested on a simple measure of activity and subjected to pretraining. This was followed by the location discrimination task for spatial pattern separation, which consisted of an initial acquisition phase followed by pattern separation probe-sessions. In order to ensure that animals were motivated to perform the task for a food reward, all mice were subjected to mild food restriction to 85-90% of their free feeding body weight.

Apparatus: automated touchscreen operant chambers were used of two similar types; Bussey-Saksida touchscreen chambers (Campden Instruments, Loughborough, UK) and testing chambers assembled from separate parts (Med Associates, Inc., St. Albans, VT, USA) in-house. For a detailed description of both types of boxes, see Horner *et al.*, 2013. In short, both types of chambers consisted of a modular chamber made out of black Perspex walls and a metal grid floor within a sound-attenuating box, a reward tray, equipped with a tray-light, was situated opposite to the screen in which either strawberry milkshake (Campden) or sugar pellets (Med-Associates) was delivered. Chambers were equipped with a light on the ceiling (house-light, 3W), a tone generator and a touch-sensitive screen using infrared photocells. Campden chambers

were additionally equipped with infrared beams at the front and back of the chamber for activity registration. a black plastic mask with response windows was used to cover the touchscreen during testing, dimensions of which were dependent on the specific task.

Learning and memory tests: for an overview of the tests see Figure 4.1 and a short description below. Detailed protocols used in this study are available elsewhere (Oomen et al., 2013; Horner et al., 2013; Mar et al., 2013). Pretraining was utilized to train mice to touch the screen for a reward and familiarize animals to common trial elements: a training session (maximum 1h) consisted of 30 trials and to start each trial, mice were required to nose-poke in the reward tray to “initiate” stimulus presentation on the screen. Upon making a correct response, touching the screen resulted in the delivery of a food reward and the sound of a tone (secondary reinforcer). An incorrect response resulted in a time-out (5s) and the presentation of a correction trial (i.e. the same stimulus and stimulus location) until a correct response was made. Correction trials were used to prevent the formation of a stimulus- or side-bias and were also utilized in the visual discrimination and reversal learning task and the paired-associates learning task. Trials were separated by an inter-trial interval lasting 20s. the first two pretraining sessions consisted of habituation to the testing chamber, during which activity registration was performed by recording the number of infrared beam breaks at the front and back of the chamber. Pretraining preceding the visual discrimination task was performed using a 2-hole mask and a range of 40 visual stimuli (randomly presented one at a time, in one of the two locations), whereas pretraining for the location discrimination task was performed without a mask and using a white square presented in 1 of 6 locations.

For visual discrimination and reversal learning (Horner et al., 2013; Mar et al., 2013), mice had to discriminate between two stimuli: “fan” (correct, S+) and “marbles” (incorrect, S-), (see Figure 3b) (Horner et al., 2013), presented in a pseudorandom location. Mice were considered to have acquired visual discrimination when they reached a performance criterion of at least 80% of trials correct (not including correction trials) on two consecutive 30-trial sessions. Mice were moved on to reversal learning individually, after they attained visual discrimination criterion. Reversal was identical to visual discrimination, except that S+ and S- were reversed. Criterion for completion of reversal learning was considered to be at least 80% correct on 2 consecutive sessions, but all mice received a minimum of 20 sessions regardless. Mice that did not attain criterion were tested for 25 sessions. the first two sessions of visual discrimination and reversal learning were each run over two days, in four sessions of 15 trials. These sessions were not counted towards the acquisition or reversal criteria.

Mice trained on visual discrimination and reversal learning were transferred to object-location paired-associates learning but were first subjected to the final phase of pretraining using a 3-hole mask. For paired-associates learning, three stimuli were used; flower, plane and spider. Whether a stimulus was correct was determined by the location in which it was presented (flower/left; plane/middle; spider/right). On each trial, one stimulus was presented in its correct location and one in its incorrect location resulting in 6 trial types (Figure 4.3) (Horner et al., 2013). Criterion for paired-associates learning acquisition was 70% correct on 2 consecutive sessions, but all mice received 50 sessions regardless.

Acquisition and extinction of a simple instrumental response (Mar et al., 2013) was done after paired-associates learning, using the same 3-hole mask. Animals were required to touch a single white square in the central window and criterion was attained when 30 trials were finished in < 14.5min for 5 consecutive days. During the subsequent extinction phase, there was no requirement to initiate, but an initiation delay was implemented (5s). the stimulus was presented in the central touchscreen window for 10s. If the stimulus was not touched during this time ("omission"), it disappeared at the end of the 10s, followed by a 5s inter-trial interval. If the stimulus was touched, it disappeared immediately and the 5s inter trial interval began. Criterion for this phase of the task was $\geq 77\%$ (23/30) omissions on 2 consecutive days, but mice were tested for a minimum of 10 sessions.

Finally, location discrimination was used to assess memory for screen locations and spatial pattern separation ability (Oomen et al., 2013; McTighe et al., 2009) in a separate cohort of mice. Animals had to discriminate and choose between two illuminated (100% white) squares that were presented at small, intermediate or large distance (separation), within a row of 6 potential locations. Inactive locations were identifiable from the background of the screen through low illumination (10% white) and no mask was used. Mice were required to respond correctly in 7 out of 8 consecutive trials (acquisition) after which reward contingencies were reversed (reversal). Mice were first trained on intermediate separation (locations 2 and 5) until they could attain the overall acquisition criterion (perform one acquisition and one reversal within a session of maximum 60 trials, for 3 out of 4 consecutive days). Subsequently, pattern separation ability was assessed during probe sessions of unlimited trials, using only small separation (locations 3 and 4) or large separation (locations 1 and 6). In total, 12 probe sessions were applied, 6 of each separation in blocks of 2 sessions.

Adult neurogenesis and BrdU injections

In order to investigate differences in adult neurogenesis in the SGZ of the DG, proliferation rate of neural stem cells in *Ehmt1*^{-/-} mice (n=7) was compared to that of WT animals (n=8) was assessed using BrdU and Ki-67 immunohistochemistry. For this, mice were intraperitoneally injected with BrdU 50 µg/g (Sigma, B9285) at postnatal day 70±10 days for four times every 4h during 12h period, as previously described (Hayes and Nowakowski, 2002). Mice were perfused transcardially, 24h after the first BrdU injection with PFA 4% and sucrose 4% in PBS 1X. Brains were removed and kept in the same perfusion solution o/n at 4 °C and then replaced with PBS 1X with NaN₃ 0.025%. Coronal 30µm thick sections throughout the hippocampus were cut with a Leica VT 1000S vibratome. One in ten brain sections were collected for BrdU and Ki-67 immunohistochemistry and kept at 4 °C in PBS 1X with NaN₃ 0.025%.

BrdU and Ki-67 immunohistochemistry and stereological counting

For BrdU immunolabeling sections were first post fixed for 2h in PFA 4%/ sucrose 4% and washed in PBS 0.1 M/ 0.1% triton. Subsequently, the sections were immersed in pre-cooled HCl 1 M for 10min at 4 °C, after 10min in HCl 2 M at room temperature, and transferred for additional 10min at 37 °C in the same solution. After this, sections were rinsed in boric acid 0.1 M (pH 8.5) for

12min at room temperature. Subsequently, sections were washed and permeabilized in PBS 1X with Triton 0.1% and then blocked with Normal Goat Serum (NGS) 10%, Normal Donkey Serum (NDS) 10% in PBS 1X/ 0.1% triton pH: 7.6 for 1h at room temperature. Primary antibodies against BrdU (1:200, Abcam ab1893), Ki67 (1:50, BD Pharmigen 550609) and H3K9me2 (1:100, Millipore 07-449) in PBS 1X/ 0.1% triton with NGS 5% and NDS 5% were incubated overnight at 4 °C. Brain sections were washed and incubated in Donkey anti-sheep Alexa Fluor 488 (1:1000, Invitrogen A11015) and Goat anti-Mouse 568 (1:1000, Invitrogen A11031) secondary antibodies in NGS 5%, NDS 5% in PBS 1X/ 0.1% triton for 1h at room temperature in darkness. Nuclear staining with Hoechst 33342 (1:5000, Invitrogen H3570) was performed after additional washing of secondary antibody excess in PBS 1X/ 0.1% triton. Free-floating sections were then washed with PBS 1X and mounted on a glass slide. Imaging was performed either with a Fluoview FV1000 confocal microscope (Olympus) for representative pictures or with a ZEISS IMAGER 2.1 epifluorescent microscope that was used for counting BrdU⁺ and Ki67⁺ cells. the total number of cells was calculated by counting the amount of either of BrdU⁺ or Ki67⁺ cells in the SGL on 8 coronal 30µm brain sections. Every section was a cranio-caudal transition of 300 µm encompassing the entire length of the hippocampus, thus the total number of cells was calculated by the summing the number of cells per section times 10 (Quadrato et al., 2012).

EHMT1 immunostaining and brain preparation

A separate group of WT, n=5 mice at postnatal 70±10 days, were sacrificed by cervical dislocation and brains were snap frozen in liquid nitrogen and stored at -80°C. Brains were embedded in the Shandon M-1 embedding matrix (Thermo Scientific). the brains were sectioned on a cryostat at -20°C in the sagittal plane from medial to lateral and mounted on Superfrost Plus glass slides (Thermo Scientific). Brain sections were first fixated onto glass slides with ice-cold methanol for 10min at -20°C. After washing with Tris buffered saline (TBS) 1X, pH: 7.6 with Tween 0.05% (TBS-T), slides were treated with hydrogen peroxide 0.3% for 10min RT and washed in TBS-T. Ultra-Tek Superblock for 5min was used to block nonspecific immunolabeling. Incubation with an EHMT1 primary antibody (1:100 Abcam, ab 41969) was conducted, initially for 30min at room temperature and then continued overnight at 4°C. the next day, the incubation box was left at room temperature for 30min before washing with TBS-T. Thereafter, the slides were incubated with the Ultra-Tek anti-polyvalent staining system. After another 5 times 10min washing steps with TBS-T, slides were incubated with Ultra/Tek HRP for 10min. After washing with Tris buffer (TB) pH: 7.6, 3,3' diaminobenzidine tetrahydrochloride 0.05% (DAB, Sigma) was added. After 10min the DAB reaction was stopped by washing in TB, followed by washing in TBS. Dehydration was done in a series of ethanol dilutions (50%, 70%, 96%, 96%, 100%, 100%; each for 1min). Then slides were treated with xylene and coverslipped with Pertex (Histolab Products AB, Göteborg, Sweden).

Analysis of EHMT1 immunostaining was performed using a bright light microscope (Leitz Dialux 22, Leitz Microscopes) and pictures were taken with a microscope camera (Nikon Coolpix 990, Nikon Corporation, Tokyo, Japan). EHMT1 intensity levels were compared between the SGZ and the granular cell layer in the DG in WT animals only (n=5). We selected the SGZ by delineating a distance of one cell layer at the border of the *hilus* and granular cell

layer. Mean density was measured by analyzing the intensity levels of EHMT1 staining in cell nuclei. Measurements were performed in 30 cells within the DG, 30 cells in the SGZ, and in the outer area for background density values. The values measured ranged between 0 (dark) and 256 (light), here reported as arbitrary units (a.u.). All the values were then transposed (i.e. subtracted from 256), in order to have a higher value corresponding to higher density. In this way, a dark stained cell was represented by a high-density value. These density values were then used to calculate the mean and standard error mean (SEM), and shown in tables and bar-graphs.

Analysis & Statistics

Touchscreen operant training. For activity assessment during habituation, total beam breaks, chamber traversals and screen touches in 30min were compared between genotypes. For pretraining, visual discrimination & reversal learning, paired-associates learning, extinction learning, the number of trials animals required to reach performance criterion was calculated for each mouse and averaged across genotypes. For extinction, it was necessary to exclude one mouse from the analysis after acquisition, due to the repeated escapes from the chamber, which resulted in WT $n=13$, *Ehmt1*^{+/-} $n=10$ (for acquisition) and $n=9$ (for extinction). In addition to the 'trials to criterion' measure, for the Reversal learning paradigm the number of errors (incorrect choices on first presentation trials) and correction trials committed were analyzed, specifically during the early reversal phase (i.e. on sessions where animals performed below 50% correct). This was done to calculate an average "perseveration index" (PI) per animal; the ratio of CTs to incorrect responses on first presentation trials (Brigman et al., 2008). For location discrimination, the number of trials and errors mice required to reach the overall acquisition criterion of Location Discrimination training at intermediate distance were calculated. Furthermore, the number of trials mice required to attain within-session acquisition, but not reversal, are reported for small and large separation probes. This was done because the within-session reversal criterion was not reached consistently. In cases where animals had not reached the acquisition criterion, the total amount of trials performed within that session + 8 was used, as this would have been the minimum amount of trials needed to be able to reach that criterion. Based on anatomical MRI scans of mice within the cohort of animals that were tested in the location discrimination task, performed after the last day of behavioral testing (data not shown here), two *Ehmt1*^{+/-} mice were excluded from location discrimination analysis, as these animals showed, bilaterally, greatly enlarged ventricles and reduced hippocampi. In addition, two WT mice did not reach the overall criterion during initial acquisition at intermediate distance (after 40 sessions) and were excluded from further analysis, resulting in WT $n=17$, *Ehmt1*^{+/-} $n=8$. Finally, for both cohorts, the average reward collection latency and response latency were calculated.

Proliferation assay. For the analysis of cell proliferation, we counted the total number of either Ki67⁺ or BrdU⁺ cells in the DG per mouse. The number of cells positive for either marker was then averaged within the genotype to subsequently perform between genotypes statistical comparisons. For EHMT1 intensity analysis density values were then used to calculate the mean and standard error mean (SEM), and shown in tables and bar-graphs.

All experiments. Data are presented as the mean±SEM. Where possible, data were analyzed using Student's t-test for independent samples, one-sample t-test and repeated-measures ANOVA (within-subject factor: session block, between-subject factor: genotype), as appropriate. Where the assumption of homogeneity of variance was rejected (Levene's test), an unequal variance t-test was used. Where the assumption of normality was rejected (Shapiro-Wilk test), attempts were made to normalize the distributions with appropriate transformations, but where data could not be normalized with transformations, the non-parametric Mann-Whitney U tests was used instead of the standard t-test. All ANOVA data were subjected to Mauchly's test of sphericity to ensure that the homogeneity of variance assumption was not violated. Where it was, the Huynh-Feldt correction was used. All statistical analyses were conducted with a significance level of $\alpha=0.05$, using SPSS version 17.0.

ACKNOWLEDGEMENTS

The research of the authors was supported by a Hypatia fellowship award of the Radboudumc [to N.N.K.]; EU-FP7 Marie Curie International Reintegration Grant 277091 [to N.N.K.]; the Jerome Lejeune Foundation [to N.N.K]; the European Union Seventh Framework Programme under the grant agreement HEALTH-F2-2009-241995 ("GENCODYS project") [to HvB]; the European Union Seventh Framework Programme under the grant agreement HEALTH-F2-2011-278948 ("TACTICS project") [to J.C.G.]; the European Union Seventh Framework Programme under the grant agreement HEALTH-F2-2012-305697 ("OPTIMISTIC project") [to J.C.G.]; the European Union Seventh Framework Programme under the grant agreement HEALTH-F2-2013-603016 ("MATRICS project") [to J.C.G.].

COMPETING FINANCIAL INTERESTS

The authors declare no competing financial interests.

AUTHOR CONTRIBUTION

Conceptualization, MB, CO, JG and NNK; Investigation, MB, CO, AH, HA, TJ, CP, CZ; Writing - original draft, MB, CO and NNK; Writing – review & editing, AH, HA, MF, TK, MK, SG, TB, LS, CvdZ, HvB and JG; Supervision, NNK and JG; Funding acquisitions, NNK and JG

REFERENCES

- Balemans, M. C. M. *et al.* Reduced Euchromatin histone methyltransferase 1 causes developmental delay, hypotonia, and cranial abnormalities associated with increased bone gene expression in Kleefstra syndrome mice. *Dev. Biol.* 386, 395–407 (2014).
- Balemans, M. C. M. *et al.* Hippocampal dysfunction in the Euchromatin histone methyltransferase 1 heterozygous knockout mouse model for Kleefstra syndrome. *Hum Mol Genet* 22, 852–866 (2013).
- Balemans, M. C. M. *et al.* Reduced exploration, increased anxiety, and altered social behavior: Autistic-like features of euchromatin histone methyltransferase 1 heterozygous knockout mice. *Behav Brain Res* 208, 47–55 (2010).
- Benevento, M., van de Molengraft, M., van Westen, R., van Bokhoven, H. & Nadif Kasri, N. the role of chromatin repressive marks in cognition and disease: a focus on the repressive complex GLP/G9a. *Neurobiol Learn Mem* 124, 88–96 (2015).
- Brigman, J.L., Feyder, M., Saksida, L.M., Bussey, T.J., Mishina, M. and Holmes, A., 2008. Impaired discrimination learning in mice lacking the NMDA receptor NR2A subunit. *Learning & memory*, 15(2), pp.50-54.
- Bussey, T.J., Padain, T.L., Skillings, E.A., Winters, B.D., Morton, A.J. and Saksida, L.M., 2008. the touchscreen cognitive testing method for rodents: how to get the best out of your rat. *Learning & Memory*, 15(7), pp.516-523.
- Chen, X., Skutt-Kakaria, K., Davison, J., Ou, Y.L., Choi, E., Malik, P., Loeb, K., Wood, B., Georges, G., Torok-Storb, B. and Paddison, P.J., 2012. G9a/GLP-dependent histone H3K9me2 patterning during human hematopoietic stem cell lineage commitment. *Genes & development*, 26(22), pp.2499-2511.
- Chen, E.S., Giguek, C.O., Rosenfeld, J.A., Diallo, A.B., Maussion, G., Chen, G.G., Vaillancourt, K., Lopez, J.P., Crapper, L., Poujol, R. and Shaffer, L.G., 2014. Molecular convergence of neurodevelopmental disorders. *The American Journal of Human Genetics*, 95(5), pp.490-508.
- Clelland, C.D., Choi, M., Romberg, C., Clemenson, G.D., Fragniere, A., Tyers, P., Jessberger, S., Saksida, L.M., Barker, R.A., Gage, F.H. and Bussey, T.J., 2009. a functional role for adult hippocampal neurogenesis in spatial pattern separation. *Science*, 325(5937), pp.210-213.
- Creer, D. J., Romberg, C., Saksida, L. M., van Praag, H. & Bussey, T. J. Running enhances spatial pattern separation in mice. *Proc Natl Acad Sci USA* 107, 2367–2372 (2010).
- Coba, M. P. *et al.* TNiK is required for postsynaptic and nuclear signaling pathways and cognitive function. *J. Neurosci.* 32, 13987–13999 (2012).
- Gilbert, P.E., Kesner, R.P. and Lee, I., 2001. Dissociating hippocampal subregions: a double dissociation between dentate gyrus and CA1. *Hippocampus*, 11(6), pp.626-636.
- Gitlin, A.D., Shulman, Z. and Nussenzweig, M.C., 2014. Clonal selection in the germinal centre by regulated proliferation and hypermutation. *Nature*, 509(7502), pp.637-640.
- Gupta, S., Kim, S.Y., Artis, S., Molfese, D.L., Schumacher, A., Sweatt, J.D., Paylor, R.E. and Lubin, F.D., 2010. Histone methylation regulates memory formation. *The Journal of neuroscience*, 30(10), pp.3589-3599.
- Gupta-Agarwal, S., Franklin, A.V., DeRamus, T., Wheelock, M., Davis, R.L., McMahon, L.L. and Lubin, F.D., 2012. G9a/GLP histone lysine dimethyltransferase complex activity in the hippocampus and the entorhinal cortex is required for gene activation and silencing during memory consolidation. *The Journal of Neuroscience*, 32(16), pp.5440-5453.
- Hayes, N.L. and Nowakowski, R.S., 2002. Dynamics of cell proliferation in the adult dentate gyrus of two inbred strains of mice. *Developmental brain research*, 134(1), pp.77-85.
- Horner, A.E., Heath, C.J., Hvoslef-Eide, M., Kent, B.A., Kim, C.H., Nilsson, S.R., Alsiö, J., Oomen, C.A., Holmes, A., Saksida, L.M. and Bussey, T.J., 2013. the touchscreen operant platform for testing learning and memory in rats and mice. *Nature protocols*, 8(10), pp.1961-1984.
- Katoh, K., Yamazaki, R., Onishi, A., Sanuki, R. and Furukawa, T., 2012. G9a histone methyltransferase activity in retinal progenitors is essential for proper differentiation and survival of mouse retinal cells. *The Journal of Neuroscience*, 32(49), pp.17658-17670.
- Kee, N., Sivalingam, S., Boonstra, R. and Wojtowicz, J.M., 2002. the utility of Ki-67 and BrdU as proliferative markers of adult neurogenesis. *Journal of neuroscience methods*, 115(1), pp.97-105.
- Kleefstra, T., Brunner, H.G., Amiel, J., Oudakker, A.R., Nillesen, W.M., Magee, A., Geneviève, D., Cormier-Daire, V., Van Esch, H., Fryns, J.P. and Hamel, B.C., 2006. Loss-of-function mutations in euchromatin histone methyl transferase 1

(EHMT1) cause the 9q34 subtelomeric deletion syndrome. *The American Journal of Human Genetics*, 79(2), pp.370-377.

Kramer, J.M., Kochinke, K., Oortveld, M.A., Marks, H., Kramer, D., de Jong, E.K., Asztalos, Z., Westwood, J.T., Stunnenberg, H.G., Sokolowski, M.B. and Keleman, K., 2011. Epigenetic regulation of learning and memory by *Drosophila* EHMT/G9a. *PLoS Biol*, 9(1), p.e1000569.

Kubicek, S., O'Sullivan, R.J., August, E.M., Hickey, E.R., Zhang, Q., Teodoro, M.L., Rea, S., Mechtler, K., Kowalski, J.A., Homon, C.A. and Kelly, T.A., 2007. Reversal of H3K9me2 by a small-molecule inhibitor for the G9a histone methyltransferase. *Molecular cell*, 25(3), pp.473-481.

Mar, A.C., Horner, A.E., Nilsson, S.R., Alsiö, J., Kent, B.A., Kim, C.H., Holmes, A., Saksida, L.M. and Bussey, T.J., 2013. the touchscreen operant platform for assessing executive function in rats and mice. *Nature protocols*, 8(10), pp.1985-2005.

McTighe, S.M., Mar, A.C., Romberg, C., Bussey, T.J. and Saksida, L.M., 2009. a new touchscreen test of pattern separation: effect of hippocampal lesions. *Neuroreport*, 20(9), pp.881-885.

Mozzetta, C., Pontis, J. and Ait-Si-Ali, S., 2015. Functional crosstalk between lysine methyltransferases on histone substrates: the case of G9A/GLP and polycomb repressive complex 2. *Antioxidants & redox signaling*, 22(16), pp.1365-1381.

Nithianantharajah, J., Komiyama, N.H., McKechnie, A., Johnstone, M., Blackwood, D.H., St Clair, D., Emes, R.D., van de Lagemaat, L.N., Saksida, L.M., Bussey, T.J. and Grant, S.G., 2013. Synaptic scaffold evolution generated components of vertebrate cognitive complexity. *Nature neuroscience*, 16(1), pp.16-24.

Nithianantharajah, J., McKechnie, A.G., Stewart, T.J., Johnstone, M., Blackwood, D.H., St Clair, D., Grant, S.G.N., Bussey, T.J. and Saksida, L.M., 2015. Bridging the translational divide: identical cognitive touchscreen testing in mice and humans carrying mutations in a disease-relevant homologous gene. *Scientific reports*, 5.

Ohno, H., Shinoda, K., Ohyama, K., Sharp, L.Z. and Kajimura, S., 2013. EHMT1 controls brown adipose cell fate and thermogenesis through the PRDM16 complex. *Nature*, 504(7478), pp.163-167.

Ogawa, H., Ishiguro, K.I., Gaubatz, S., Livingston, D.M. and Nakatani, Y., 2002. a complex with chromatin modifiers that occupies E2F-and Myc-responsive genes in G0 cells. *Science*, 296(5570), pp.1132-1136.

Oomen, C.A., Hvoslef-Eide, M., Heath, C.J., Mar, A.C., Horner, A.E., Bussey, T.J. and Saksida, L.M., 2013. the touchscreen operant platform for testing working memory and pattern separation in rats and mice. *Nature protocols*, 8(10), pp.2006-2021.

Parkel, S., Lopez-Atalaya, J.P. and Barco, A., 2013. Histone H3 lysine methylation in cognition and intellectual disability disorders. *Learning & Memory*, 20(10), pp.570-579.

Pereira, J.D., Sansom, S.N., Smith, J., Dobenecker, M.W., Tarakhovsky, A. and Livesey, F.J., 2010. Ezh2, the histone methyltransferase of PRC2, regulates the balance between self-renewal and differentiation in the cerebral cortex. *Proceedings of the National Academy of Sciences*, 107(36), pp.15957-15962.

Quadrato, G., Benevento, M., Alber, S., Jacob, C., Floriddia, E.M., Nguyen, T., Elnaggar, M.Y., Pedroarena, C.M., Molkentin, J.D. and Di Giovanni, S., 2012. Nuclear factor of activated T cells (NFATc4) is required for BDNF-dependent survival of adult-born neurons and spatial memory formation in the hippocampus. *Proceedings of the National Academy of Sciences*, 109(23), pp.E1499-E1508.

Schaefer, A., Sampath, S.C., Intrator, A., Min, A., Gertler, T.S., Surmeier, D.J., Tarakhovsky, A. and Greengard, P., 2009. Control of cognition and adaptive behavior by the GLP/G9a epigenetic suppressor complex. *Neuron*, 64(5), pp.678-691.

Schones, D.E., Chen, X., Trac, C., Setten, R. and Paddison, P.J., 2014. G9a/GLP-dependent H3K9me2 patterning alters chromatin structure at CpG islands in hematopoietic progenitors. *Epigenetics & chromatin*, 7(1), p.1.

Vedadi, M., Baryte-Lovejoy, D., Liu, F., Rival-Gervier, S., Allali-Hassani, A., Labrie, V., Wigle, T.J., DiMaggio, P.A., Wasney, G.A., Siarheyeva, A. and Dong, A., 2011. a chemical probe selectively inhibits G9a and GLP methyltransferase activity in cells. *Nature chemical biology*, 7(8), pp.566-574.

Willemsen, M.H., Vulto-van Silfhout, A.T., Nillesen, W.M., Wissink-Lindhout, W.M., van Bokhoven, H., Philip, N., Berry-Kravis, E.M., Kini, U., van Ravenswaaij-Arts, C.M.A., Delle Chiaie, B. and Innes, A.M.M., 2012. Update on Kleefstra syndrome. *Molecular syndromology*, 2(3-5), pp.202-212.

Zylicz, J.J., Dietmann, S., Günesdogan, U., Hackett, J.A., Cougot, D., Lee, C. and Surani, M.A., 2015. Chromatin dynamics and the role of G9a in gene regulation and enhancer silencing during early mouse development. *eLife*, 4, p.e 09571.



five

GENERAL DISCUSSION

Since the advent of Next Generation Sequencing (NGS), mutations affecting more than 700 genes have been shown to be causative for Intellectual Disability (ID) in humans (Vissers et al., 2016). Functional genomic studies highlighted that one of the main pathways affected in ID consists of genes involved in synaptic function and epigenetic factors (Parikshak et al., 2013; van Bokhoven, 2011; Vissers et al., 2016). At the same time, there is a staggering amount of studies showing that epigenetic control of gene expression is pivotal to learning and memory (Benevento et al., 2015; Barco et al., 2014). However, the molecular mechanisms behind the epigenetic regulation of gene expression during synaptic plasticity, learning and memory are far from being clarified. During my *PhD*, I studied in depth the role of the epigenetic factor Euchromatic Histone Methyltransferase 1 (EHMT1). This gene was described in our department to be causative for KS (Kleefstra et al., 2006). Here, I focused my attention in further understanding the function of EHMT1 in molecular and cellular processes underlying synaptic plasticity and cognition.

EHMT1, A KEY HOMEOSTATIC TUNER

Neuronal activity-dependent gene regulation is a prominent mechanism through which the nervous system responds to environmental challenges, like learning & memory, brain development and neuronal network formation and maintenance. Contrary to Hebbian-synapse specific mechanisms, homeostatic synaptic plasticity acts to maintain a fine tuning of overall neuronal activity by monitoring and scaling globally all synapses. These global synaptic modifications, besides being dynamic, are dependent on epigenetic regulation of gene function. I found that EHMT1 is an epigenetic tuner required for homeostatic synaptic scaling. This epigenetic factor responds to chronic network deprivation by tuning a gene repression program in order to scale up synapses (Figure 5.1). This is achieved through EHMT1-dependent dynamic increase in the di-methylation at lysine 9 (K9) of Histone H3 (H3K9me2). H3K9me2 levels were bi-directionally altered in response to enduring stimulatory and inhibitory in neuronal network activity.

Overall, this finding is very exciting because previously histone methylations were not considered as dynamic and only thought to be passively changing through cell divisions (Bannister et al., 2002). Therefore, my study contributes to the idea that histone methylations have a dynamic nature.

Gene expression analysis before and after induction of homeostatic plasticity on WT and neurons lacking EHMT1 revealed interesting changes in gene expression patterns. Specifically, I found that during synaptic scaling up 263 genes were downregulated after TTX treatment. However, only a fraction of these genes was downregulated in EHMT1 lacking neurons, which fail to exhibit scaling up under the same inhibitory conditions. This suggests a critical role for EHMT1 in synaptic scaling, mediated by increased H3K9 dimethylation affecting the expression of a subset of genes. Interestingly, little or no changes were observed under basal condition. Going more into details to investigate the individual targets, I found that EHMT1 directly regulated *Bdnf* repression by specifically binding and increasing H3K9me2 levels at the *Bdnf* promoter IV, both *in vitro* and *in vivo* (Figure 5.1). In line with other studies, BDNF repression

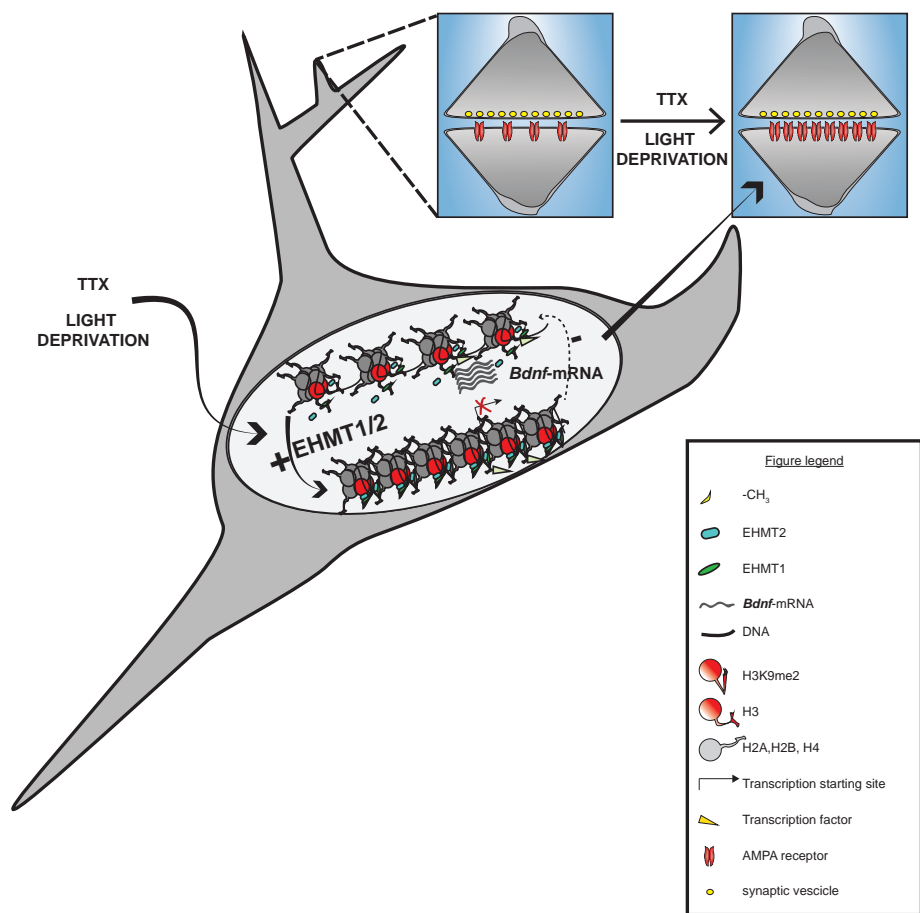


Figure 5.1. Model depicting the epigenetic synaptic scaling action of EHMT1/2 in repressing *Bdnf* expression, by compacting chromatin locally at *Bdnf* promoter IV and subsequent increase in AMPA receptors (up right insert), in conditions of neuronal network activity deprivation.

was shown to be necessary to scale up synapses (Rutherford et al., 1998). Interestingly, BDNF regulation is achieved at several levels, including DNA-methylation and histone methylation. For instance, *Bdnf* expression misregulation and impaired synaptic scaling was found in loss-of-function studies of *Mecp2* and *Tet3* in primary cortical neurons (Qiu et al., 2012; Blackman et al., 2012; Yu et al., 2015). Moreover, downscaling was impeded in *Tet3*-knock down neurons, as the result of the inability to de-methylate DNA specifically at *Bdnf* promoter IV (Yu et al., 2015). *BDNF* gene is a key-master regulator that is involved in different neuronal functions, like learning and memory, neuronal survival and AMPA receptor trafficking (Cunha et al., 2010). Therefore, it is not surprising that BDNF gene regulation relies on different fine-tuned epigenetic mechanisms that control globally neuronal physiology. It can be hypothesized that EHMT1 acts either in parallel or sequentially to other epigenetic regulators to finely tune

BDNF expression. For example, EHMT1 through H3K9me2 could function as a permissive tag to recruit a machinery that adds more stable repressive markers such as H3K9me3, H3K27me3 and DNA methyltransferases through HP1 recruitment (Mozzetta et al., 2014; Rothbart and Strahl, 2014; Yearim et al., 2015). Taken together a picture is emerging in which H3K9me2 could act as an epigenetic mark that represents the activity state of a neuronal network and could serve as a general mechanism for poising a state in the genome in a “ready to repress” mode. Histone methylations, therefore, represent an important epigenetic component that contributes to genomic metaplasticity that tunes gene expression in dynamic states that can be promptly reversed in order to serve rapid changes, characteristic of neuronal activity. This hypothesis is in line with my data showing that under basal condition we observed few and modest changes in gene expression. However, neurons lacking EHMT1 (and having reduced H3K9me2) were unable to repress certain genes (including *Bdnf*), and therefore respond to changes in activity. Therefore, H3K9me2 can thus be viewed as a dynamic regulatory histone mark in euchromatic regions, as opposed to only a mark for heterochromatin only.

Growing evidence is correlating strongly the relation between cognitive disorders and impairments in homeostatic synaptic plasticity. Strikingly, a common denominator between KS and other well-known neurodevelopmental disorders are perturbations in the regulation of key synaptic regulators like BDNF (reviewed in Dickman and Wondolowski, 2013). Furthermore, deficits in homeostatic plasticity have now been described in models for Fragile X syndrome, Rett syndrome and Tuberous sclerosis (Lee et al., 2016). Deficits in homeostatic synaptic scaling could therefore potentially be used as a biomarker for early diagnosis of neurodevelopmental disorders, like Intellectual disability.

EHMT1, AN EVOLUTIONARILY CONSERVED EPIGENETIC TRANSLATOR

The ability to generate human *in vitro* models to study neurodevelopmental disorders represents an enormous biotechnological revolution for studying the molecular and functional mechanisms underlying intellectual disabilities and more generally, brain development and function. The results described in chapter 3, contributed to a project that aimed to induce neurons (iN) from human induced pluripotent stem cells (hiPSCs) from human donors. By using a modified protocol previously described by Zhang and colleagues (Zhang et al., 2013), we have successfully generated hiPSCs-induced neurons (iN-hiPSCs) that formed functional synapses and were organized in active neuronal networks. The adapted protocol from Zhang et al. (2013) allowed us to obtain a fast and highly efficient differentiation protocol that ensures us with the possibility to derive highly homogenous and synchronized iN-hiPSCs population (i.e. cortical upper layer excitatory neurons). This is clearly a great asset for the reason that it allows us to perform developmental time course studies of neuronal network formation in synchronized differentiated iN-hiPSCs populations.

Besides EHMT1, a number of other epigenetic regulators have been found to play a role in the development of KS phenotypic spectrum (KSS). Kleefstra and colleagues (Kleefstra et

al., 2012) described four genes which were found to be defective in KSS patients: *MBD5*, *MLL3*, *SMARCB1* and *NR1I3*. Of these, *MBD5*, *MLL3* and *NR1I3* genetically interacted with *EHMT1*, and *SMARCB1* influenced *EHMT1* through its interaction with *MLL3*. *EHMT1* is thus part of a larger epigenetic module underlying human cognitive disorders. Having iN-hiPSCs production optimized, an exciting application is to functionally study iN-hiPSCs neuronal network activity by using Multi Electrode Array (MEA) technology. Culturing neurons on MEA plates allows recording of neuronal network activity through a high-dense array of micro-electrodes that sense changes in ionic concentrations that are typical of neuronal activity. These signals are readily amplified and recorded as single electrode activity. This information integrated with other electrodes, provides temporal data of how neurons communicate and form functionally mature neuronal networks (Taketani et al., 2006; Frega et al., 2016). By using MEA in high throughput-put studies, we can compare the neuronal network activity and developmental profile in iN-hiPSCs from control and KSS related genes (*EHMT1*, *MBD5*, *NR1/3*, *SMARCB1*, *MLL3*) (Kleefstra et al., 2012). This will allow us to collect signatures of the temporal and neurophysiological activity associated with mutations in these KSS genes, and to establish their roles in the maturation of neuronal network activity.

The derivation of iN-hiPSCs represents a breakthrough for research into the molecular and cellular mechanisms of disease in human neurodevelopmental (and degenerative) disorders. However, there are a number of limitations that still require further advancement. For example, although the cellular homogeneity is considered to be a desired trait, this also represents a disadvantage, because the iN-hiPSCs cultures are represented by only excitatory neurons. This limits our power to determine *in toto* the properties of *in vivo* networks, because the lack of inhibitory neurons. Therefore, further efforts should be performed in establishing and optimizing protocols for fast and high efficient production of both inhibitory and excitatory neuronal populations in iN-hiPSCs cultures.

In the experiments described in chapter 3, we tested whether *EHMT1* function in regulating homeostatic synaptic scaling up is conserved in humans. In agreement with what I and others described previously using rodent *in vitro* and *in vivo* models (Benevento et al., 2016; Desai et al., 2002; Turrigiano et al., 1998), we are, to the best of our knowledge, the first research group showing that iN-hiPSCs from control human donors scaled up synapses in response to chronic neuronal activity suppression. Excitingly, we are finding that synaptic scaling up in a KS iN-hiPSCs line is blocked after TTX-treatment, suggesting that *EHMT1* is required also in humans for synaptic scaling up.

The evolutionarily conserved role of *EHMT1* in regulating homeostatic synaptic scaling reflects the importance of this epigenetic factor in determining aspects of central nervous system development. The information provided by evolutionary cross-comparison between murine and human *in vitro* models, like iN-hiPSCs, represents a potent translational interface that will be extremely beneficial for further biomedical research. For example, by using pharmacological and novel gene editing approaches, like CRISPR-Cas9, directly on iN-hiPSCs we could functionally study and hopefully reverse some symptoms associated with cognitive disorders and in our case, Kleefstra syndrome.

THE COGNITIVE PARADOX OF EHMT1

In chapter four, I focused on the role of EHMT1 in cognition. I found that *Ehmt1*^{+/-} mice, surprisingly, showed an improvement in pattern separation. Loosely defined, pattern separation is the process of making similar patterns or memorized contingencies, different. For example, pattern separation refers to the capacity to remember, every day, where exactly our car is parked in our neighborhood. This function depends on the Dentate gyrus function (Leutgeb et al., 2007). In parallel to enhanced pattern separation in the *Ehmt1*^{+/-} mice, I show an increase in hippocampal neural stem cell (nsc) proliferation in the adult dentate gyrus. These findings are in line with seminal studies showing a direct relation between increases in pattern separation ability and nsc proliferation in the adult hippocampus (Clelland et al., 2009). For example, better performances in memory retention and pattern separation abilities were described in mice that were subjected to physical exercise or were maintained in enriched environments. the same studies, described that this correlated with an increase in nsc proliferation and neuronal differentiation, compared to animals kept in standard environments (Kempermann et al., 1997). By analyzing the molecular mechanisms underlying adult hippocampal neurogenesis, others highlighted that increases in BDNF expression positively correlated with enhanced nsc proliferation, neuronal differentiation and pattern separation, tested with the spatial reversal paradigm in the Morris water maze (Bekinschtein et al., 2014). For example, impaired pattern separation, a reduction in adult hippocampal nsc proliferation and neurogenesis was reported in mouse models in which genes downstream to BDNF activity, like *NFATc4*, was knocked-down (Quadrato et al., 2012). the abnormal increase and lack of regulation of the *Bdnf* gene I described in *Ehmt1*-KD neurons and in *Ehmt1*^{+/-} mice, could thus explain the increase in nsc proliferation in the adult hippocampus. However, this finding should be corroborated by further quantifying which proportion of the nsc proliferating cells effectively differentiates into granular neurons in the adult Dentate gyrus of the *Ehmt1*^{+/-} mice.

Patients with KS have recognizable physical, developmental and behavioral phenotypes. ID is a prominent feature of KS patients, however, comorbidity with other behavioral disturbances, like autism spectrum disorder, epilepsy, catatonia during childhood and puberty complicates even more the diagnosis and the patient treatment.

The *Ehmt1*^{+/-} mice were previously described to manifest ID and autism-like features like, reduction in social interaction, lack of interest in exploring novel environments, impairments in fear-memory extinction and spatial object recognition. Indicating that this mouse model is a face validated model for KS (Balemans et al., 2010, 2013). Paradoxically to these previous results, I found that *Ehmt1*^{+/-} mice were outperforming WT mice in the location discrimination task, showing an increase in pattern separation abilities. An increase in cognitive performance in *Ehmt1*^{+/-} mice has actually already been described by Balemans and collaborators (2013). For example, *Ehmt1*^{+/-} mice showed an increase in fear memory retention in the contextual fear conditioning (CFC) paradigm and a non-significant trend towards an increase in fear memory in the cued-CFC version. the characteristic of cued-CFC is to use negative reinforcers as conditioning stimuli, like foot-shock and loud acoustic pulses. Potentially, these negative-stimuli

could be confounding parameters for the interpretation of changes in the freezing scores to assess fear-memory retention. Balemans et al., understood the confounding effects of negative reinforcers and tested for differences in sensitivity to painful stimuli in the *Ehmt1*^{-/-} mice. They found that the *Ehmt1*^{-/-} mice have increased startle responses to gradually increased acoustical stimuli (Balemans et al., 2013). This correlates well to previous descriptions in which increased freezing during CFC were observed in rat models for autism and for post-traumatic stress disorders (PTSD) (Markram et al., 2008; Imanaka et al., 2006). Moreover, recently a study reported that peripheral mechanoreception is altered in different and well-established autism-related mouse models (Orefice et al., 2016). This could explain the hypersensitivity and altered tactile experiences in patients with KS, who suffer from severe intellectual disability and exhibit significant behavioral and psychiatric problems including anxiety and stress to novel contexts (personal communication). Integrating these findings could explain why using low aversive behavioral tasks such as operant chambers coupled with touch screens (Oomen et al., 2013), represent a valuable new behavioral paradigm strategy to assess cognitive abilities in mouse models that show hypersensitivity to environmental stressors. Further studies should foster the redesign of canonical behavioral paradigms in order to use positive reinforcers and isolate stress-related brain function to assess cognition. This may lead to surprising new discoveries that could explain paradoxical behaviors in cognitive impairments. Ultimately, these findings could be applied to change therapy strategy for treatment of ID and Autism-like patients.

Appendix

SUMMARY

LIST OF ABBREVIATIONS

LIST OF PUBLICATIONS

ACKNOWLEDGEMENTS (DANKWOORD)

SUMMARY

The findings described in this thesis provided mechanistic insights into the role of EHMT1 in synaptic plasticity and in cognition, by using a mouse model haploinsufficient for *Ehmt1* (*Ehmt1*^{-/-}) and a human cellular model for Kleefstra syndrome. Specifically, the findings described in this thesis contribute to increase our understanding of the underlying causes of circuit malfunction provoked by *EHMT1* haploinsufficiency.

In **chapter 2** of this thesis the role of EHMT1 as a key neuronal homeostatic tuner required for synaptic scaling is described. First, we report the histone H3 lysine K9 di-methylation (H3K9me2) levels to be dynamically and bidirectionally regulated in function of neuronal network chronic manipulations to induce synaptic scaling. Subsequently, through genetic and pharmacological manipulations of EHMT1 function, we describe that this epigenetic factor is required for the increases in H3K9me2 levels after chronic activity suppression. By performing electrophysiological experiments, we give evidence of EHMT1 to be necessary for the increases in the miniature excitatory post-synaptic currents amplitude (mEPSC) and AMPA receptor abundance in response to activity deprivation. Mechanistically, via a series of biochemical experiments, we explore how EHMT1 activation is triggered in response to chronic network activity deprivation. We describe that EHMT1 and its paralog, EHMT2, increase their interaction and augment their catalytic activity by increasing H3K9me2 levels in response to prolonged suppression of neuronal firing. Subsequently, through RNA-sequencing experiments, we show that EHMT1 participates in the control an epigenetic repressive genetic program required to scale up synapses in response to chronic network activity deprivation. This led us to validate the dynamics of EHMT1 and EHMT2 gene expression regulation. We report EHMT1 and EHMT2 to bind and increase H3K9me2 levels directly at *Bdnf* promoter IV, leading to *Bdnf* repression after neuronal activity suppression. We conclude chapter 2, by studying whether EHMT1 is required for synaptic scaling *in vivo*. By using a mouse model haploinsufficient for *Ehmt1*, we indicate that EHMT1 function is required for the increase in H3K9me2 levels, in the mEPSC amplitude in layer II/III of primary visual cortex after a light deprivation paradigm. Together the data presented in chapter 2 show that EHMT1 and EHMT2 assemble in a repressive epigenetic complex that is engaged during synaptic scaling.

In **Chapter 3**, we describe a procedure to induce neuronal differentiation from human induced pluripotent stem cells (iN-hiPSCs). We first report that the iN-hiPSCs express synaptic markers already at early stages of neuronal induction. In a series of electrophysiological experiments, the iN-hiPSCs are described to elicit action potentials when evoked and to spontaneously organize in active neuronal networks. Having validated the synaptic and active properties of the iN-hiPSCs, we use this model to derive iN-hiPSCs from control volunteers and Kleefstra syndrome (KS) patients. We, next, test whether human derived neurons from KS were defective in expressing synaptic scaling, similar to the experiments we described in chapter 2 of this manuscript. We report that synaptic scaling is expressed in human neurons and that EHMT1 function is required for homeostatic plasticity. Together these results suggest that defects on synaptic scaling could be one of the underlying causes of KS.

In **chapter 4**, we study cognition in the *Ehmt1* haploinsufficient mouse model by using non-aversive touchscreen-equipped operant chambers. In these series of studies, we report the *Ehmt1*^{+/-} mice to perform similarly to control littermates when tested for visual discrimination, object-location paired-associates learning and extinction learning. Together, these data indicate that the *Ehmt1*^{+/-} mice are generally unimpaired at learning and memory tasks when tested in a low-stress and unaversive environment. When instead testing the *Ehmt1*^{+/-} mice for reversed contingencies by using location discrimination test, a paradigm used to study pattern separation, we describe that *Ehmt1*^{+/-} mice manifested increased performances compared to control littermates. To investigate the cellular correlates, we indicate an increase in neural stem cell (nsc) proliferation in the subgranular zone of the dentate gyrus of the *Ehmt1*^{+/-} mice. Together, the data described in chapter 4 suggests that EHMT1 function is required to restrict developmental genetic programs for correct nsc proliferation and that *Ehmt1*^{+/-} mice are generally unimpaired at learning and memory tasks when tested in a low-stress and unaversive environment.

The findings described in this thesis suggest that EHMT1 functions as an evolutionarily conserved epigenetic factor important for synaptic plasticity and cognition.

LIST OF ABBREVIATIONS

AAV-Cre	Adeno-associated virus with Cre recombinase
AMPA	alpha-Amino-3-hydroxy-5-methyl-4-isoxazolepropionic acid
ANOVA	Analysis of Variance
APV	D-(-)-2-Amino-5-phosphonopentanoic acid
ASD	Autism spectrum disorders
BAF	BRG1 associated factors
BDNF	Brain derived neurotrophic factor
BIX-01924	G9a inhibitor
BrdU	Bromo de-oxy Uridine
bp	base pairs
C57Bl6/J	WT-mouse strain
CA1	Cornu Ammonis 1
CaCl ₂	Calcium Chloride
CANTAB	Cambridge Neuropsychological test automated battery
ChIP	Chromatin Immunoprecipitation
CNS	Central Nervous System
cDNA	complementary DNA
CNQX	6-Cyano-7-nitroquinoxaline-2,3-dione (AMPA antagonist)
CO ₂	Carbon di-oxyde
CsCl	Cesium Chloride
CsMeSO ₃	Cesium Metan-sulfonate
DG	Dentate <i>gyrus</i>
DIV	Days <i>in vitro</i>
Dlg2	Disc large homolog 2
DMEM	Dulbecco modified Eagle medium
DNA	Deoxyribonucleic acid
DNMT3A	DNA (Cytosine-5)-Methyltransferase 3 Beta
DR	Dark reared
Drd1	Dopamine receptor d1
Drd2	Dopamine receptor d2
DSG	Disuccinimidil glutarate
DTT	Dithiothreitol
EC	Entorhinal cortex
EDTA	Ethylenediaminetetraacetic acid
EGTA	Ethylene-glycol-bis(2-aminoethylether)-N,N,N',N'-tetraacetic acid
EHMT1 (GLP/KMT1D)	Euchromatin histone lysine n-methyltransferase 1
EHMT2 (G9a/KMT1C)	Euchromatin histone lysine n-methyltransferase 2
ELISA	Enzymatic-linked immunosorbent assay
ERK	Extracellular signal-regulated kinase

EtOH	Ethanol
Ezh2	Enhancer of zeste homolog 2
FBS	Fetal bovine serum
Gabra1/Gabra2/Gabrb2	Gamma-aminobutyric acid (GABA)A receptor, subunit alpha 1,2/ beta 2
(e)GFP	(enhanced) Green Fluorescence Protein
GLP	G9a-like protein; a histone methyltransferase
GluA1/GluA2	Subunits 1 and 2 of the AMPA receptor
GluN2A/GluN2B	Subunits a and B of the NMDA receptor
Grin2B (Nr2B)	Glutamate (NMDA) receptor subunit epsilon-2
H2A, 2B, 3, 4	Histone 2A, 2B, 3, 4
H3K4me1	Monomethylated 4 th lysine residue of histone H3
H3K4me3	Trimethylated 4 th lysine residue of histone H3
H3K9me2	Dimethylated 9 th lysine residue of histone H3
H3K27me3	Trimethylated 27 th lysine residue of histone H3
HAT	Histone acetyltransferase
HBSS	Hank's buffered salt solution
HDAC	Histone deacetylase
HDM	Histone demethylase
HEK293T	Human Embryonic Kidney clone 293T cells
hiPSc	human induced Pluripotent Stem cells
HMT	Histone methyltransferase
HP1	Histone protein 1
h	hour/-s
iN(-hiPSCs)	induced Neurons-hiPSCs
K	Lysine
KCl	Potassium Chloride
Ki-67	Marker of proliferation Ki67
KS (9qSTDS)	Kleefstra syndrome (9q subtelomeric deletion syndrome)
LA	Lateral amygdala
LiCl	Lithium Chloride
LSD1	Lysine (K)-specific demethylase 1, also KDM1a
LTM	Long-term memory
LTP	Long-term potentiation
MAP2	Microtubule associated protein 2
MEA	Multi Electrode Array
MeCP2	Methyl-CpG Binding Protein 2
mEPSC	Miniature excitatory postsynaptic current
MgCl ₂	Magnesium chloride
min	minutes
mIPSC	Miniature inhibitory postsynaptic current

mRNA	Messenger Ribonucleic acid
MS-275	Etinostat (HDAC1 inhibitor)
nAc	nucleus <i>Accumbens</i>
NaCl	Sodium chloride
NaHCO ₃	Sodium Carbonate
NaHPO ₄	Sodium monohydrogen phosphate
NaH ₂ PO ₄	Sodium di-hydrogen phosphate
NDS	Normal donkey serum
Ngn2	Neurogenin-2
NGS	Normal goat serum
NGS	Next generation sequencing
NP-40 (IGEPAL)	Octyl phenoxypolyethoxyethano
NR	Normal reared
Nsc	Neural stem cells
NMDAR	N-methyl-D-aspartate receptor
O ₂	Oxygen
PBB	Protein binding buffer
PBS	Phosphate buffered solution
PCR-(q)-(RT)	Polymerase chain reaction-(quantitative)-(Reverse Transcription)
PDL	Poli-(D)-lysine
PPIA	Peptidylpropyl Isomerase A
PRC2	Polycomb Repressive complex 2
Prnp	Prion protein
PSD-95	Post-synaptic density protein 95
PTM	Post-translational modification
PTX	Picrotoxin
Puro	Puromycin
R	Arginine
Rab3b	Member RAS oncogene family 3b
RNA	Ribonucleic acid
rtTA	reverse tetracycline-controlle transactivator
s	seconds
SDS	Sodium-dodecyl sulfate
Setdb1	SET domain bifurcated 1
SEM	Standard error mean
SGZ	Subgranular zone
shRNA	short hairpin RNA
SMARCB1	SWI/SNF-related matrix-associated actin-dependent regulator of chromatin subfamily B member 1
STO-609	7-Oxo-7H-benzimidazo[2,1-1]benz[de]isoquinoline-3-carboxylic acid acetate

Suv39 h1	Suppressor of variegation 3-9 homolog 1
SYBR	N',N'-dimethyl-N[4-[€-(3-methyl-1,3-benzothiazol-2-ylidene)methyl]-1-phenylquinolin-1-ium-2-y]-N-propylpropane-1,3-diamine
TALE	Transcription activator like effector
TB	Tris Base
TBS-(T)	Tris base solution-(tween or triton)
TrkB-(Fc)-(Ig)	TyrosinereceptorkinaseB-(Fragmentcristallizable)-(Immunoglobulin)
TTX	Tetrodotoxin
VGlut	Vescicular Glutamate transporter
VSVG	Vescicular Stomatitis virus
VTA	Ventral-Tegmental Area
WT	Wild type
ZFP	Zinc finger protein

REFERENCES

- Aimone, J.B., Deng, W. and Gage, F.H., 2010. Adult neurogenesis: integrating theories and separating functions. *Trends in cognitive sciences*, 14(7), pp.325-337.
- Akbarian, S., and Huang, H.-S. (2009). Epigenetic regulation in human brain-focus on histone lysine methylation. *Biol Psychiatry* 65, 198–203.
- Akbarian, S., Beeri, M.S., and Haroutunian, V. (2013). Epigenetic determinants of healthy and diseased brain aging and cognition. *JAMA Neurol* 70, 711–718.
- Asperger, Hans (June 1944). "Die "Autistischen Psychopathen" im Kindesalter [Autistic psychopaths in childhood]". *Archiv für Psychiatrie und Nervenkrankheiten* (in German) 117: 76–136. doi:10.1007/BF01837709. Retrieved 2016-01-01.
- Bannister, A.J., Schneider, R. and Kouzarides, T., 2002. Histone methylation: dynamic or static?. *Cell*, 109(7), pp.801-806.
- Balemans, M.C.M., Ansar, M., Oudakker, A.R., van Caam, A.P.M., Bakker, B., Vitters, E.L., van der Kraan, P.M., de Bruijn, D.R.H., Janssen, S.M., Kuipers, A.J., et al. (2014). Reduced Euchromatin histone methyltransferase 1 causes developmental delay, hypotonia, and cranial abnormalities associated with increased bone gene expression in Kleefstra syndrome mice. *Dev. Biol.* 386, 395–407.
- Balemans, M.C.M., Huibers, M.M.H., Eikelenboom, N.W.D., Kuipers, A.J., van Summeren, R.C.J., Pijpers, M.M.C.A., Tachibana, M., Shinkai, Y., van Bokhoven, H., and Van der Zee, C.E.E.M. (2010). Reduced exploration, increased anxiety, and altered social behavior: Autistic-like features of euchromatin histone methyltransferase 1 heterozygous knockout mice. *Behav Brain Res* 208, 47–55.
- Balemans, M.C.M., Kasri, N.N., Kopanitsa, M.V., Afinowi, N.O., Ramakers, G., Peters, T.A., Beynon, A.J., Janssen, S.M., van Summeren, R.C.J., Eeftens, J.M., et al. (2013). Hippocampal dysfunction in the Euchromatin histone methyltransferase 1 heterozygous knockout mouse model for Kleefstra syndrome. *Hum Mol Genet* 22, 852–866.
- Bannister, A.J., Schneider, R., and Kouzarides, T. (2002). Histone Methylation: Dynamic or Static? 1–6.
- Barco, A. (2014). Neuroepigenetic disorders: progress, promises and challenges. *Neuropharmacology* 80, 1–2.
- Banerjee-Basu, S. and Packer, A., 2010. SFARI Gene: an evolving database for the autism research community. *Disease Models and Mechanisms*, 3(3-4), pp.133-135.
- Bekinschtein, P., Cammarota, M. and Medina, J.H., 2014. BDNF and memory processing. *Neuropharmacology*, 76, pp.677-683.
- Benelkebir, H., Hodgkinson, C., Duriez, P.J., Hayden, A.L., Bulleid, R.A., Crabb, S.J., Packham, G., and Ganesan, A. (2011). Enantioselective synthesis of tranlycypromine analogues as lysine demethylase (LSD1) inhibitors. *Bioorg. Med. Chem.* 19, 3709–3716.
- Benevento, M., Iacono, G., Selten, M., Ba, W., Oudakker, A., Frega, M., ... & Stunnenberg, H. G. (2016). Histone Methylation by the Kleefstra Syndrome Protein EHMT1 Mediates Homeostatic Synaptic Scaling. *Neuron* 2016. <http://dx.doi.org/10.1016/j.neuron.2016.06.003>
- Binda, C., Valente, S., Romanenghi, M., Pilotto, S., Cirilli, R., Karyinos, A., Ciossani, G., Botrugno, O.A., Forneris, F., Tardugno, M., et al. (2010). Biochemical, structural, and biological evaluation of tranlycypromine derivatives as inhibitors of histone demethylases LSD1 and LSD2. *J. Am. Chem. Soc.* 132, 6827–6833.
- Borovecki, F., Lovrecic, L., Zhou, J., Jeong, H., Then, F., Rosas, H.D., Hersch, S.M., Hogarth, P., Bouzou, B., Jensen, R.V., et al. (2005). Genome-wide expression profiling of human blood reveals biomarkers for Huntington's disease. *Proc Natl Acad Sci USA* 102, 11023–11028.
- Cahoy J.D., Emery, B., Kaushal, A., Foo, L.C. et al. a transcriptome database for astrocytes, neurons, and oligodendrocytes: a new resource for understanding brain development and function. *the Journal of neuroscience: the official journal of the Society for Neuroscience*, 28(1):264– 278, Jan 2008.
- Cedar, H., and Bergman, Y. (2009). Linking DNA methylation and histone modification: patterns and paradigms. *Nat Rev Genet* 10, 295–304.
- Cellot, G., Cherubini, E. (2014). GABAergic Signaling as Therapeutic Target for Autism Spectrum Disorders. *Front. Pediatr.* 2:70
- Chang, Y., Zhang, X., Horton, J.R., Upadhyay, A.K., Spannhoff, A., Liu, J., Snyder, J.P., Bedford, M.T., and Cheng, X. (2009). Structural basis for G9a-like protein lysine methyltransferase inhibition by BIX-01294. *Nat. Struct. Mol. Biol.* 16, 312–317.
- Chase, K.A., and Sharma, R.P. (2013). Nicotine induces chromatin remodelling through decreases

- in the methyltransferases GLP, G9a, Setdb1 and levels of H3K9me2. *Int. J. Neuropsychopharmacol.* 16, 1129–1138.
- Chen, X., Skutt-Kakaria, K., Davison, J., Ou, Y.-L., Choi, E., Malik, P., Loeb, K., Wood, B., Georges, G., Torok-Storb, B., et al. (2012). G9a/GLP-dependent histone H3K9me2 patterning during human hematopoietic stem cell lineage commitment. *Genes Dev* 26, 2499–2511.
- Comoglio, F., and Paro, R. (2014). Combinatorial modeling of chromatin features quantitatively predicts DNA replication timing in *Drosophila*. *PLoS Comp Biol* 10, e1003419.
- Cougot, D., Lee, C., & Surani, M. A. (2015) Chromatin dynamics and the role of G9a in gene regulation and enhancer silencing during early mouse development. eLife doi: <http://dx.doi.org/10.7554/eLife.09571.001>
- Cunha, C., Brambilla, R. and Thomas, K.L., 2010. a simple role for BDNF in learning and memory?. *Frontiers in molecular neuroscience*, 3, p.1.
- Day, J.J., and Sweatt, J.D. (2011a). Epigenetic modifications in neurons are essential for formation and storage of behavioral memory. *Neuropsychopharmacology* 36, 357–358.
- Day, J.J., and Sweatt, J.D. (2011b). Cognitive neuroepigenetics: a role for epigenetic mechanisms in learning and memory. *Neurobiol Learn Mem* 96, 2–12.
- de Pretis, S., and Pelizzola, M. (2014). Computational and experimental methods to decipher the epigenetic code. *Front Genet* 5, 335.
- Del Rio, A., & Varchi, G. (2016). Molecular Design of Compounds Targeting Histone Methyltransferases. *Epi-Informatics: Discovery and Development of Small Molecule Epigenetic Drugs and Probes*, 257.
- Dickman, D. and Wondolowski, J., 2013. Emerging links between homeostatic synaptic plasticity and neurological disease. *Frontiers in cellular neuroscience*, 7, p.223.
- Dixon, C.I., Morris, H.V., Breen, G., Desrivieres, S., Jugurnauth, S., Steiner, R.C., Vallada, H., Guindalini, C., Laranjeira, R., Messas, G., et al. (2010). Cocaine effects on mouse incentive-learning and human addiction are linked to alpha2 subunit-containing GABAA receptors. *Proc Natl Acad Sci USA* 107, 2289–2294.
- Espinosa, J.S., Wheeler, D.G., Tsien, R.W., and Luo, L. (2009). Uncoupling dendrite growth and patterning: single-cell knockout analysis of NMDA receptor 2B. *Neuron* 62, 205–217.
- Felsenfeld, G., and Groudine, M. (2003). Controlling the double helix. *Nature* 421, 448–453.
- Fischer, A. (2014). Neuropharmacology. *Neuropharmacology* 1–8.
- Fischer, A., Sananbenesi, F., Wang, X., Dobbin, M., and Tsai, L.-H. (2007). Recovery of learning and memory is associated with chromatin remodelling. *Nature* 447, 178–182.
- Fonseca, R. (2016). the aging memory: Modulating epigenetic modifications to improve cognitive function. *Neurobiology of Learning and Memory*.
- Frost, B., Hemberg, M., Lewis, J., and Feany, M.B. (2014). Tau promotes neurodegeneration through global chromatin relaxation. *Nat Neurosci* 17, 357–366.
- Gardian, G., Browne, S.E., Choi, D.-K., Klivenyi, P., Gregorio, J., Kubilus, J.K., Ryu, H., Langley, B., Ratan, R.R., Ferrante, R.J., et al. (2005). Neuroprotective effects of phenylbutyrate in the N171-82Q transgenic mouse model of Huntington's disease. *J Biol Chem* 280, 556–563.
- Graham, D.L., Edwards, S., Bachtell, R.K., DiLeone, R.J., Rios, M., and Self, D.W. (2007). Dynamic BDNF activity in nucleus accumbens with cocaine use increases self-administration and relapse. *Nat Neurosci* 10, 1029–1037.
- Gray, J.A., Shi, Y., Usui, H., During, M.J., Sakimura, K., and Nicoll, R.A. (2011). Distinct modes of AMPA receptor suppression at developing synapses by GluN2A and GluN2B: single-cell NMDA receptor subunit deletion in vivo. *Neuron* 71, 1085–1101.
- Gräff, J., and Mansuy, I.M. (2008). Epigenetic codes in cognition and behavior. *Behav Brain Res* 192, 70–87.
- Gräff, J., Rei, D., Guan, J.-S., Wang, W.-Y., Seo, J., Hennig, K.M., Nieland, T.J.F., Fass, D.M., Kao, P.F., Kahn, M., et al. (2012a). An epigenetic blockade of cognitive functions in the neurodegenerating brain. *Nature* 483, 222–226.
- Gräff, J., Woldemichael, B.T., Berchtold, D., Dewarrat, G., and Mansuy, I.M. (2012b). Dynamic histone marks in the hippocampus and cortex facilitate memory consolidation. *Nat Comms* 3, 991.
- Gupta, S., Kim, S.Y., Artis, S., Molfese, D.L., Schumacher, A., Sweatt, J.D., Paylor, R.E., and Lubin, F.D. (2010). Histone methylation regulates memory formation. 30, 3589–3599.
- Gupta-Agarwal, S., Franklin, A.V., Deramus, T., Wheelock, M., Davis, R.L., McMahon, L.L., and Lubin, F.D. (2012). G9a/GLP Histone Lysine Dimethyltransferase Complex Activity in the Hippocampus and the Entorhinal Cortex Is

- Required for Gene Activation and Silencing during Memory Consolidation. *J. Neurosci.* 22, 5440–5453.
- Gupta-Agarwal, S., Jarome, T.J., Fernandez, J., and Lubin, F.D. (2014). NMDA receptor- and ERK-dependent histone methylation changes in the lateral amygdala bidirectionally regulate fear memory formation. *Learn. Mem.* 21, 351–362.
- Hall, B.J., Ripley, B., and Ghosh, A. (2007). NR2B signaling regulates the development of synaptic AMPA receptor current. *J. Neurosci.* 27, 13446–13456.
- He, X., Caluseriu, O., Srivastava, R., Denny, A. M., & Bolduc, F. V. (2016). Reversible white matter lesions associated with mutant EHMT1 and Kleefstra syndrome. *Neurology Genetics*, 2(2), e58.
- Heller, E.A., Cates, H.M., Peña, C.J., Sun, H., Shao, N., Feng, J., Golden, S.A., Herman, J.P., Walsh, J.J., Mazei-Robison, M., et al. (2014). Locus-specific epigenetic remodeling controls addiction- and depression-related behaviors. *Nat Neurosci* 17, 1720–1727.
- Imanaka, A., Morinobu, S., Toki, S. and Yamawaki, S., 2006. Importance of early environment in the development of post-traumatic stress disorder-like behaviors. *Behavioral brain research*, 173(1), pp.129-137.
- Kato, S., Inoue, K. and Youn, M.Y., 2010. Emergence of the osteo-epigenome in bone biology. *IBMS BoneKEy*, 7(9), pp.314-324.
- Katoh, K., Yamazaki, R., Onishi, A., Sanuki, R., and Furukawa, T. (2012). G9a histone methyltransferase activity in retinal progenitors is essential for proper differentiation and survival of mouse retinal cells. *J. Neurosci.* 32, 17658–17670.
- Kelly, T.K., De Carvalho, D.D., and Jones, P.A. (2010). Epigenetic modifications as therapeutic targets. *Nat Biotechnol* 28, 1069–1078.
- Kanner L. Autistic disturbances of affective contact. *Nerv Child* 2. 1943. pp. 217–250.
- Kempermann, G., Kuhn, H.G. and Gage, F.H., 1997. More hippocampal neurons in adult mice living in an enriched environment. *Nature*, 386(6624), pp.493-495.
- Kennedy, P.J., Feng, J., Robison, A.J., Maze, I., Badimon, A., Mouzon, E., Chaudhury, D., Damez-Werno, D.M., Haggarty, S.J., Han, M.-H., et al. (2013). Class I HDAC inhibition blocks cocaine-induced plasticity by targeted changes in histone methylation. *Nat Neurosci* 16, 434–440.
- Kessels, H.W., and Malinow, R. (2009). Synaptic AMPA receptor plasticity and behavior. *Neuron* 61, 340–350.
- Kleefstra, T., van Zelst-Stams, W.A., Nillesen, W.M., Cormier-Daire, V., Houge, G., Foulds, N., van Dooren, M., Willemsen, M.H., Pfundt, R., Turner, A., et al. (2009). Further clinical and molecular delineation of the 9q subtelomeric deletion syndrome supports a major contribution of EHMT1 haploinsufficiency to the core phenotype. *J Med Genet* 46, 598–606.
- Kleefstra, T., Brunner, H.G., Amiel, J., Oudakker, A.R., Nillesen, W.M., Magee, A., Geneviève, D., Cormier-Daire, V., van Esch, H., Fryns, J.-P., et al. (2006). Loss-of-function mutations in euchromatin histone methyltransferase1 (EHMT1) cause the 9q34 subtelomeric deletion syndrome. *the American Journal of Human Genetics* 79, 370–377.
- Kleefstra, T., Kramer, J.M., Neveling, K., Willemsen, M.H., Koemans, T.S., Vissers, L.E.L.M., Wissink-Lindhout, W., Fencikova, M., van den Akker, W.M.R., Kasri, N.N., et al. (2012). Disruption of an EHMT1-Associated Chromatin-Modification Module Causes Intellectual Disability. *Am. J. Hum. Genet.* 91, 73–82.
- Kleefstra, T., Schenck, A., Kramer, J., and van Bokhoven, H. (2014). the genetics of cognitive epigenetics. *Neuropharmacology*.
- Kramer, J.M. (2013). Epigenetic regulation of memory: implications in human cognitive disorders. *Biomol Concepts* 4, 1–12.
- Kramer, J.M., Kochinke, K., Oortveld, M.A.W., Marks, H., Kramer, D., de Jong, E.K., Asztalos, Z., Westwood, J.T., Stunnenberg, H.G., Sokolowski, M.B., et al. (2011). Epigenetic regulation of learning and memory by Drosophila EHMT/G9a. *PLoS Biol.* 9, e1000569.
- Kubicek, S., O'Sullivan, R.J., August, E.M., Hickey, E.R., Zhang, Q., Teodoro, M.L., Rea, S., Mechtler, K., Kowalski, J.A., Homon, C.A., et al. (2007). Reversal of H3K9me2 by a Small-Molecule Inhibitor for the G9a Histone Methyltransferase. *Mol Cell* 25, 473–481.
- Lee, M.-C., Yasuda, R., and Ehlers, M.D. (2010). Metaplasticity at single glutamatergic synapses. *Neuron* 66, 859–870.
- Lee, E., Lee, J. and Kim, E., 2016. Excitation/inhibition Imbalance in Animal Models of ASDs. *Biological Psychiatry*.
- Lesne, A., Foray, N., Cathala, G., Forné, T., Wong, H., and Victor, J.-M. (2015). Chromatin fiber allostery and the epigenetic code. *J Phys Condens Matter* 27, 064114.
- Levenson, J.M., and Sweatt, J.D. (2005). Epigenetic mechanisms in memory formation. 6, 108–118.

- Leutgeb, J.K., Leutgeb, S., Moser, M.B. and Moser, E.I., 2007. Pattern separation in the dentate gyrus and CA3 of the hippocampus. *Science*, 315(5814), pp.961-966.
- Lipsky, R.H. (2013). Epigenetic mechanisms regulating learning and long-term memory. *Int. J. Dev. Neurosci.* 31, 353–358.
- Liu, F., Chen, X., Allali-Hassani, A., Quinn, A.M., Wasney, G.A., Dong, A., Barsyte, D., Kozieradzki, I., Senisterra, G., Chau, I., et al. (2009). Discovery of a 2,4-diamino-7-aminoalkoxyquinazoline as a potent and selective inhibitor of histone lysine methyltransferase G9a. *J. Med. Chem.* 52, 7950–7953.
- Liu, Q., & Wang, M. W. (2016). Histone lysine methyltransferases as anti-cancer targets for drug discovery. *Acta Pharmacologica Sinica*.
- Lopez-Atalaya, J. P., Valor, L. M., & Barco, A. (2014). Epigenetic factors in intellectual disability: the Rubinstein-Taybi syndrome as a paradigm of neurodevelopmental disorder with epigenetic origin. *Prog Mol Biol Transl Sci*, 128, 139-76.
- Lubin, F.D., Gupta, S., Parrish, R.R., Grissom, N.M., and Davis, R.L. (2011). Epigenetic Mechanisms: Critical Contributors to Long-Term Memory Formation. *Neuroscientist* 17, 616–632.
- Lyons, D.B., Magklara, A., Goh, T., Sampath, S.C., Schaefer, A., Schotta, G., and Lomvardas, S. (2014). Heterochromatin-mediated gene silencing facilitates the diversification of olfactory neurons. *Cell Reports* 9, 884–892.
- Makino, H., and Malinow, R. (2009). AMPA Receptor Incorporation into Synapses during LTP: the Role of Lateral Movement and Exocytosis. *Neuron* 64, 381–390.
- Malenka, R.C., and Malinow, R. (2011). Alzheimer’s disease: Recollection of lost memories. *Nature* 469, 44–45.
- Malinow, R., and Malenka, R.C. (2002). AMPA receptor trafficking and synaptic plasticity. *Annu. Rev. Neurosci.* 25, 103–126.
- Markram, K., Rinaldi, T., La Mendola, D., Sandi, C. and Markram, H., 2008. Abnormal fear conditioning and amygdala processing in an animal model of autism. *Neuropsychopharmacology*, 33(4), pp.901-912.
- Maze, I., Chaudhury, D., Dietz, D.M., Schimmelfmann, Von, M., Kennedy, P.J., Lobo, M.K., Sullivan, S.E., Miller, M.L., Bagot, R.C., Sun, H., et al. (2014). G9a influences neuronal subtype specification in striatum. *Nat Neurosci* 17, 533–539.
- Maze, I., Covington, H.E., Dietz, D.M., LaPlant, Q., Renthal, W., Russo, S.J., Mechanic, M., Mouzon, E., Neve, R.L., Haggarty, S.J., et al. (2010). Essential role of the histone methyltransferase G9a in cocaine-induced plasticity. *Science* 327, 213–216.
- Miller, C.A., Gavin, C.F., White, J.A., Parrish, R.R., Honasoge, A., Yancey, C.R., Rivera, I.M., Rubio, M.D., Rumbaugh, G., and Sweatt, J.D. (2010). Cortical DNA methylation maintains remote memory. *Nat Neurosci* 13, 664–666.
- Mozzetta, C., Pontis, J., Fritsch, L., Robin, P., Portoso, M., Proux, C., Margueron, R., and Ait-Si-Ali, S. (2014). the histone H3 lysine 9 methyltransferases G9a and GLP regulate polycomb repressive complex 2-mediated gene silencing. *Mol Cell* 53, 277–289.
- Nelson, S.B., Valakh, V. (2015). Excitatory/Inhibitory Balance and Circuit Homeostasis in Autism Spectrum Disorders. *Neuron* 19;87(4):684-98
- Nestler, E.J. (2014a). ΔFosB: a transcriptional regulator of stress and antidepressant responses. *Eur. J. Pharmacol.*
- Nestler, E.J. (2014b). Epigenetic mechanisms of drug addiction. *Neuropharmacology* 76 Pt B, 259–268.
- Nillesen, W.M., Yntema, H.G., Moscarda, M., Verbeek, N.E., Wilson, L.C., Cowan, F., Schepens, M., Raas-Rothschild, A., Gafni-Weinstein, O., Zollino, M., et al. (2011). Characterization of a novel transcript of the EHMT1 gene reveals important diagnostic implications for Kleefstra syndrome. *Hum. Mutat.* 32, 853–859.
- Parkel, S., Lopez-Atalaya, J.P., and Barco, A. (2013). Histone H3 lysine methylation in cognition and intellectual disability disorders. *Learn. Mem.* 20, 570–579.
- Parikhshak, N.N., Luo, R., Zhang, A., Won, H., Lowe, J.K., Chandran, V., Horvath, S. and Geschwind, D.H., 2013. Integrative functional genomic analyses implicate specific molecular pathways and circuits in autism. *Cell*, 155(5), pp.1008-1021.
- Penney, J., and Tsai, L. -H. (2014). Histone deacetylases in memory and cognition. *Sci Signal* 7, re12.
- Peña, C.J., Bagot, R.C., Labonté, B., and Nestler, E.J. (2014). Epigenetic Signaling in Psychiatric Disorders. *J. Mol. Biol.*
- Portela, A., and Esteller, M. (2010). Epigenetic modifications and human disease. *Nat Biotechnol* 28, 1057–1068.
- Qiang, M., Denny, A., Lieu, M., Carreon, S., and Li, J. (2011). Histone H3K9 modifications are a local chromatin event involved in ethanol-induced neuroadaptation of the NR2B gene. *Epigenetics* 6, 1095–1104.
- Quadrato, G., Benevento, M., Alber, S., Jacob, C., Floriddia, E. M., Nguyen, T., ... & Di Giovanni, S.

- (2012). Nuclear factor of activated T cells (NFATc4) is required for BDNF-dependent survival of adult-born neurons and spatial memory formation in the hippocampus. *Proceedings of the National Academy of Sciences*, 109(23), E1499–E1508.
- Rando, O.J. (2012). Combinatorial complexity in chromatin structure and function: revisiting the histone code. *Curr. Opin. Genet. Dev.* 22, 148–155.
- Rodenas-Ruano, A., Chávez, A.E., Cossio, M.J., Castillo, P.E., and Zukin, R.S. (2012). REST-dependent epigenetic remodeling promotes the developmental switch in synaptic NMDA receptors. *Nat Neurosci* 15, 1382–1390.
- Ronan, J.L., Wu, W., and Crabtree, G.R. (2013). From neural development to cognition: unexpected roles for chromatin. *Nat Rev Genet* 14, 347–359.
- Roopra, A., Qazi, R., Schoenike, B., Daley, T.J., and Morrison, J.F. (2004). Localized domains of G9a-mediated histone methylation are required for silencing of neuronal genes. *Mol Cell* 14, 727–738.
- Rose, N.R., and Klose, R.J. (2014). Understanding the relationship between DNA methylation and histone lysine methylation. *Biochim Biophys Acta* 1839, 1362–1372.
- Rothbart, S.B., and Strahl, B.D. (2014). Interpreting the language of histone and DNA modifications. *Biochim Biophys Acta* 1839, 627–643.
- Rothman, R.B. (1990). High affinity dopamine reuptake inhibitors as potential cocaine antagonists: a strategy for drug development. *Life Sci* 46, PL17–PL21.
- Russo, S.J., Wilkinson, M.B., Mazei-Robison, M.S., Dietz, D.M., Maze, I., Krishnan, V., Renthal, W., Graham, A., Birnbaum, S.G., Green, T.A., et al. (2009). Nuclear factor kappa B signaling regulates neuronal morphology and cocaine reward. *J. Neurosci.* 29, 3529–3537.
- Ryu, H., Lee, J., Hagerty, S.W., Soh, B.Y., McAlpin, S.E., Cormier, K.A., Smith, K.M., and Ferrante, R.J. (2006). ESET/SETDB1 gene expression and histone H3 (K9) trimethylation in Huntington's disease. *Proc Natl Acad Sci USA* 103, 19176–19181.
- Sahay, A., Scobie, K. N., Hill, A. S., O'Carroll, C. M., Kheirbek, M. A., Burghardt, N. S., ... & Hen, R. (2011). Increasing adult hippocampal neurogenesis is sufficient to improve pattern separation. *Nature*, 472(7344), 466–470.
- Schaefer, A., Sampath, S.C., Intrator, A., Min, A., Gertler, T.S., Surmeier, D.J., Tarakhovsky, A., and Greengard, P. (2009). Control of cognition and adaptive behavior by the GLP/G9a epigenetic suppressor complex. *Neuron* 64, 678–691.
- Schaefer, A., Tarakhovsky, A., and Greengard, P. (2011). Epigenetic mechanisms of mental retardation. *Prog Drug Res* 67, 125–146.
- Schneider, R., Bannister, A.J., Myers, F.A., Thorne, A.W., Crane-Robinson, C., and Kouzarides, T. (2004). Histone H3 lysine 4 methylation patterns in higher eukaryotic genes. *Nat Cell Biol* 6, 73–77.
- Schones, D.E., Chen, X., Trac, C., Setten, R., and Paddison, P.J. (2014). G9a/GLP-dependent H3K9me2 patterning alters chromatin structure at CpG islands in hematopoietic progenitors. *Epigenetics Chromatin* 7, 23.
- Sharma, M., Razali, N. B., & Sajikumar, S. (2016). Inhibition of G9a/GLP Complex Promotes Long-Term Potentiation and Synaptic Tagging/Capture in Hippocampal CA1 Pyramidal Neurons. *Cerebral Cortex*, bhw170.
- Sheng, M., Cummings, J., Roldan, L.A., Jan, Y.N., and Jan, L.Y. (1994). Changing subunit composition of heteromeric NMDA receptors during development of rat cortex. *Nature* 368, 144–147.
- Shi, Y., Lan, F., Matson, C., Mulligan, P., Whetstone, J.R., Cole, P.A., Casero, R.A., and Shi, Y. (2004). Histone demethylation mediated by the nuclear amine oxidase homolog LSD1. *Cell* 119, 941–953.
- Subbanna, S., Nagre, N.N., Shivakumar, M., Umapathy, N.S., Psychoyos, D., and Basavarajappa, B.S. (2014). Ethanol induced acetylation of histone at G9a exon1 and G9a-mediated histone H3 dimethylation leads to neurodegeneration in neonatal mice. *Neuroscience* 258, 422–432.
- Subbanna, S., and Basavarajappa, B.S. (2014). Pre-administration of G9a/GLP inhibitor during synaptogenesis prevents postnatal ethanol-induced LTP deficits and neurobehavioral abnormalities in adult mice. *Experimental Neurology* 261, 34–43.
- Subbanna, S., Shivakumar, M., Umapathy, N.S., Saito, M., Mohan, P.S., Kumar, A., Nixon, R.A., Verin, A.D., Psychoyos, D., and Basavarajappa, B.S. (2013). G9a-mediated histone methylation regulates ethanol-induced neurodegeneration in the neonatal mouse brain. *Neurobiol. Dis.* 54, 475–485.
- Sugars, K., and Rubinshtein, D.C. (2003). Transcriptional abnormalities in Huntington disease. *Trends Genet.* 19, 1–6.
- Sweatt, J. D. (2016). Dynamic DNA methylation controls glutamate receptor trafficking and synaptic scaling. *Journal of neurochemistry*, 137(3), 312–330.
- Tachibana, M., Matsumura, Y., Fukuda, M., Kimura, H., and Shinkai, Y. (2008). G9a/GLP complexes

independently mediate H3K9 and DNA methylation to silence transcription. *Embo J* 27, 2681–2690.

Tachibana, M., Sugimoto, K., Nozaki, M., Ueda, J., Ohta, T., Ohki, M., Fukuda, M., Takeda, N., Niida, H., Kato, H., et al. (2002). G9a histone methyltransferase plays a dominant role in euchromatic histone H3 lysine 9 methylation and is essential for early embryogenesis. *Genes Dev* 16, 1779–1791.

Tachibana, M., Ueda, J., Fukuda, M., Takeda, N., Ohta, T., Iwanari, H., Sakihama, T., Kodama, T., Hamakubo, T., and Shinkai, Y. (2005). Histone methyltransferases G9a and GLP form heteromeric complexes and are both crucial for methylation of euchromatin at H3-K9. *Genes Dev* 19, 815–826.

Taketani, M. and Baudry, M., 2006. Advances in network electrophysiology. *US: Springer*.

Traynor, B.J., and Renton, A.E. (2015). Exploring the epigenetics of Alzheimer disease. *JAMA Neurol* 72, 8–9.

Turrigiano, G. G. (2008). the self-tuning neuron: synaptic scaling of excitatory synapses. *Cell*, 135(3), 422–435.

Ulanir, S.K., Kim, J.-E., Hall, B.J., Deerinc, T., Ellisman, M., and Ghosh, A. (2007). Regulation of spine morphology and spine density by NMDA receptor signaling in vivo. *Proc Natl Acad Sci USA* 104, 19553–19558.

Ungless, M.A., Whistler, J.L., Malenka, R.C., and Bonci, A. (2001). Single cocaine exposure in vivo induces long-term potentiation in dopamine neurons. *Nature* 411, 583–587.

van Bokhoven, H., 2011. Genetic and epigenetic networks in intellectual disabilities. *Annual review of genetics*, 45, pp.81–104.

Vedadi, M., Barsyte-Lovejoy, D., Liu, F., Rival-Gervier, S., Allali-Hassani, A., Labrie, V., Wigle, T.J., Dimaggio, P.A., Wasney, G.A., Siarheyeva, A., et al. (2011). a chemical probe selectively inhibits G9a and GLP methyltransferase activity in cells. *Nat. Chem. Biol.* 7, 566–574.

Verhoeven, W.M.A., Egger, J.I.M., Vermeulen, K., van de Warrenburg, B.P.C., and Kleefstra, T. (2011). Kleefstra syndrome in three adult patients: Further delineation of the behavioral and neurological phenotype shows aspects of a neurodegenerative course. *Am. J. Med. Genet.* 155, 2409–2415.

Walker, M.P., LaFerla, F.M., Oddo, S.S., and Brewer, G.J. (2013). Reversible epigenetic histone modifications and Bdnf expression in neurons with aging and from a mouse model of Alzheimer's disease. *Age (Dordr)* 35, 519–531.

Willemsen, M.H., Vulto-van Silfhout, A.T., Nillesen, W.M., Wissink-Lindhout, W.M., van Bokhoven, H., Philip, N., Berry-Kravis, E.M., Kini, U., van Ravenswaaij-Arts, C.M.A., Delle Chiaie, B., et al. (2012). Update on Kleefstra Syndrome. *Mol Syndromol* 2, 202–212.

Williams, K., Russell, S.L., Shen, Y.M., and Molinoff, P.B. (1993). Developmental switch in the expression of NMDA receptors occurs in vivo and in vitro. *Neuron* 10, 267–278.

Willsey, A. J., Sanders, S. J., Li, M., Dong, S., Tebbenkamp, A. T., Muhle, R. A., ... & Murtha, M. T. (2013). Coexpression networks implicate human midfetal deep cortical projection neurons in the pathogenesis of autism. *Cell*, 155(5), 997–1007.

Wood, J.G., Hillenmeyer, S., Lawrence, C., Chang, C., Hosier, S., Lightfoot, W., Mukherjee, E., Jiang, N., Schorl, C., Brodsky, A.S., et al. (2010). Chromatin remodeling in the aging genome of *Drosophila*. *Aging Cell* 9, 971–978.

Yankner, B.A., Lu, T., and Loerch, P. (2008). the aging brain. *Annu Rev Pathol* 3, 41–66.

Yashiro, K., and Philpot, B.D. (2008). Regulation of NMDA receptor subunit expression and its implications for LTD, LTP, and metaplasticity. *Neuropharmacology* 55, 1081–1094.

Yu, H., Su, Y., Shin, J., Zhong, C., Guo, J. U., Weng, Y. L., ... & Song, H. (2015). Tet3 regulates synaptic transmission and homeostatic plasticity via DNA oxidation and repair. *Nature neuroscience*, 18(6), 836–843.

Zeisel, A., Muñoz-Manchado, A. B., Codeluppi, S., Lönnerberg, P., La Manno, G., Juréus, A., ... & Rolny, C. (2015). Cell types in the mouse cortex and hippocampus revealed by single-cell RNA-seq. *Science*, 347(6226), 1138–1142.

Zhang, Tuo, Ausma Termanis, Burak Özkan, Xun X. Bao, Jayne Culley, Flavia de Lima Alves, Juri Rappsilber, Bernard Ramsahoye, and Irina Stancheva. "G9a/GLP complex maintains imprinted DNA methylation in embryonic stem cells." *Cell reports* 15, no. 1 (2016): 77–85.

Zhang et al., An RNA-Sequencing Transcriptome and Splicing Database of Glia, Neurons, and Vascular Cells of the Cerebral Cortex. *The Journal of Neuroscience*, 35(2), 864–866.

Zhao, M.-G., Toyoda, H., Lee, Y.-S., Wu, L.-J., Ko, S.W., Zhang, X.-H., Jia, Y., Shum, F., Xu, H., Li, B.-M., et al. (2005). Roles of NMDA NR2B subtype receptor in prefrontal long-term potentiation and contextual fear memory. *Neuron* 47, 859–872.

Zovkic, I.B., Guzman-Karlsson, M.C., and Sweatt, J.D. (2013). Epigenetic regulation of memory formation and maintenance. *Learn. Mem.* 20, 61–74.

LIST OF PUBLICATIONS

- 2017 **Marco Benevento**, Charlotte A. Oomen, Alexa E. Horner, Houshang Amiri, Tessa Jacobs, Charlotte Pauwels, Monica Frega, Tjitske Kleefstra, Maksym V. Kopanitsa, Seth G. N. Grant, Timothy J. Bussey, Lisa M. Saksida, Catharina E.E.M. Van der Zee, Hans van Bokhoven, Jeffrey C. Glennon, Nael Nadif Kasri
- Haploinsufficiency of EHMT1 improves pattern separation and increases hippocampal cell proliferation.*
- Scientific Reports** 2017, 10; 7:40284. doi: 10.1038/srep40284
- 2016 **Marco Benevento**, Giovanni Iacono, Martijn Selten, Monica Frega, Wei Ba, Astrid Oudakker, Roberta Mancini, Elly Lewerissa, Tjitske Kleefstra, Hendrick Stunnenberg, Huiqing Zhou, Hans van Bokhoven and Nael Nadif Kasri
- Histone methylation by the Kleefstra Syndrome protein EHMT1 mediates homeostatic synaptic scaling.*
- Neuron** 2016, 91:341-55. doi: 10.1016/j.neuron.2016.06.003
- 2016 Marijn Martens, Monica Frega, Jessica Classen, Lisa Epping, Elske Bijvank, **Marco Benevento**, Hans Bokhoven, Paul Tiesinga, Dirk Schubert and Nael Nadif Kasri
- Euchromatin histone methyltransferase 1 regulates cortical neuronal network development*
- Scientific reports** 2016, 6:35756. doi: 10.1038/srep35756
- 2016 Wei Ba, Martijn M. Selten, Jori van der Raadt, Herman van Veen, Li L.Li, **Marco Benevento**, Astrid R Oudakker, R.S.E. Lasabuda, S.J. Letteboer. R. Roepman, R.J.A. van Wezel, M.J. Courtney, H. van Bokhoven, Nael Nadif Kasri
- ARHGAP12 functions as a developmental brake on excitatory synapse function.*
- Cell Reports** 2016, 14:1355-68. doi: 10.1016/j.celrep.2016.01.037
- 2015 **Marco Benevento**, Marise van de Molengraft, Rhode van Westen, Hans van Bokhoven and Nael Nadif Kasri
- The role of chromatin repressive marks in cognition and disease: a focus on the repressive complex GLP/G9a.*
- Neurobiology of Learning and Memory** 2015, 124:88-96. doi: 10.1016/j.nlm.2015.06.013
- 2015 Zafar Iqbal, Marjolein H Willemsen, Marie-Amélie Papon, Luciana Musante, **Marco Benevento**, Hao Hu, Willemijn M Wissink-Lindhout, Anneke T Vulto-van Silfhout, Lisenka E L M Vissers, Arjan P M de Brouwe, Sylviane Marouillat, Thomas F Wienker, Hans Hilger Ropers, Kimia Kahrizi, Nael Nadif Kasri, Hossein Najmabadi, Frédéric Laumonnier, Tjitske Kleefstra and Hans van Bokhoven

Homozygous SLC6A17 Mutations Cause Autosomal-Recessive Intellectual Disability with Progressive Tremor, Speech Impairment, and Behavioral Problems.

The American Journal of Human Genetics 2015, 96: 386-96. doi: 10.1016/j.ajhg.2015.01.010

- 2014 Monique C M Balemans, Muhammad Ansar, Astrid R. Oudakker, Arjan P M van Caam, Elly L Vitters, Peter M van der Kraan, Diederik R H de Bruijn, Sanne M Janssen, Manon M H Huibers, Eliza M Maliepaard, Frank Walboomers, **Marco Benevento**, Nael Nadif Kasri, Tjitske Kleefstra, Huiqing Zhou, Catharina E E M Van der Zee, Hans van Bokhoven

Reduced Euchromatin histone methyltransferase 1 causes developmental delay, hypotonia, and cranial abnormalities associated with increased bone gene expression in Kleefstra syndrome mice.

Developmental Biology 2014, 386: 395-407. doi: 10.1016/j.ydbio.2013.12.016

- 2013 Monique C.M. Baleman, Nael Nadif Kasri, Maksym V. Kopanitsa, Nurudeen O. Afinowi, Ger Ramakers, Theo A. Peters, Andy J. Beynon, Sanne M. Janssen, Rik C.J. van Summeren, Jorine M. Eeftens, Nathalie Eikelenboom, **Marco Benevento**, Makoto Tachibana, Yoichi Shinkai, Tjitske Kleefstra, Hans van Bokhoven and Catharina E.E.M. Van der Zee

Hippocampal dysfunction in the Euchromatin histone methyltransferase 1 heterozygous knockout mouse model for Kleefstra syndrome.

Human Molecular Genetics 2013, 22: 852-66. doi: 10.1093/hmg/ddt490

- 2012 Giorgia Quadrato, **Marco Benevento**, Stefanie Alber, Caroline Jacob, Tuan Nguyen, Elisa M. Floriddia, Mohamed Y Elnaggar, Jeffrey D. Molkentin, Simone Di Giovanni.

Nuclear factor of activated T cells (NFATc4) is required for BDNF-dependent survival of adult-born neurons and spatial memory formation in the hippocampus.

PNAS 2012, 109(23):E1499-508. doi: 10.1073/pnas.1202068109

- 2011 Gisella Vetere, Cristina Marchetti, **Marco Benevento**, Elisiana Tafi, Hélène Marie, Martine Ammassari-Teule

Viral-mediated expression of a constitutively active form of CREB in the dentate gyrus does not induce abnormally enduring fear memory.

Behavioral brain research 2011; 222(2):394-6. doi: 10.1016/j.bbr.2011.04.004

ACKNOWLEDGEMENTS (DANKWOORD)

I would like to thank my daily supervisor Dr. Nael Nadif Kasri, my mentor Prof. Dr. Hans van Bokhoven, Dr. Tjtske Kleefstra, Dr. Giovanni Iacono, Dr. Huiqing Zhou, Prof. Dr. Hendrik Stunnenberg, Dr. Jeffrey Glennon, Dr. Ineke van der Zee and Dr. Dirk Schubert for their scientific support.

Thanks to all my colleagues with whom I had the pleasure to work with in these years in Nijmegen. In particular, to: Martijn Selten, Wei (Vivien) Ba, Astrid Oudakker, Monica Frega, Giovanni Iacono, Roberta Mancini, Jori van der Raadt, Stephanie Miceli, Marijn Martens, Katrin Linda, Jason Keller, and Jon Ruben van Rijn.

Cesar Robles, Martin Perescis, Ganesh Manjeri, Izabela Mikula, Roberta Mancini, Silvia Albert, Riccardo Sangermano, Monica Frega, Martijn Selten and Wei Ba. My friends, thank you for the very cheerful moments spent together in Nijmegen, you are all greatly missed!

I am grateful to my father, Giuseppe Benevento, my mother, Silvana Marchese, and my brother, Alessandro Benevento, for being always and unconditionally present in my life and supportive with my choices.

Finally, I would like to particularly thank my partner Sandra Siegert, who I met in a conference in the beautiful landscape of Tuscany, and with whom I am happily sharing my life now in Vienna. These are also the beautiful consequences of a *PhD*.

